THERMAL ASSESSMENT OF RICE HUSK AND STRAW

Assessment of Thermal Decomposition of Rice Husk and its Blend with Rice Straw

Raúl Andrés Serrano Bayona

Dissertation for the Postulation to the Degree of Master of Science in Mechanical Engineering

Director
Yesid Javier Rueda Ordoñez
Ph.D. in Chemical Engineering.

Co director
María Paola Maradei García
Ph.D. in Chemical Engineering.

Co director
Omar Armando Gélvez Arocha
M.Sc. in Informatics.

Universidad Industrial de Santander
Facultad de Ingenierías Físico – Mecánicas
Escuela de Ingeniería Mecánica
Maestría en Ingeniería Mecánica
Bucaramanga
2020

Dedication

To my mom, Luz Mery, my stepfather, Yovinacio, and my sisters Laura and Mayra, who have been always at my side even in the tough moments in my life.

To María Alejandra, my love, the woman who makes me want to be a better person everyday.

To my dad, Raúl Serrano Cabrera, who has been and will be my inspiration and motivation for the life project I chose to live.

My relatives by the side of my mom, my aunts Sandra and Claudia, my grandmother María Telma, their fraternal love and patience are present always in my mind.

My grandparents related to dad, Isaías and María Francelina, their hospitality and kindness will never be forgotten.

María Alejandra's relatives, they are the best example of a united and lovely family.

To all those friends that supported to me in the development of this whole program.

Acknowledgements

To the Interfase Research Group from the School of Chemical Engineering at UIS, in attention to the professor Paola Maradei, for giving me an excellent notion and example of how a research group works.

To the professors Yesid Rueda from the School of Mechanical Engineering at UIS, for his help and dedication with the performance of this research process and to the professor Alberto Pertuz also from the School of Mechanical Engineering for his assistance with the university requirements for the use of the metallography laboratory and other devices in the tests performance step.

To the laboratory crew of the School of Chemical Engineering at UIS, Mr. Eduardo and Mr. Wilson, for their patience and help with the several test and preparation of material performed in there.

To the CIDES research group, professor Viatcheslav Kafarov, for its support with laboratory devices to the Laboratory of Combustion, needed for experimental tests performance in the present research project.

My sister, Laura Ximena, who helped me in tasks related with the assistance and participation to academic events for the knowledge spreading required in the research process.

To the Enterprise Molinos El Yopal Ltda, in attention to the CEO, Margarita Ardila, for their support with information related to the rice industry processes.

Table of contents

Pag.

Introduction. 13
1. Theoretical framework. 18
1.1. Biomass use advantages 18
1.2. State of the art 19
2. Rice waste biomasses. 22
2.1. Sample biomasses 22
2.2. Physico-chemical characterization 23
2.3. Structural composition 24
2.4. Experimental setup (Thermogravimetric analysis – TGA) 24
2.5. Results from laboratory tests 25
2.5.1. Proximate analysis. 25
2.5.2. Ultimate analysis. 28
2.5.3. Structural composition. 28
2.5.4. Heating value. 29
2.6. Thermal decomposition of biomasses. 30
2.6.1. Rice straw content influence in an inert atmosphere (N2) 33
2.6.2. Rice straw addition influence in the oxidative atmosphere (synthetic air) 35
3. Kinetic Modeling 37
3.1. Global reaction mechanism 38
3.2. Independent parallel reactions model 43
3.3. Consecutive reactions model 46
3.4. Results – performance of models from experimental results 48
3.4.1. Global reaction model – inert atmosphere. 48
3.4.2. Parallel reaction scheme – inert atmosphere. 56
3.4.3. Consecutive reaction scheme – inert atmosphere. 61
3.4.4. Parallel reaction scheme – oxidative atmosphere 66
3.4.5. Consecutive reaction scheme – oxidative atmosphere. 71
3.4.6. Comparison of the Arrhenius parameters. 75
4. Enhancement technologies. 78
4.1. Combustion chamber 78
4.2. Pyrolysis reactor 80
4.3. Gasification reactor 82
4.4. Stoichiometric analysis and reactor bed design for the thermochemical processes 85
4.4.1. Pyrolysis. 85
4.4.2. Combustion. 86

4.4.3. Gasification. 88
4.5. Experimental design for products composition test 90
4.6. Results from the experimental designs performance 93
4.6.1. Pyrolysis. 93
4.6.2. Syngas composition (Gasification) 96
5. Conclusions 113
References 116
Appendixes 140

List of figures

Pag.

Figure 1. Comparison among gross energy potential with electric energy consumption in Casanare. 14
Figure 2. Emissions of greenhouse gases sorted by component per year from 2010 to 2014**.** 15
Figure 3. Greenhouse gases emitted from 2010 to 2014 sorted by economic activity. 16
Figure 4. Normalized mass loss (straight line) and its derivative data (dotted line) as a function of the temperature of thermal decomposition of rice blend husk-straw samples in inert atmosphere. 31
Figure 5. Normalized mass loss (straight line) and its derivative data (dotted line) as a function of the temperature of thermal decomposition of rice blend husk-straw samples in oxidative atmosphere. 32
Figure 6. Comparison for blend husk-straw sample at inert and oxidative atmospheres of normalized mass loss (straight line) and its derivative data (dotted line) as a function of the temperature of thermal decomposition at 5ºC/min. 33
Figure 7. Normalized mass loss and its derivative data as a function of **the** temperature of thermogravimetry tests applied to rice husk (RH), straw (RS) and its blend (B H-S) at inert atmosphere for a heating rate of 10 °C/min. 34
Figure 8. Normalized mass loss curves and their derivative data as a function of temperature from thermal decomposition of rice husk (RH), blend husk straw (B H-S) and straw (RS) samples in oxidative atmospheres at a heating rate of 5 °C/min. 36
Figure 9. Independent Parallel Reaction Scheme development. 44
Figure 10. Consecutive reaction scheme development. 47
Figure 11. Comparison between Friedman and Vyazovkin methods results – Blend husk-straw sample. 49
Figure 12. Master plots for the blend husk-straw sample. 51
Figure 13. Results of the method for pre-exponential factor determination for blend husk-straw sample with the linear regression equation and the fitting coefficient (R^2). 52
Figure 14. Comparison between experimental data and results from global reaction model performance for the blend husk-straw sample in terms of conversion level (upper plot) and its derivative as a function of time (downer plot). 55
Figure 15. Parallel reaction scheme application to blend husk-straw mass conversion and its comparison with experimental results, $\beta = 5$ [°C/min], N_2 atmosphere, $d\alpha/dt$ variable is named as dalpha_dt. 59
Figure 16. Consecutive reactions scheme performance and a contrast with experimental values, to blend husk-straw sample, $\beta = 5$ [°C/min], N_2 atmosphere. 64
Figure 17. Curves of normalized mass and its derivative, from the performance of independent parallel reaction model for the blend husk-straw sample and a contrast with experimental data, $\beta = 10$ °C/min, synthetic air atmosphere. 70
Figure 18. Consecutive reaction scheme development and its comparison with experimental results to blend husk-straw sample, $\beta = 5$ °C/min, synthetic air atmosphere. 74
Figure 19. Sorting of pre-exponential factor values in natural logarithm magnitude vs activation energies in all the reactions for all the kinetic models in inert and oxidative atmospheres.. 76

Figure 20. Linear regression and assessment with its fitting from the obtained data of pre-exponential factor values in natural logarithm magnitude vs activation energies, in all the reactions for all the kinetic models in nitrogen and synthetic air atmospheres. 77
Figure 21. Scheme of the combustion chamber and boiler for steam obtainment at a laboratory scale and used for this study. 78
Figure 22. Reactor set-up used for the pyrolysis analysis of biomasses in this study. 82
Figure 23. Laboratory-scale reactor set-up used for the gasification analysis of biomass samples. 84
Figure 24. Contour plots with the results obtained from the bio-oil mass yield following the experimental design carried out using rice waste biomasses. 94
Figure 25. Contour plots with the results obtained from the biochar mass yield measurement following the experimental design performed using rice waste biomasses. 95
Figure 26. Comparison of measurements of CO content from the tests performed following the central composed design applied to this thermal decomposition process. 99
Figure 27. Comparison among calculations of H_2/CO ratio from the tests performed following the experimental design stablished to the gasification process. 101
Figure 28. Comparison of measurements of CH_4 content from the tests carried out following the experimental design applied to the gasification process. 103
Figure 29. Comparison among calculations of high heating value (HHV) from the tests performed following the central composed design applied to this thermochemical process. 105
Figure 30. Contour plot with data obtained from the CO emissions measurement in the combustion tests performance following the central composed design for rice waste biomasses. 108
Figure 31. Contour plot with data obtained from the NO/NO_X content measurement in the combustion tests performance following the central composed design for rice waste biomasses. 110
Figure 32. Contour plot with data obtained from the C_XH_Y concentration measurement in the combustion tests performance following the central composed design for rice waste biomasses. 111
Figure 33. Contour plot with data obtained from the chamber temperature measurement in the combustion tests performance following the central composed design for rice waste biomasses. 112
Figure 34. Parametric curve of operation of centrifugal fan with a rotor diameter of 108 mm, working at 1800 rpm*. 141
Figure 35. Control features of various tested dampers (Millers & Pelite, 2016) at similar air flow velocities, approaching in the single blade damper without a sealing (SB-l) in the present study. 142
Figure 36. Calibration curve and equation for the temperature measured by the furnace and the measured through an additional thermocouple connected to a multimeter. 143
Figure 37. Temperature profiles measured all along the pyrolysis reactor, at the center of its cross-sectional area, at various constant temperatures [°C] set in the furnace. 143
Figure 38. Calibration curve for the flux regulation of nitrogen in the rotameter. 144
Figure 39. Linear regression performance over the nitrogen content measurement in the gas chromatograph in terms of its peak area, as a function of the volume percentage of this component in the gas sample. 145

Figure 40. Linear regression performance over the hydrogen content measurement in the gas chromatograph in terms of its peak area, as a function of the volume percentage of this component in the gas sample. 145
Figure 41. Linear regression performance over the methane content measurement in the gas chromatograph in terms of its peak area, as a function of the volume percentage of this component in the gas sample. 146
Figure 42. Linear regression performance over the carbon monoxide content measurement in the gas chromatograph in terms of its peak area, as a function of the volume percentage of this component in the gas sample. 146
Figure 43. Linear regression performance over the carbon dioxide content measurement in the gas chromatograph in terms of its peak area, as a function of the volume percentage of this component in the gas sample. 147
Figure 44. Correlation for the linear regression performed to the experimental data obtained from the loose bulk density measurement as a function of the rice straw mass percentage in the sample. 148
Figure 45. Correlation from the linear regression applied in the experimental results of the ash content measurement as a function of the rice straw content in the biomass blend. 148
Figure 46. Linear regression performance over the tests data obtained for the carbon content measurement, as a function of the rice straw mass percentage in the sample. 149
Figure 47. Correlation obtained since the linear regression application over the experimental results of the hydrogen content determination, as a function of the rice straw content in the biomass blend..... 149
Figure 48. Linear regression application in the experimental results obtained from the nitrogen content measurement in the biomass sample, as a function of its rice straw content. 150
Figure 49. Linear regression performance in the tests data obtained for the oxygen content determination, as a function of the rice straw content in the biomass sample. 150
Figure 50. Temperature profile measured in the quartz reactor using the tubular furnace at 805 °C in the experimental set-up for the fixed bed gasification analysis. 151
Figure 51. Comparison of measurements of H_2 content from the tests performed following the central composed design applied to the gasification process analysis..... 155

List of tables

Pag.

Table 1. Bibliometric study for state of the art from the present research project. 20
Table 2. Standards used for the characterization of biomass samples. 24
Table 3. Standards used for the biomass structural composition determination..... 25
Table 4. Results obtained from the proximate, ultimate analysis, heating value and structural composition determination, and a comparison with data from previous studies. 27
Table 5. Ranges for values of Arrhenius equation in parallel reaction scheme taken from previous studies. 46
Table 6. Reaction functions mostly used in previous works in their general and integral form, expressed as a function of α. 50
Table 7. Obtained data for parameters and deviation with experimental results in the isoconversional reaction scheme for rice husk (RH), rice straw (RS) and blend husk-straw (B H-S) samples. 53
Table 8. Obtained data from the iterations performed in independent parallel reaction scheme on inert atmosphere. 57
Table 9. Obtained data of coefficients from the iteration process and its deviation value in consecutive reaction scheme performance for all samples on inert atmosphere. 61
Table 10. Obtained results for coefficients values and the deviation with experimental data from parallel reaction scheme for all samples in oxidative atmosphere. 67
Table 11. Obtained results for consecutive reaction scheme performance and its deviation from the experimental data in oxidative atmosphere for all samples. 72
Table 12. Factors and values of high and low levels stated from the central composed designs for each thermochemical process performed using the biomass samples. 91
Table 13. Response variables stablished from the central composed designs for each thermochemical process assessment using the biomass samples. 92
Table 14. Typical gasification reactions used in previous studies concerning this thermochemical process using air in a fixed bed condition. 97
Table 15. List of reaction models used for the reaction kinetics description used by Jankovic (Jankovic, 2008). 140
Table 16. Equations applied for the real air flow determination and the opening angle calculation in the damper. 141
Table 17. Results of bio-oil and solid char mass yields obtained from the tests performed in the pyrolysis reactor. 152
Table 18. Mass balance calculation from the products mass yields obtained in the gasification tests performance. 152
Table 19. Results of syngas composition measurement through the gas chromatograph and its calculated heating value following the experimental design carried out for gasification process tests for rice waste biomass samples. 153
Table 20. Results obtained from flue gas composition and its temperature measurements performed from the combustion experimental tests. 153

List of appendixes

Pag.

Appendix A 140
Appendix B 141
Appendix C 143
Appendix D 145
Appendix E 148
Appendix F 151
Appendix G 152
Appendix H 154

Resumen

TÍTULO: EVALUACIÓN DE LA DESCOMPOSICIÓN TÉRMICA DE LA CASCARILLA DE ARROZ Y SU MEZCLA CON PAJA DE ARROZ[1].

AUTORES: SERRANO BAYONA, Raúl Andrés[2].

Palabras clave: Termogravimetría, Pirólisis, Combustión, Gasificación, Modelado Cinético, Rendimiento Másico.

Actualmente, en países en desarrollo, el residuo agrícola de la industria arrocera, específicamente la cascarilla de arroz la cual es recogida en los molinos es quemada para obtener calor en calderas para vapor y en secadores de aire, y la paja de arroz que es obtenida en la etapa de cosecha, es dejada en el campo como un fertilizante complementario. Este trabajo tiene como objetivo el estudiar la mejora de las características térmicas y evaluar el rendimiento en masa de productos y sus composiciones obtenidas de la combustión, pirólisis y gasificación de los residuos de la industria arrocera en el departamento de Casanare, mediante la adición de paja de arroz a la cascarilla de arroz. Así, este trabajo comparó el comportamiento de la descomposición térmica de estos dos materiales de biomasa mediante análisis termogravimétrico en atmósfera inerte y oxidativa. El mecanismo de reacción que describe el proceso de descomposición térmica fue determinado también, seleccionado de los modelos de reacción global, reacciones paralelas independientes y reacciones consecutivas. Un analizador de gases fue usado en el montaje experimental del proceso de combustión para la medición de emisiones. Las pruebas de pirólisis fueron realizadas mediante un montaje con un reactor usando N_2 como gas de arrastre y variando la temperatura del proceso, con el fin de medir los rendimientos de masa de bioaceite y biochar. Para la realización del proceso de gasificación, un montaje similar fue usado, donde aire comprimido fue suministrado de acuerdo con la relación de equivalencia (ER). Después, la composición del gas de síntesis obtenido fue medida en un cromatógrafo de gases. Los análisis próximos, últimos y estructurales fueron llevados a cabo bajo estándares de la ASTM, al igual que el análisis de calorimetría en base húmeda para determinación del poder calorífico. El porcentaje de desviación promedio (AD %) menor al 5% fue considerado como un criterio estadístico para evaluar la exactitud en los resultados experimentales. Los resultados obtenidos de este trabajo presentaron un valor mayor de poder calorífico en las muestras de paja de arroz, siendo más adecuada para el proceso de combustión. Sin embargo, la relación de aire en exceso dió la influencia directa más representativa sobre este mismo proceso. Esto es opuesto a la tendencia encontrada en la pirólisis y gasificación, donde la temperatura del reactor fue establecida como un factor y fue la más influyente sobre estas conversiones térmicas. Finalmente, el modelo cinético que representó mejor el proceso de descomposición térmica fue el de reacciones consecutivas.

---

[1] Trabajo de Investigación, Tesis de Maestría.

[2] Facultad de Ingenierías Físicomecánicas, Escuela de Ingeniería Mecánica. Director: RUEDA-ORDÓÑEZ, Yesid Javier, Ph.D. en Ingeniería Química. Codirectores: GAUTHIER-MARADEI, María Paola, Ph.D. en Ingeniería Química; GÉLVEZ-AROCHA, Omar Armando, M.Sc. en Informática.

Abstract

TITLE: ASSESSMENT OF THERMAL DECOMPOSITION OF RICE HUSK AND ITS BLEND WITH RICE STRAW[1].

AUTHORS: SERRANO BAYONA, Raúl Andrés[2].

Keywords: Thermogravimetry, Pyrolysis, Combustion, Gasification, Kinetic Modeling, Mass Yield.

Currently, in developing countries, the agricultural residue of the rice industry, specifically rice husk which is collected in the rice mills is burned to obtain heat in steam boilers and air driers, and the rice straw, obtained in the harvesting stage, is left in the field as a complementary fertilizer. This work aimed to study the improvement of the thermal characteristics and to assess the mass yields of products and their compositions obtained from combustion, pyrolysis and gasification of rice industry wastes in the department of Casanare, by the addition of rice straw to the rice husk waste. Thus, this work compared the thermal decomposition behavior of these two biomass materials by thermogravimetry analysis in inert and oxidative atmospheres. The reaction mechanism which governed the thermal decomposition process was determined as well, selected from the single-step global reaction, independent parallel reactions, and consecutive reactions models. A gas analyzer was used in the experimental set up of the combustion process for the emissions measurement. Pyrolysis tests were performed through a set-up with a reactor using N2 as a carrier gas and varying the process temperature, in order to measure the bio-oil and the solid char mass yields. For gasification performance, a similar set-up was used, where compressed air was supplied according to the equivalence ratio (ER). Later, the obtained syngas composition was measured in a gas chromatograph. Proximate, ultimate and structural analysis tests under ASTM standards, and heating value tests on a wet basis through calorimeter were performed. An average deviation percentage (AD %) lower than 5% was regarded as a statistical criterion to assess the accuracy in the experimental results. Results obtained from this work presented a higher heating value in the rice straw sample rather than the rice husk being more profitable for combustion processes. However, the air excess ratio gave the most remarkable direct influence over the combustion process. This is opposite to the trend found in pyrolysis and gasification, where the temperature of the reactor was set as a factor and was the most influent over these thermal conversions. At the same time, the rice straw content in the sample took place with a lower or negligible effect, including the equivalence ratio for the gasification analysis. Finally, the reactions model which better represented the decomposition processes was the consecutive reactions. However, independent parallel reactions also showed a good agreement with the non-isothermal decomposition curves.

---

[1] Research Work, Master Thesis.

[2] Facultad de Ingenierías Físicomecánicas, Escuela de Ingeniería Mecánica. Director: RUEDA-ORDÓÑEZ, Yesid Javier, Ph.D. in Chemical Engineering. Co-directors: GAUTHIER-MARADEI, María Paola, Ph.D. in Chemical Engineering; GÉLVEZ-AROCHA, Omar Armando, M.Sc. in Informatics.

Introduction.

a) Problem Formulation

Waste biomasses in rice industry

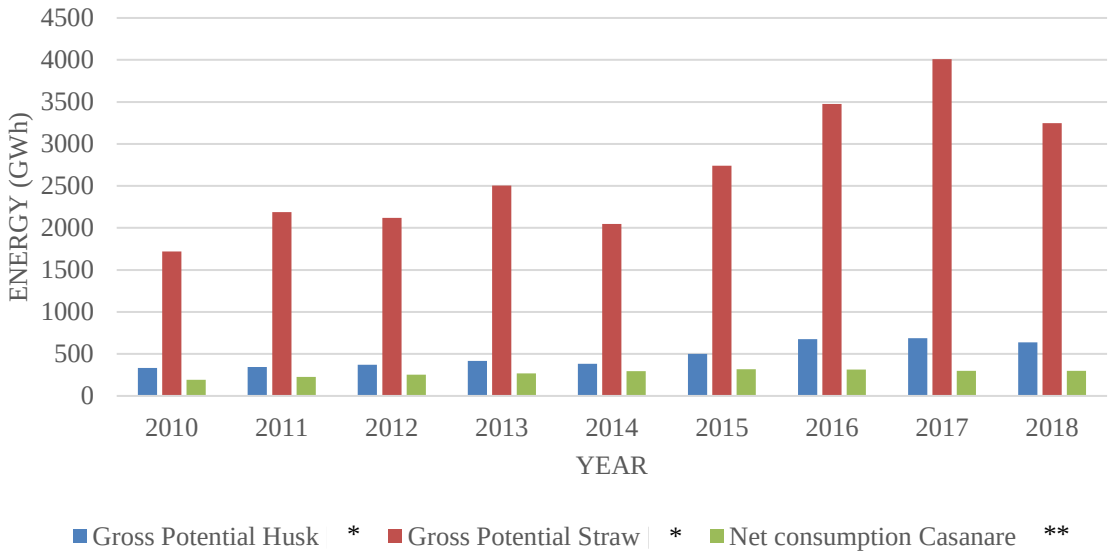
Colombia has some relevant features regarding its agricultural nature, as its high production of waste from agro-industry, referring to the rice industry biomasses which reached a 30.5% on a mass basis over the national obtainment in 2017 (DANE, 2017). In the department of Casanare, considering the rice straw generation ratio as 5 t/ha of paddy rice harvested (Parés-Casanova et al., 2017), 900.765 t of this biomass were obtained in 2017 as well; also, the other residue produced is the rice husk, corresponding to the 20 % on a mass basis of the whole paddy rice grain (Aguilar, 2009), and in this year reached 172.675 t (DANE, 2017).

Energy Consumption in rice industry

In Figure 1 is presented the comparison of the energy potential between the selected biomasses and contrasted to the data of electric energy consumption in Casanare, Colombia, from 2010 to 2018 (CREG, 2019). In 2017, it was presented the highest ratio of energy potential/consumption, with values of 13.35 and 2.29 for rice straw and rice husk, respectively. However, the lowest ratio of energy potential/consumption registered was in 2014 with a value of 6,97 for the rice straw and 1,3 for the rice husk.

Figure 1.

Comparison among gross energy potential with electric energy consumption in Casanare.



[*] (DANE, 2017); [**] (CREG, 2019).

Fuel production in Casanare

The highest consumption of natural gas in Casanare was 19 million m^3 and occurred in 2018 (CREG, 2019), with a distribution of 67.15% and 32.85% for residential and industrial use, respectively. On the other hand, in 2016 was produced the highest amount of liquefied petroleum gas (LPG), over 226 million kg (CREG, 2019).

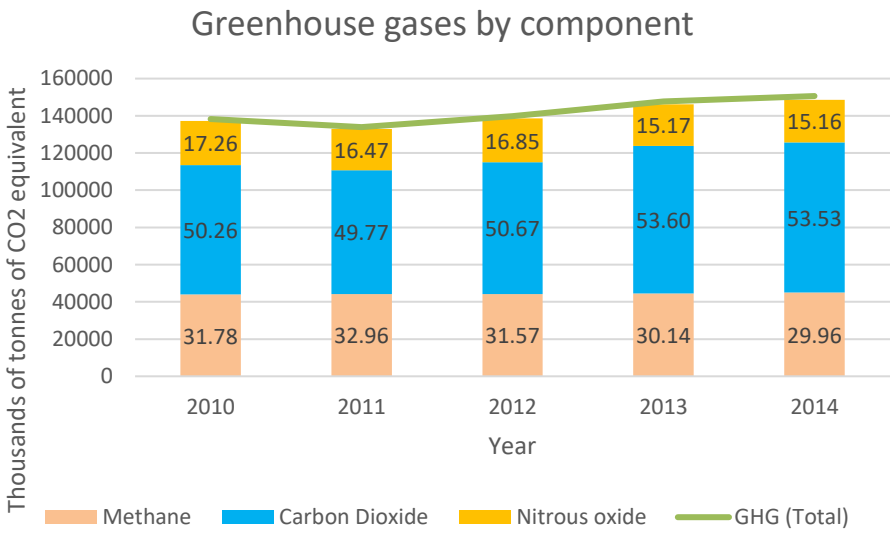
Environmental issues

According to the United States Environmental Protection Agency (EPA, 2014), in 2010 was released 65% of carbon dioxide because of using these fossil fuels and several

industrial processes all over the world. In Figure 2 is presented the production of greenhouse gases in Colombia from 2010 to 2014, following the latest data exposed by the Organisation for Economic Co-operation and Development (OECD). The main component was carbon dioxide with 51%, followed by 31% methane, and 15% nitrous oxide (OECD - 2020).

Figure 2.

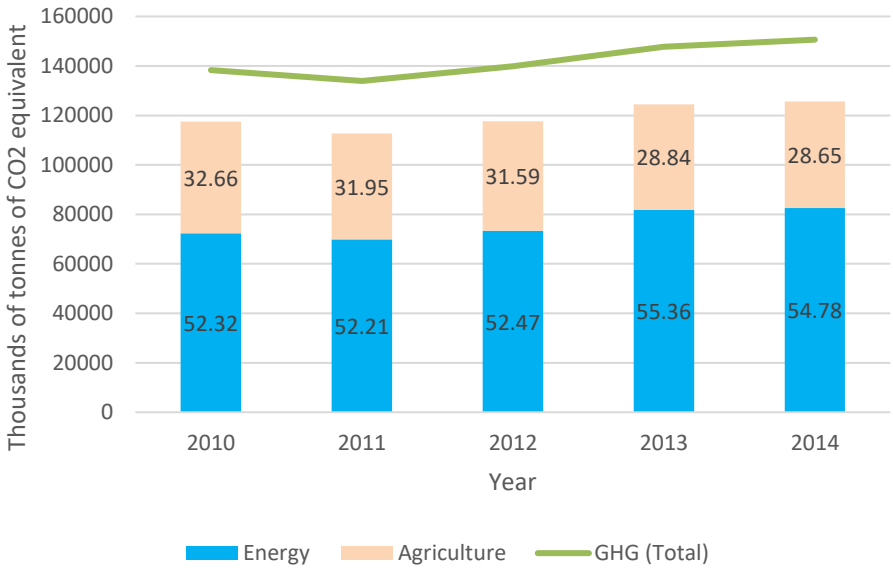
Emissions of greenhouse gases sorted by component per year from 2010 to 2014.



In this way, in Figure 3 are exposed the GHG emissions with activities related to energy generation (including manufacturing industries and construction, residential and transportation sectors) and agriculture, representing approximately 53 %, and 31 %, respectively (OECD - 2020).

Figure 3.

Greenhouse gases emitted from 2010 to 2014 sorted by economic activity.



b) Objectives

General objective

To assess the effect of adding of rice straw to rice husk produced in the department of Casanare, in their thermal, energy and compositional features for fuels production or derivates obtained for industrial purposes, in combustion, gasification and pyrolysis processes.

Specific Objectives

To find physico-chemical and thermal properties of biomass through the:

- Proximate analysis (moisture, ash, volatile matter and fixed carbon contents).

- Ultimate analysis (carbon, hydrogen, nitrogen and oxygen contents).
- Structural composition (extractives, hemicellulose, cellulose and lignin contents).
- Higher heating value of biomasses.

To perform a kinetic reaction model of thermal decomposition process under an atmosphere of nitrogen and synthetic air for the obtainment of:

- The chemical reactions involved in the process.
- The kinetic parameters to reactions, such as activation energy, frequency (pre-exponential) factor and conversion function.
- The reaction mechanisms based in Arrhenius law, which predicts thermal behavior of biomass samples.

To obtain mass yields of solid, liquid and syngas products in combustion, pyrolysis and gasification in a fixed bed reactor at lab-scale.

1. Theoretical framework.

1.1. Biomass use advantages

Waste biomass using as raw material for fuel production has been widely evidenced, such as syngas production through gasification, which has reached yields of H_2, CO and CH_4 of 25, 39 and 14 % (volume fraction), respectively (Khonde and Chaurasia, 2016). On the other hand, in the pyrolysis process the products are composed by non-condensable gases, bio-char (solid), and bio-oil (liquid), in which the last one could achieve up to 40% of mass yield (Tsai and Chang, 2007). However, in the bio-oil, large amounts of oxygen have been found, resulting in low pH value and low heating value. Finally, in biomass processing through combustion, the main interest is the thermal energy release. However, the flue gas composition quantification is needed to verify that the greenhouse gases (GHG) emissions are into the admitted limit standards (Duan et al., 2013).

In this sense, in the present study, the three thermochemical conversion processes will be analyzed, aiming to obtain product composition and their variation according to factors changes in their values, and, observing their influence in the parameters above.

1.2. State of the art

Several studies have been performed in both biomasses (rice straw and rice husk), referring to compositional analysis, physico-chemical characterization and thermal decomposition. The determination of the mass yield of products is more common in pyrolysis processes. In contrast, for the combustion process, the temperature of operation is usually measured rather than the mass yield, as same as flue gas emissions. For gasification, the measuring of the mass of products is required to check the mass balance. Besides, the syngas composition for the heating value calculation and other derived values are also considered due to its interest in biofuels synthesis. Research studies about rice husk and rice straw have been performed and reported in the scientific literature such as measurements for rice husk mixed with seaweed (Hu, Y. et al., 2019) in co-pyrolysis mechanism and studies using this biomass blended with mineral coal (Lignite) (Qi et al., 2017) in chemical-looping co-gasification.

A brief bibliometric analysis can be observed in Table 1, where several studies about these topics were quantified based on data obtained in Scopus database (Scopus®, 2020) through the ‘Analyze search results’ tool. This one allows checking the number of studies performed in each topic by year, by authors, by the origin countries, subject area, type of documents and funding sponsor (among others). The keywords used in this analysis, including those shown in the first column, were Rice & Husk & Straw & Blend. Furthermore, considering the workshops undertaken in Colombia, shown in parenthesis in

Table 1, highlights also the lack of research studies in this topic nationwide. As seen in this chart, the structural composition measured in both biomasses is the most commonly studied, followed by the thermal decomposition analysis and then, the physico-chemical characterization. It is worth noting that, in the firsts two topics mentioned previously, it is usual to find proximate and ultimate analysis results as well.

Table 1.

Bibliometric study for state of the art from the present research project.

Research Topic (Keywords)	**Rice Husk**	**Blend Husk-Straw (Rice waste biomasses)**	**Rice Straw**	**Total**
Proximate – Ultimate analysis	44 (2)	1 (1)	21 (1)	66 (4)
Hemicellulose, cellulose, lignin.	114 (8)	0	337 (1)	451 (9)
Thermogravimetry (Inert)	51 (1)	0	43 (0)	94 (1)
Thermogravimetry - Combustion	23 (0)	1 (0)	21 (0)	45 (0)
Kinetics modeling - pyrolysis	24 (1)	0	23 (0)	47 (1)
Kinetics modeling - combustion	9 (0)	0	13 (0)	22 (0)
Air gasification – fixed bed	19 (2)	0	2 (0)	21 (2)
Air combustion – fixed bed	12 (0)	0	5 (0)	17 (0)
Pyrolysis – fixed bed - Nitrogen	15 (0)	0	13 (0)	28 (0)

Note: Contrast among the global amounts with the number of studies performed nationwide (represented in parenthesis).

The studies based in fixed bed reactors in thermochemical conversions were the less performed because the fluidized bed reactors are more common, regarding its preference at large scales (Hrbek and Vreugdenhil, 2020). Finally, there are no studies

focused on the effect assessments of the addition of rice straw to rice husk as blend samples, on their composition, thermal and energy characteristics; further, the determination of the products from pyrolysis, gasification or combustion processes using these blends is not done yet.

2. Rice waste biomasses.

2.1. Sample biomasses

Biomasses selected for this study were rice husk and rice straw, obtained from paddy rice crops, brought from the department of Casanare, in its capital, Yopal. Rice husk dwas given by Molinos el Yopal Ltda. (5°19'38.1"N 72°24'26.1"W), and rice straw has been supplied by a local farmer in Tilodirán, a county from the same city (5°07'58.5"N 72°11'53.4"W). Initially, for a better milling process, biomass was dried in the open air, for two months; this preliminar step avoids the biomass agglomeration in the knives mill, allowing to achieve higher milling efficiency using this device, obtaining higher amounts of sample mass with the required particle size at the end of the process. After that, it was milled using a Wiley knives mill, getting particle sizes lower than 1 mm, and it was sieved using a portable sieve shaker CE Tyler RX - 24. In this stage, the particle size of 250 µm for TGA, heating value, volatile matter and moisture contents analyses, 180 µm for ash analysis and 150 µm for ultimate analysis -sieves N° 60, N° 80 and N° 100 respectively, according to standard ASTM E11 (ASTM E11, 2020)- were used to separate biomass samples. In this study, three levels of biomass composition were used in samples; this is, 0, 50 and 100 mass% of rice straw, balanced with rice husk.

2.2. Physico-chemical characterization

The characterization was performed through the ASTM standards shown in Table 2. For proximate analysis, a Terrígeno D8 Furnace was used, and the mass measurements for moisture, ash and volatile materials were determined in a high precision balance (0.1 mg). In this analysis, fixed carbon content was calculated by difference.

On the other hand, a SUNDY SDCHN435 analyzer is used for the determination of ultimate analysis. Following ASTM specifications related to this measurement, the moisture content is extracted from this composition, determined previously from an oven-heated sample at 105 °C and using the remaining product for this test. All these standards are exposed in Table 2.

Finally, for the lower heating value (LHV) analysis, a Parr 6200 calorimeter was used, and the ASTM standards considered in this measurement are mentioned in Table 2. The specification for the higher heating value determination states that the moisture content is measured apart, and its value is extracted from the amount determined in the calorimetry test.

Table 2.

Standards used for the characterization of biomass samples.

Type of characterization	Standard code	Measured value
Proximate analysis	ASTM E1756 – 08	Moisture content
	ASTM E872 – 82	Volatile matter
	ASTM E1755 – 01	Ash content
Ultimate analysis	ASTM D5373 – 16	Carbon, hydrogen and nitrogen measurement.
Higher heating value	ASTM D5865/D5865M - 19	Higher heating value determination for coal and coke.

2.3. Structural composition

This analysis was performed through a set of tests to measure the aqueous and organic extractives and, contents of hemicellulose, cellulose and lignin from the biomass samples (the last values were calculated through the previous determination of α-cellulose and holocellulose, respectively). For this analysis, the protocol used follows the standards exposed in Table 3. The raw material is oven-dried to decrease the moisture content of the biomass sample. The dried biomass is used to determine the aqueous and organic extractives, which are subtracted using a Soxhlet system.

2.4. Experimental setup (Thermogravimetric analysis – TGA)

Thermogravimetric tests were carried out using a TGA analyzer (5500, TA Instruments). To study the biomass behavior on inert atmosphere, nitrogen was chosen as reactive gas with a flux of 50 mL/min. For the test, three heating rates were used (2.5 °C/min, 5 °C/min and 10 °C/min). The oven temperature was programmed from 25 ºC to

900 °C. Besides, tests at the oxidative atmosphere are also performed. For that, synthetic air was used with 20 vol% O_2 (in N_2 balance) as reactive gas at the flux mentioned above, heating rates and temperature limits in the oven. For all tests, an initial mass of approximately 10 mg was used.

Table 3.

Standards used for the biomass structural composition determination.

Type of characterization	Standard code/Reference	Title
Aqueous and organic extractives	ASTM D1110 – 84	Standard Test Methods for Water Solubility of Wood
	TAPPI T-264 (ASTM D1105 – 96)	Preparation of Wood for Chemical Analysis (Including Procedures for Removal of Extractive and Determination of Moisture Content).
Holocellulose	(Evtuguin et al., 2003)	Characterization of an acetylated heteroxylan from *Eucalyptus globulus* Labill.
	(Marques, 2010)	Recovery for different lignocellulosic crops for paper paste manufacturing.
Alphacellulose	ASTM D1103 – 60 (1977)	Method of Test for Alpha-Cellulose in Wood (Withdrawn 1985).
	TAPPI T203 05-1974	Alpha-, Beta-, and Gamma-Cellulose in Pulp.
Klason Lignin	ASTM D1106 – 96	Standard Test Method for Acid-Insoluble Lignin in Wood.
	(Moore and Johnson, 1967)	Procedures for the chemical analysis of wood and wood products.

2.5. Results from laboratory tests

2.5.1. Proximate analysis.

According to Table 4, the moisture of biomasses is held below 10 mass%, being suitable as a raw material in thermochemical processes following previous studies (Lopes,

I. et al., 2018; Han et al., 2020) which state that a value below 15 mass% is optimal for its use in these conversions. It worths noting that the moisture of biomass does not need to follow a linear trend because of the inference of other factors such as the environment (either weather or the year season), the geography (Sasauchi, 2019), the type of biomass storage, among others. A direct effect from the straw content in the biomass sample is detected for the volatile matter, and the fixed carbon content, while for the ash content measured an inverse influence is observed from this parameter as well. However, the reference data exposed in Table 4 shows similar values for both biomass samples, evidencing an absence of influence from the straw addition in the biomass blend over these components. A higher amount of fixed carbon content may lead to a higher char production through a pyrolysis process. However, it is not the same fact for the volatile matter with the bio-oil production, due to the possible release of non-condensable gases from the devolatilization of biomass as well.

Table 4.

Results obtained from the proximate, ultimate analysis, heating value and structural composition determination, and a comparison with data from previous studies.

Biomass Samples		This study			Rice husk references			Rice straw references		
		RH	B H–S	RS	[A]	[B]	[C]	[D]	[E]	[F]
Moisture content		8.88	8.73	9.78	-	6.92	7.3	-	8.9	5.73
Proximate analysis (mass%)*	Volatile matter	65.64	67.07	68.47	68.25	60.00	61.92	75.8	69.30	61.4
	Fixed carbon**	12.46	13.37	13.80	16.92	19.23	21.14	9.3	19.87	17.6
	Ash content	21.90	19.56	17.73	14.83	20.77	16.94	14.9	10.83	21
Ultimate analysis (mass%)	Carbon	34.62	38.46	40.79	39.5	33.87	42.80	38.7[+]	42.04	35.5
	Hydrogen	4.58	5.06	5.30	5.71	4.57	4.48	5.8[+]	6.26	4.62
	Oxygen	38.02	35.89	34.90	39.3	41.28	29.33	55.2[+]	39	37.83
	Nitrogen	0.87	1.04	1.29	0.66	0.84	0.37	0.7[+]	1.23	0.99
	Hemicellulose***	9.3	9.7	10.55	27.30[G]	24.50	28[H]	33.6	19.02[I]	32.98[J]
	Cellulose***	58.7	51.4	32.7	34.10[G]	39.65	34[H]	38.0	34.98[I]	37.47[J]
	Lignin***	27	22.1	16.5	17.90[G]	35.84	18[H]	23.8	26.53[I]	18.68[J]
Lower heating value (MJ/kg)		14.36	15.17	16.02	16.10*	13.11	15.70	15.5*	19.44	13.29

RH: Rice husk; B H – S: Blend Husk-Straw and RS: Rice straw
**dry basis; ** calculated by difference; ***Extractives-free basis; [+]Moisture, ash-free basis.*

[A] (Abu Bakar and Titiloye, 2013); [B] (Marrugo et al., 2016); [C] (Janvijitsakul and Kuprianov, 2008); [D] (Fukuda, 2016); [E] (Okasha, 2007); [F] (Migo-Sumagang et al., 2020); [G] (Goenka et al, 2015); [H] (Kumar Gupta et al., 2016) ; [I] (Ashoor and Sukumaran, 2020); [J] (Chang et al., 2018)

2.5.2. Ultimate analysis.

An inverse effect is detected from the straw mass percentage in the sample over the oxygen content, as seen in Table 4, being consistent with the trend detailed for the ash content in the previous measurement. In the other hand, a direct influence is observed for the carbon, hydrogen and nitrogen composition in the biomass sample from the factor mentioned above as well; this effect is also evidenced in the volatile matter and fixed carbon content from the previous analysis. These influences from the addition of rice straw might improve the composition of the syngas obtained in the gasification process by the increase in the carbon and hydrogen content in the raw material, including the higher fixed carbon content achieved in the sample as well. Despite, results from the literature were with similar magnitudes among both biomass samples and with the local experimental data, although an absence of effect from the straw addition is observed in these previous studies.

2.5.3. Structural composition.

In Table 4 the results obtained from the hemicellulose, cellulose and lignin contents measurement in the present biomass samples are exposed; however, these results are not coherent with the data collected from previous studies applied to the same biomass materials. In the reference data, the cellulose content does not exceed the 40 mass% for both rice straw and husk materials; moreover, if Cellulose/Hemicellulose and Cellulose/Lignin ratios were defined for the assessment of these proportions in the samples,

these ratio values would be found between 1 and 2 for both biomasses. On the other hand, these ratios are calculated above 2 and even higher for the husk and blend samples in the present study; worth noticing other biomass samples with ratios higher than 2 such as the banana tree fiber (Santos et al., 2017) and biomass materials with ratios lower than 1, which is the case of the palm kernel shell (Marrugo et al., 2016). Therefore, for the following sections and chapters which require a discussion related to this composition, the information obtained from previous studies is taken into account for the rice waste biomass samples here analyzed, which are shown in Table 4 as well.

2.5.4. Heating value.

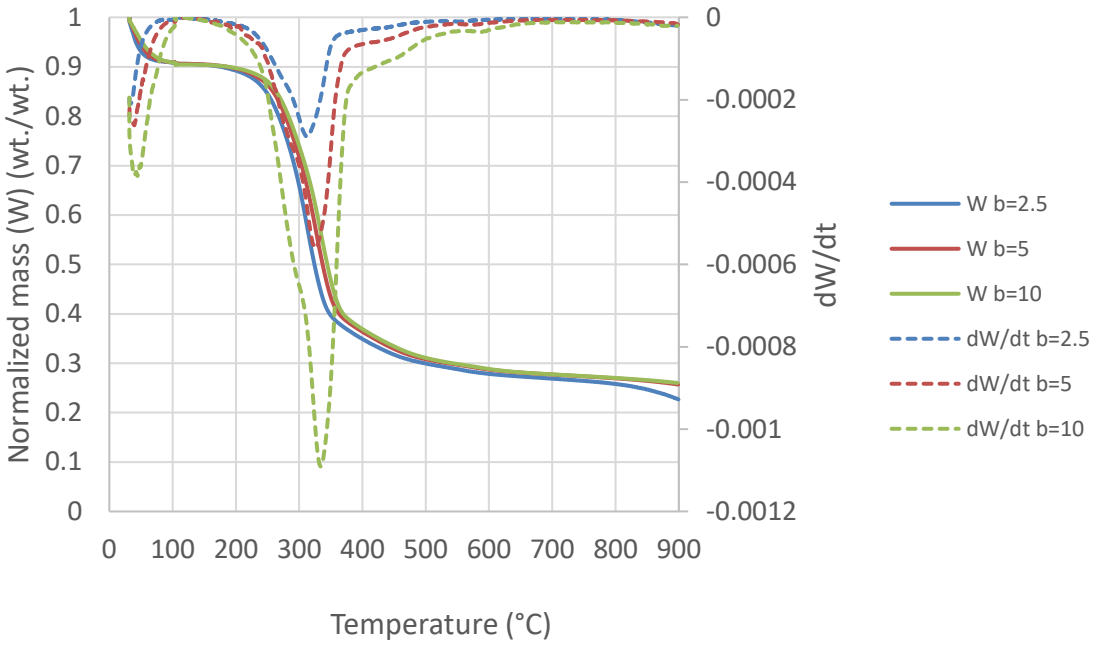
A direct effect from the rice straw addition to the sample is remarked, being consistent with the carbon and hydrogen content, and with the fixed carbon and volatile matter behavior in the proximate analysis performance. This effect might show an improvement in the combustion process due to a higher thermal energy release with the addition of rice straw to the rice husk, although this fact will be proved and discussed deeply in section 5.6.3.; moreover, data obtained from previous researches do not reveal a significant trend for this property for the biomasses here analyzed.

2.6. Thermal decomposition of biomasses.

TGA methodology was performed to study the thermal behavior of biomasses at three different heating rates (2.5 ºC/min, 5ºC/min and 10 ºC/min), in the three levels of rice straw content in the biomass sample managed in the previous compositional analysis and in inert and oxidative atmospheres. Figures 4 and 5 show that the heating rate change has not a significative effect in the mass loss produced by the thermal decomposition. However, the influence over their derivatives is observed as directly proportional, in the absence of overlapping of curves which is suitable for correct performance of the kinetic modeling at the thermal decomposition of these samples, avoiding mass and heat transfer effects (Rueda-Ordóñez and Tannous, 2015). The drying stage is exposed as the first mass loss from the biomass sample (Sattar et al., 2020), with a 10% of the decomposition from the initial mass, coincident with the values of moisture content measured in the proximate analysis results (See section 3.5.1.). Besides, the figure shows that the decomposition at inert atmosphere happened by two main stages, identified as two pronounced peaks in the derivative data and separated by a change of slope in the mass loss curve, consistent in the two atmospheres here regarded. According to previous studies (Lopes, F. et al., 2016; Lopes, F. et al., 2018), the first and most pronounced loss of mass belongs to the devolatilization stage which occurs in a short temperature interval for the nitrogen environment as seen in Figure 4. The last degradation is identified as the carbonaceous material degradation which is featured by its slow rate in the absence of oxidation reaction.

Figure 4.

Normalized mass loss (straight line) and its derivative data (dotted line) as a function of the temperature of thermal decomposition of rice blend husk-straw samples in inert atmosphere.

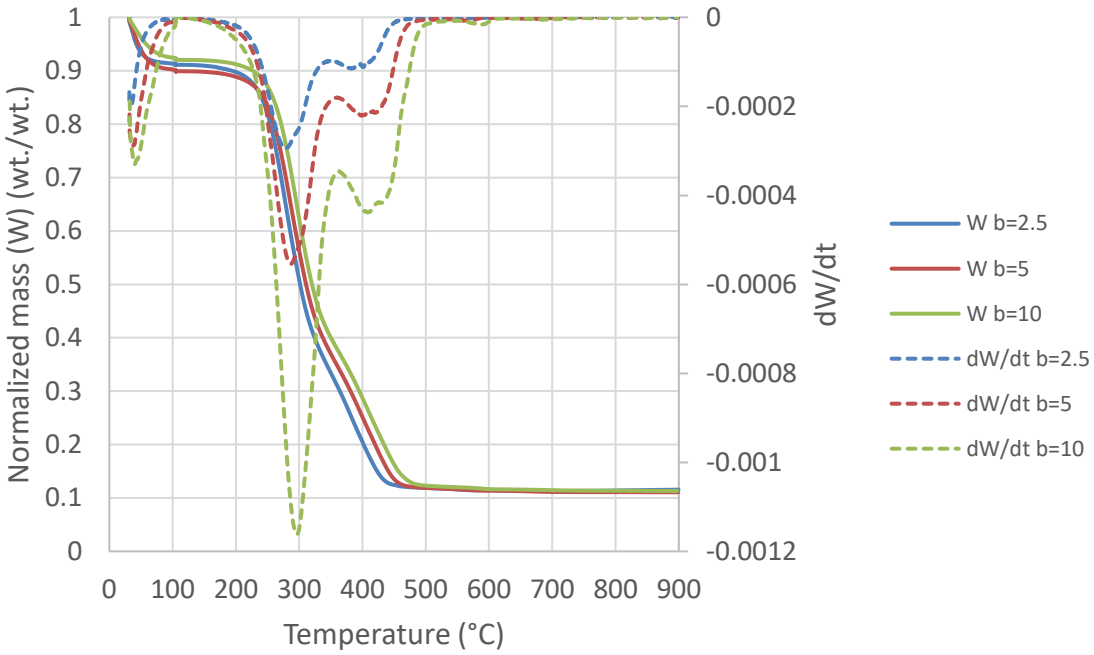


Note: Three different heating rates (2.5 ºC/min, 5ºC/min and 10 ºC/min).

Moreover, from the thermal degradation of these biomass samples in an oxidative atmosphere, as exposed in Figure 5, the normalized mass loss curve presents two decomposition zones revealed by their different slopes. The first stage is identified as the release and combustion of the volatile matter with the oxygen content present in the synthetic air (Paniagua et al., 2015; Ghaly and Mansaray, 1999) and subsequently, the second decomposition zone is associated to the oxidation of the solid char remained from the previous stage (Yin et al., 2020; Havilah et al., 2019). Finally, over 450 °C a zone with an absence of reaction is observed, which is related to the ash content in the sample; its value over the normalized mass is similar to the measured in the proximate analysis (see Table 4).

Figure 5.

Normalized mass loss (straight line) and its derivative data (dotted line) as a function of the temperature of thermal decomposition of rice blend husk-straw samples in oxidative atmosphere.



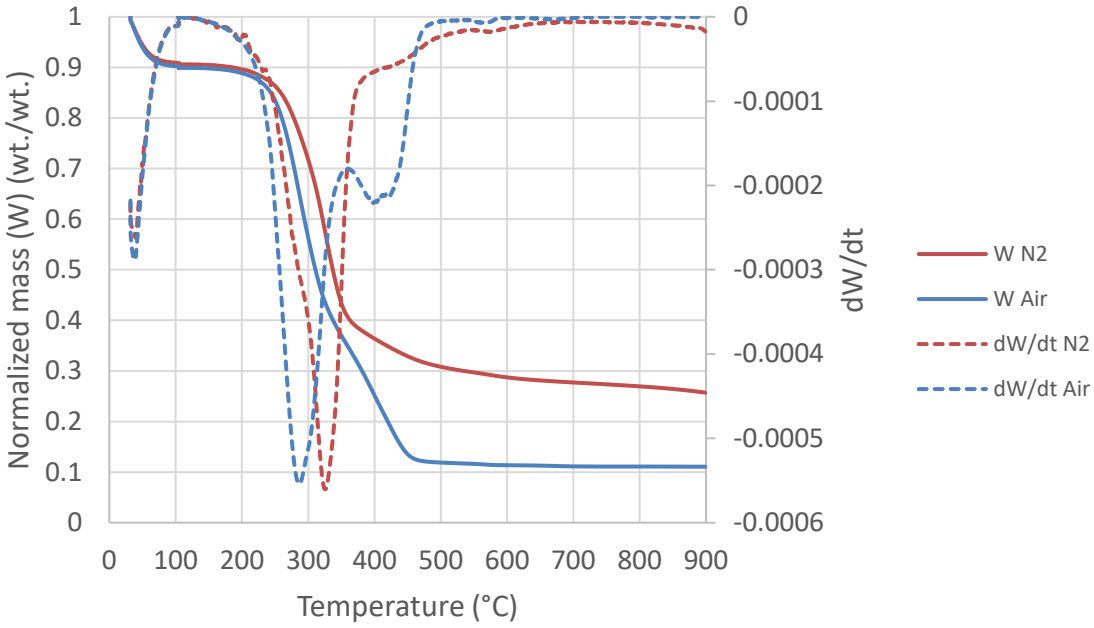
Note: Three different heating rates (2.5 ºC/min, 5ºC/min and 10 ºC/min).

A comparison between the results in inert and oxidative atmospheres is shown in Figure 6. For both devolatilization and solid char reaction stages, these occur faster under synthetic air rather than nitrogen achieving the maximum on the derivative curve of mass loss at a lower temperature. This contrast took place due to specified thermochemical reactions occurring at different atmospheres; this is, the oxidative reactions in the air environment produced higher thermal decomposition rates (Ghaly and Mansaray, 1999) than those involving the breakage of the main structural components in the biomass by the temperature increase and the absence of oxygen in the surroundings. Commonly, the behavior observed under nitrogen is linked to the pyrolysis process, while the trend denoted

during the thermal process under air, is generally associated with gasification or combustion processes.

Figure 6.

Comparison for blend husk-straw sample at inert and oxidative atmospheres of normalized mass loss (straight line) and its derivative data (dotted line) as a function of the temperature of thermal decomposition at 5ºC/min.



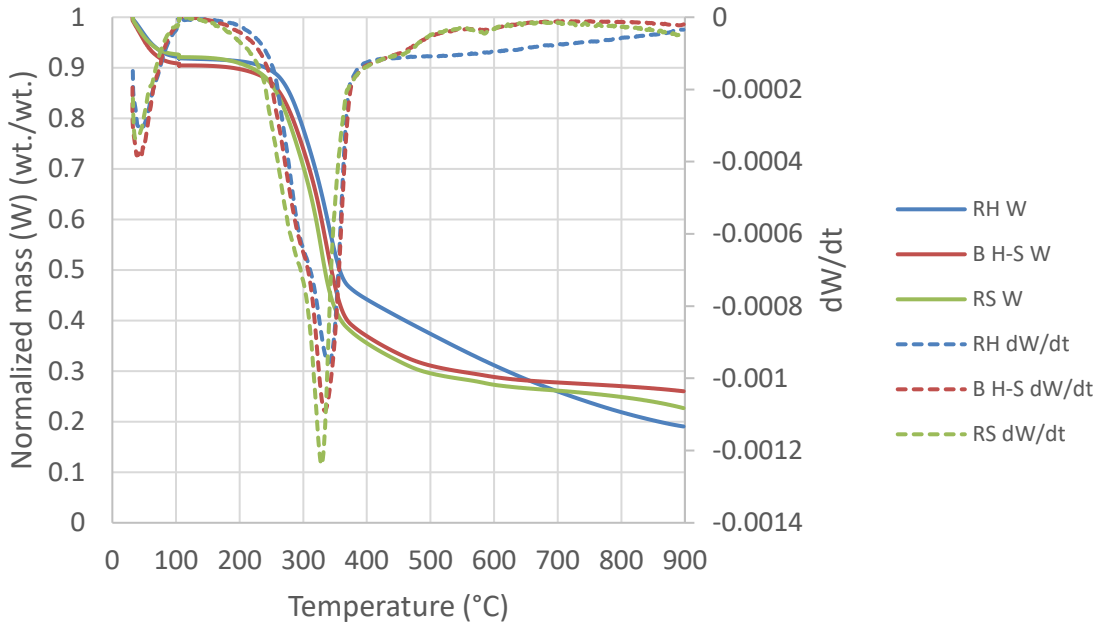
2.6.1. Rice straw content influence in an inert atmosphere (N2)

Now, referring to results shown in Figure 7, it is possible to assess biomass blend concentration influence in thermal decomposition on the inert environment. Curves for each heating rate show an equal slope all along the temperature zone for volatile release; results for straw and blend data displayed a higher volatile matter release than rice husk sample, which is in agreement with the proximate analysis performed previously. After

that, in the char formation zone, the mass loss maintained a constant slope in the rice husk sample, while for straw and blend samples this slope gets reduced by the temperature increase with a parallel shape among them. At this temperature range, the degradation rate for rice straw and rice husk took separate ways. This reveals an extra-component on rice husk reacting in this atmosphere or a missing component in the straw and blend samples decomposition.

Figure 7.

*Normalized mass loss and its derivative data as a function of **the** temperature of thermogravimetry tests applied to rice husk (RH), straw (RS) and its blend (B H-S) at inert atmosphere for a heating rate of 10 °C/min.*



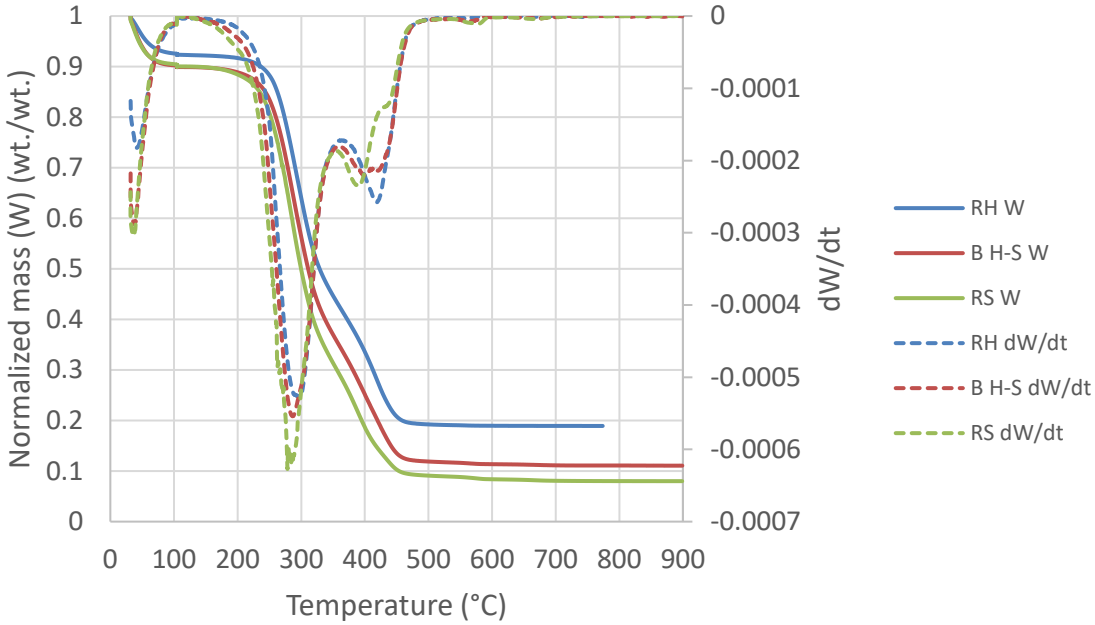
2.6.2. Rice straw addition influence in the oxidative atmosphere (synthetic air)

As plotted in Figure 8, higher moisture contents were detected in the blend and straw samples with parallel W curves in the volatile release stage, despite points of switch from this zone to the fixed carbon oxidation exposed a higher mass loss in the straw material rather than the blend sample. In turn, both these samples displayed a higher volatile release than rice husk, is this consistent with the proximate analysis data. Moreover, regarding the fixed carbon content in the husk, this content was lower than the other biomass samples, evidenced with the higher amount of ash content; these facts are in agreement with the results obtained in the proximate analysis as well, shown in section 3.5.1.

From the mass loss rate curves, the highest decomposition rate at the devolatilization stage is achieved in the rice straw sample, similar to the behavior at the inert atmosphere. Besides, a component in the rice husk sample analysis is reacting above 400 °C in the char oxidation zone, which is partially absent in the blend husk-straw decomposition and totally in the straw sample. This contrast arises due to the presence of higher amounts of ash in the husk sample, which acts as a catalyst for the thermal degradation of biomass (Fukuda, 2015), and higher contents of cellulose and lignin in this biomass waste as well, regarding its role in the char formation as discussed in section 5.6.3. and its wide range of temperature for the thermal decomposition, respectively (Sullivan and Ball, 2012).

Figure 8.

Normalized mass loss curves and their derivative data as a function of temperature from thermal decomposition of rice husk (RH), blend husk straw (B H-S) and straw (RS) samples in oxidative atmospheres at a heating rate of 5 °C/min.



3. Kinetic Modeling

After this stage, various reaction schemes were applied to determine a predictive model for thermal decomposition of biomasses to draw from the TGA results. First of all, TGA data are processed through the Savitzki-Golay smoothing method using Origin Pro© 8.0 software, suppressing the noise observed in the derivative data of mass loss as a function of time (in seconds) to improve the fitting among the theoretical models and the experimental data; worth notice the suppression of the baseline from the experimental results, according to the stated from the Laboratories of the School of Chemical Engineering of the University, giving the guarantee of the device calibration for the tests performance The smoothed values were, consequently, exported to Microsoft Excel, and new data were selected considering a time interval of 5 seconds. Finally, this new data list was ready to apply all reaction models studied in this work.

A normalized mass, w, will be used for standardized management of the experimental results, considering that all TG tests handle with a different value of initial mass. That was calculated through Equation (1), in which, m_i corresponds to actual mass and m_0 is the initial sample mass.

$$w = \frac{m_i}{m_0} \quad (1)$$

To determine the variation of w as a function of time, $\frac{dw}{dt}$, the Equation (2) is used, in which, $\frac{dm}{dt}$, is mass derivative as a function of time.

$$\frac{dw}{dt} = \frac{dm}{dt} * \left(\frac{1}{m_0}\right) \quad (2)$$

Besides, the biomass conversion, $\propto$, represents the amount of mass from the sample that is lost in the thermal degradation (Santos et al., 2020), which value is calculated using Equation (3), where, w_0, is the initial normalized mass, w_i, is the actual one and, w_f, is the last one.

$$\propto = \frac{w_0 - w_i}{w_0 - w_f} \quad (3)$$

Finally, the conversion rate, $\frac{d\propto}{dt}$, was calculated using Equation (4).

$$\frac{d \propto}{dt} = -\left(\frac{dw}{dt}\right) * \left(\frac{1}{w_0 - w_f}\right) \quad (4)$$

3.1. Global reaction mechanism

The *global reaction mechanism* is based on the assumption that the thermal decomposition process can be represented with a different reaction in a defined temperature range. In this model, the fitting is made using the conversion rate determined at same

conversion but different heating rates; for this study, three heating rates were tested, and three different tests were used to fit the model as well. A total of 19 conversion levels were then chosen in each test; starting at $\propto = 0.05$ and finishing in $\propto = 0.95$, to use fewer data and, thus, decrease the computation time.

The reaction rate, $\frac{d\propto}{dt}$, defined as a function of conversion, $\propto$, is shown in Equation (5). In this work, $f(\propto)$ is known as *conversion function* in reaction rate.

$$\left(\frac{d\propto}{dt}\right)_{theoretical} = k[f(\propto)] = A[f(\propto)]\left[exp\left(\frac{-E}{RT}\right)\right] \quad (5)$$

Kinetic constant, k, in Equation (5) is assumption according to Arrhenius (Logan, 1982), in which, E is the activation energy expressed in kJ/mol, A is the pre-exponential factor and, R is the universal constant of gases ($8.314\ \frac{\mathrm{J}}{\mathrm{mol}*\mathrm{K}}$).

For *Friedman method*, Equation (5) is used for the activation energy calculation through the linearization of the rate equation using natural logarithm (Friedman, 1964). The linear equation is shown in Equation (6), in which, $\left(\frac{d\propto}{dt}\right)$ is expressed as function of the inverse value of temperature, $\frac{1}{T}$ and, E, is determined from the value of the slope obtained, for all TG tests performed at the three heating rates.

$$ln\left(\frac{d\propto}{dt}\right) = \ln(A) + \ln\left(f(\propto)\right) - \left(\frac{E}{RT}\right) \quad (6)$$

$\ln\left(\frac{d\propto}{dt}\right)$ vs $\frac{1}{T}$ was plotted for each level of $\propto$ allowing obtaining 19 straight lines. For this study, the activation energy, E, was determined as the average of values obtained from all slopes of linear rate equations.

In *Vyazovkin method* (Vyazovkin and Wight, 1999), the activation energy is determined through the finding of a minimum value, $\emptyset$, presented in Equation (7), between the mathematical functions, *I*, obtained from Arrhenius equation and expressed as $I\left(E_{\propto}, T_{\propto,i}\right)$ which is calculated using expression (8), and β_j correspond to heating rate.

$$\emptyset = \sum_{i=1}^{n}\sum_{j\neq i}^{n}\frac{I\left(E_{\propto}, T_{\propto,i}\right)\beta_j}{I\left(E_{\propto}, T_{\propto,j}\right)\beta_i} \quad (7)$$

$$I\left(E_{\propto}, T_{\propto,i}\right) = \frac{E_{act_{\propto}}}{R} * \ p(x) \quad (8)$$

In Equation (8), $p(x)$ corresponds to 8th grade rational approach developed by Pérez-Maqueda and Criado (Pérez-Maqueda and Criado, 2000) as is shown in equation (9). X is calculated by expression (10).

$$p(x) = \left(\frac{e^{-x}}{x}\right)\left(\frac{x^7 + 70x^6 + 1886x^5 + 24920x^4 + 170136x^3 + 577584x^2 + 844560x + 357120}{x^8 + 72x^7 + 2024x^6 + 28560x^5 + 216720x^4 + 880320x^3 + 1794240x^2 + 1572480x + 403200}\right) \quad (9)$$

$$x = \left(\frac{E_{act_{\propto}}}{RT_{\propto}}\right) \quad (10)$$

For this study, regarding three heating rates used in TG analysis, the Equation for minimum value $\emptyset$ becomes the Equation (11), with six terms composing it.

$$\emptyset = \frac{I(E_\propto, T_{\propto,1})\beta_2}{I(E_\propto, T_{\propto,2})\beta_1} + \frac{I(E_\propto, T_{\propto,1})\beta_3}{I(E_\propto, T_{\propto,3})\beta_1} + \frac{I(E_\propto, T_{\propto,2})\beta_1}{I(E_\propto, T_{\propto,1})\beta_2} + \frac{I(E_\propto, T_{\propto,2})\beta_3}{I(E_\propto, T_{\propto,3})\beta_2} + \frac{I(E_\propto, T_{\propto,3})\beta_1}{I(E_\propto, T_{\propto,1})\beta_3} + \frac{I(E_\propto, T_{\propto,3})\beta_3}{I(E_\propto, T_{\propto,2})\beta_3} \quad (11)$$

Finally $\emptyset$, is calculated for the 19 levels of $\propto$, through an iterative process using the EES® V8.4 software. This is performed by the variation of the activation energy between [50 – 300] kJ/mol creating a parametric table, and then the lowest value of $\emptyset$ is found through Min/Max tool; the respective activation energy value is selected as well. The same energy value is kept as constant for all the three heating rates in each level.

Once the calculation of activation energy was performed through two methods described before, the values are compared using the standard deviation value, s (%), defined in Equation (12), in which, N is the number of data points taken as a sample, y_i are the reference values, μ is average value obtained from y_i and $y_{máx}$ belongs to the maximum value taken from the experimental data related to the assessed variable. The lowest value of the average deviation of both methods was chosen for the determination of conversion function, $f(\propto)$.

$$s\ (\%) = \frac{\sqrt{\frac{1}{N-1}\sum_{i=1}^{N}(y_i - \mu)^2}}{y_{máx}} * 100 \quad (12)$$

Next step in this mathematical procedure is the determination of the conversion function, which provide the best fitting result for the chemical process. This is selected by *Master Plots* chart through the comparison between the experimental TGA data and the

theoretical functions, selected from those proposed by Jankovic (Jankovic, 2008) which are shown in Appendix A. First of all, the heating rate, β, is introduced for the dynamic analysis of non-isothermal results obtained from TGA tests, and this can be expressed in terms of the conversion rate, $\left(\frac{d\propto}{dt}\right)$, according to (Kumar et al., 2020) and shown in expression (13); then, $f(\propto)$ is moved to the left term and the temperature differential is set to the right side to apply an integration, as exposed in equation (14) and defined as the function $g(\propto)$ as well. Regarding that this integer function presents a lack of analytical solution, it is replaced by the term $\left(\frac{E}{R}\right) * p(x)$ as shown in expression (15), in which, x is defined by equation (10), and the most stable activation energy value is chosen between Friedman and Vyazovkin methods values, according to Lopes, F. et al. (Lopes, F. et al., 2016). Now, as seen before, to find a solution for $p(x)$, Equation (9) is applied, as stated by Pérez-Maqueda and Criado (Pérez-Maqueda and Criado, 2000).

$$\frac{d\propto}{dT} = \left(\frac{A}{\beta}\right) f(\propto) exp\left(-\frac{E}{RT}\right) \tag{13}$$

$$\int_{\propto_0}^{\propto_f} \frac{d\propto}{f(\propto)} = \left(\frac{A}{\beta}\right) \int_0^{T_f} exp\left(-\frac{E}{RT}\right) dT = g(\propto) \tag{14}$$

$$g(\propto) = \frac{AE}{\beta R}\left[\frac{-e^x}{x} - \int_x^{\infty} \frac{e^{-x}}{x^2} dx\right] = \frac{AE}{\beta R} p(x) \tag{15}$$

Finally, *Master Plots* graphics are obtained by expression (16), in which, functions $g(\propto)$ and $p(x)$ are calculated respect to themselves, assessed in the middle point of conversion range, *i.e.*, $\propto = 0.5$. The theoretical functions were stated in a study performed by Jankovic (Jankovic, 2008) and shown in Appendix A. From their assessment with the

experimental data through visual comparison, three models were chosen for the final selection of the most accurate function using statistical criterion (see equation 12). This function is used further in the pre-exponential factor determination.

$$\frac{g(\propto)}{g(0.5)} = \frac{\frac{AE}{\beta R}p(x)}{\frac{AE}{\beta R}p(x_{0.5})} = \frac{p(x)}{p(x_{0.5})} \quad (16)$$

The procedure performed to find the frequency factor is initially using Equation (6) but moving $f(\propto)$ to the left side of the equation; it simplifies in one only logarithm, as shown in Equation (17). In this way, the left term is calculated as a function of the inverse of the temperature, $\frac{1}{T}$. The fitting model process uses experimental data of $f(\propto)$, E and $\frac{d\propto}{dt}$, previously obtained by TGA. Finally, the values of A and E are obtained from linear model expressed in Equation (17) using the 19 conversion levels as mentioned earlier. A higher value of R^2 gives the reliable of the model.

$$\text{Ln}\left[\frac{\frac{d\propto}{dt}}{f(\propto)}\right] = \ln A - \frac{E}{RT} \quad (17)$$

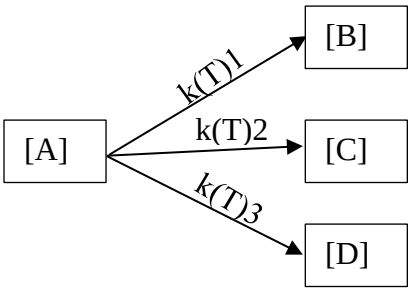
3.2. Independent parallel reactions model

The global reaction mechanism was presented before, in which only a global reaction is supposed to occur during the thermal decomposition process instead of considering all reactions present independently. The chemical mechanism of independent parallel reactions (Figure 9) recognizes a set of decomposition reactions where each one

belongs to a biomass structural component (hemicellulose, cellulose and lignin) and takes place as independent and concurrent (Lopes, F. et al., 2018).

Figure 9.

Independent Parallel Reaction Scheme development.



The mathematical model using this chemical reaction mechanism establishes that reactions take place at a temperature range between 125ºC and 700 °C; in this context, three independent reactions are taken into account in this study; each one of them involving one polymer composing of biomass.

As in the case of global reaction models, the kinetic constant was defined through the Arrhenius equation for each reaction (see Equation 18). To consider all reactions occurring during thermal decomposition of biomass, the total conversion rate, $\left(\frac{d\propto}{dt}\right)$ was defined as the sum of partial conversion rates associated to each independent reactions affected by the mass fraction of the respective component involved in the reaction, x_i, as is shown in Equation (19) where, m, is the maximum number of reactions to be used.

$$\left(\frac{d\propto}{dt}\right)_i = f(\propto)_i\, k(T)_i \tag{18}$$

$$\frac{d\propto}{dt} = \sum_{i=1}^{m} x_i \left(\frac{d\propto}{dt}\right)_i \tag{19}$$

The conversion function, $f(\propto)$, declared in Equation (18), was considered as an n-reaction order in this study, as listed in the research performed by Jankovic (Jankovic, 2008), and shown in Equation (20).

$$f(\propto) = (1-\propto)^n \tag{20}$$

Fourth order Runge – Kutta method (Press et al., 2007) was used to determine the value of α, by the integration of $\left(\frac{d\propto}{dt}\right)$ considering the chemical reaction of three main compounds of biomass (cellulose, hemicellulose and lignin). This method is shown in equations 21 to 25, where P is the value of the time step in seconds.

$$\propto_{n+1} = \propto_n + \left[\frac{P}{6} * \left(k_{1_n} + 2 * k_{2_n} + 2 * k_{3_n} + k_{4_n}\right)\right] \tag{21}$$

$$k_{1_n} = [A * e^{\frac{-E}{R*T_n}}](1-\propto_n)^m \tag{22}$$

$$k_{2_n} = A * e^{\frac{-E}{R*\left(\frac{T_n+T_{n+1}}{2}\right)}} * \left[1 - \left(\propto_n + \frac{k_{1_n}}{2}\right)\right]^m \tag{23}$$

$$k_{3_n} = A * e^{\frac{-E}{R*\left(\frac{T_n+T_{n+1}}{2}\right)}} * \left[1 - \left(\propto_n + \frac{k_{2_n}}{2}\right)\right]^m \tag{24}$$

$$k_{4_n} = A * e^{\frac{-E}{R*T_{n+1}}} * \left[1 - \left(\propto_n + k_{3_n}\right)\right]^m \tag{25}$$

Solver of Microsoft® Excel® 16.0 was used because it allows to manage several variables and equations, and it performs iterative processes to fit results with the experimental data, in this case by the setting of the average deviation (see Equation 12) as the objective to minimize. For this scheme performance, intervals for activation energy, pre-exponential factor, fractions and conversion function degrees were established. These ranges are shown in Table 5, which are taken from previous research performed for sugarcane straw (Rueda-Ordóñez et al., 2015).

Table 5.

Ranges for values of Arrhenius equation in parallel reaction scheme taken from previous studies.

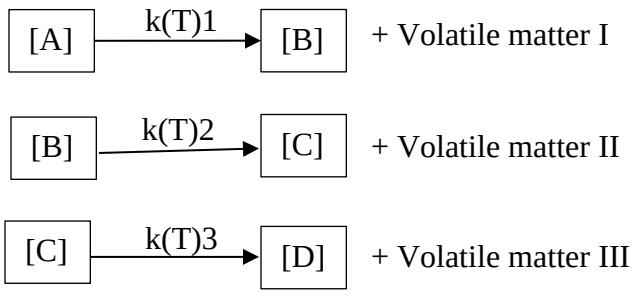
Biomass component	**Hemicellulose**	**Cellulose**	**Lignin**
Activation Energy [kJ/mol]	100 – 150	180 - 220	10 – 100
Pre-exponential factor [s^{-1}]	10^{6} - 10^{18}	10^{10} - 10^{20}	1 – 10^{5}
Mass fraction	0.2 – 0.35	0.35 – 0.55	0.15 – 0.35

3.3. Consecutive reactions model

This chemical reaction mechanism consists in supposing that more than one reaction occurs in chain, consequently, as seen in Figure 10. In this case, the thermal decomposition of only the main components of biomass (cellulose, hemicellulose and lignin) are considered as occurring in parallel.

Figure 10.

Consecutive reaction scheme development.



In contrast to other models, the reaction rate described using this mechanism must be written using the mass concentration as an independent variable instead of the mass conversion. As in both mechanisms mentioned above, the kinetic constant was defined with the Arrhenius equation for each reaction (see Equation 18). The temperature interval of 150 - 700 °C is defined for the scheme compilation and the fourth-order method of Runge - Kutta is also performed for the integration of $\left(\frac{d\propto}{dt}\right)$; Microsoft® Excel® 16.0 Solver Add-in is used as well. About this point, the ranges of values for activation energy, frequency factor and component fraction shown in Table 5 were also used. The utilization of same range allows comparing the behavior of a component reacting in both parallel and consecutive reaction mechanisms. Component fraction refers to a value of normalized mass in which the corresponding reaction starts.

For statistical assessment, to reach the highest accuracy, the standard deviation value, s (%), was used and showed in Equation (26), in which, N is the number of data points taken as a sample, y_i are the reference values and $y_{máx}$ belongs to the maximum value of the variable, from the experimental (*exper*) and theoretical (*theo*) data.

$$s\,(\%) = \frac{\sqrt{\frac{1}{N}\sum_{i=1}^{N}\left(y_{i_{theo}} - y_{i_{exper}}\right)^2}}{y_{máx_{exper}}} * 100 \quad (26)$$

3.4. Results – performance of models from experimental results

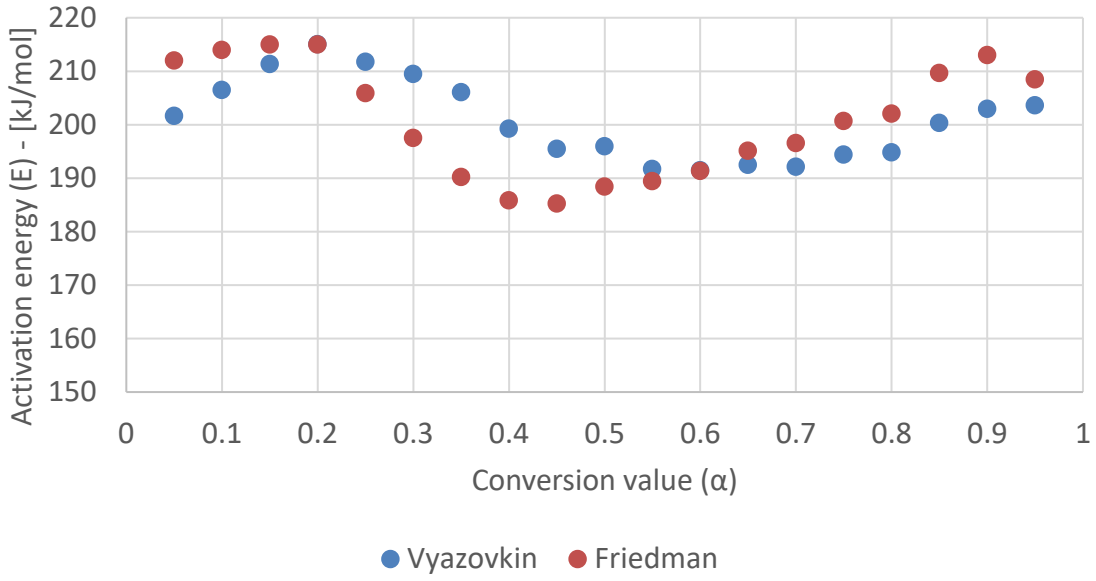
3.4.1. Global reaction model – inert atmosphere.

First of all, activation energy was calculated and selected from both methods shown in section 4.1. This value indicates the minimum energy required for the start of the thermal decomposition of a material; it can be interpreted as a barrier imposed by physical and chemical features, which needs to be overcome for the reactions to take place (Santos et al., 2020). As seen in Figure 11, higher activation energy and lower dispersion of data from the average value is achieved using the Vyazovkin method for all biomass samples. In this method the 8th grade rational approach stated by Perez-Maqueda and Criado (Pérez-Maqueda and Criado, 2000) is used as well. The dispersion mentioned before obeys to the fact of modeling an entire decomposition zone with one reaction. This follows the concept of the Arrhenius equation which was adapted for studying the kinetic behavior of gases in a one-step global reaction (Rueda-Ordóñez and Tannous, 2015). On the other hand, thermal degradation could comprise multiple components, highlighting the cellulose, hemicellulose and lignin decompositions (Kumar et al., 2020); other authors also confirms this trend in biomass kinetics analysis, conferring this behavior to the complex multistep mechanism (Mishra and Bhaskar, 2014). As a contrast with studies for other biomass samples (Lopes, F. et al., 2018; Laougé and Merdun, 2020; Mishra and Bhaskar, 2014; Singh and Sawarkar,

2020), the reactions of structural components from the rice husk and straw samples were modeled with higher activation energies in similar temperature zones. Therefore, their reaction mechanisms are slower or a higher energy input is required to take place.

Figure 11.

Comparison between Friedman and Vyazovkin methods results – Blend husk-straw sample.



Now, the conversion functions are compared with the experimental results to choose the most accurate of them, as seen in Figure 12. Five models from the stablished functions group shown in Appendix A and proposed by Jankovic (Jankovic, 2008) were selected and exposed in Table 6. Besides, these functions were also used in studies involving reactions mechanism functions as well (Kumar et al., 2020; Santos et al., 2020; Rueda-Ordóñez and Tannous, 2015; Mishra and Bhaskar, 2014; Saffe et al., 2019; Reshad et al., 2016; Singh and Sawarkar, 2020) and also based in the remarks from the International Confederation of Thermal Analysis and Calorimetry (ICTAC) (Vyazovkin et al., 2011).

For all biomass samples, D3 function was chosen because it was the closest with TG data results.

Table 6.

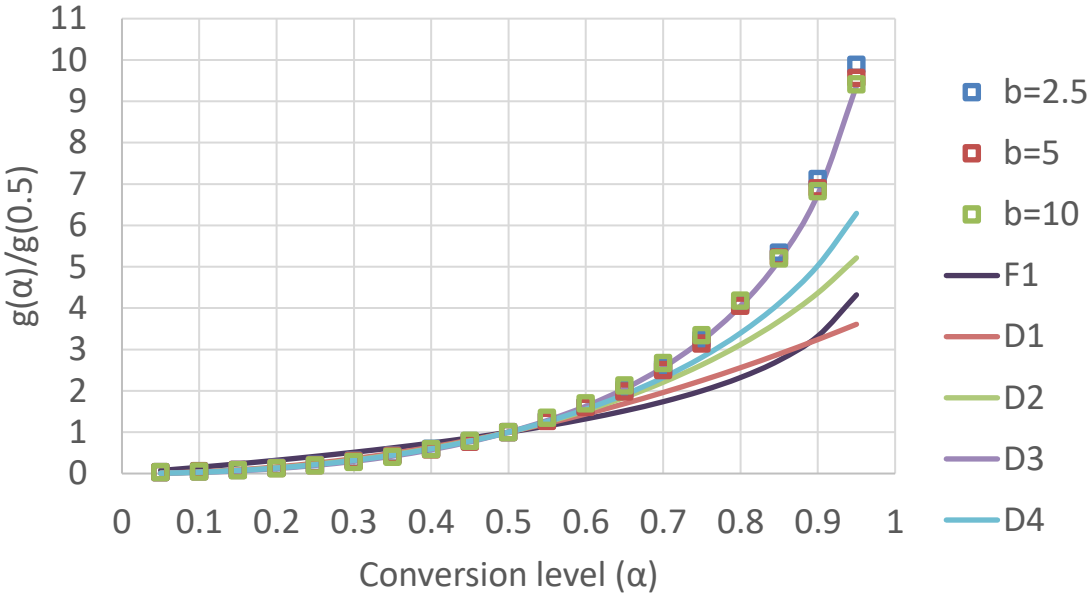
Reaction functions mostly used in previous works in their general and integral form, expressed as a function of α.

Code	Reaction model	f(α)	g(α)
D1	One-dimensional diffusion	$1/(2\alpha)$	α^2
D2	Two-dimensional diffusion: Valensi equation	$[-\ln(1-\alpha)]^{-1}$	$(1-\alpha)\ln(1-\alpha)+\alpha$
D3	Three-dimensional diffusion: Jander equation	$(3/2)(1-\alpha)^{2/3}[1-(1-\alpha)^{1/3}]^{-1}$	$[1-(1-\alpha)^{1/3}]^2$
D4	Three-dimensional diffusion: Ginstling-Brounshtein	$(3/2)[(1-\alpha)^{-1/3}-1]^{-1}$	$\left(1-(2\alpha/3)\right)-(1-\alpha)^{2/3}$
F1-R1	First-order (Mampel)	$(1-\alpha)$	$-ln(1-\alpha)$

This function was proposed by W. Jander in 1927 as the diffusion-controlled core-shell model. This model arises from the supposition that the particles of solid reactants had a sphere shape (3D dimension). Moreover, the reaction product increase rate was assumed to be inversely proportional to the particle size, following a parabolic law (Luo et al., 2010). Considering previous researches for biomass samples which performed this step as well, evidence of use of conversion functions related to dimensional diffusion -D1, D2, D3 and D4- were selected at least in a short interval, performing an Invariant Kinetic Parameter (IKP) method (Reshad et al., 2016), carrying out the Z(α) master plots function (Kumar et al., 2020; Santos et al., 2020; Mishra and Bhaskar, 2014). and using the same *master plots* method in this study (Rueda-Ordóñez and Tannous, 2015).

Figure 12.

Master plots for the blend husk-straw sample.

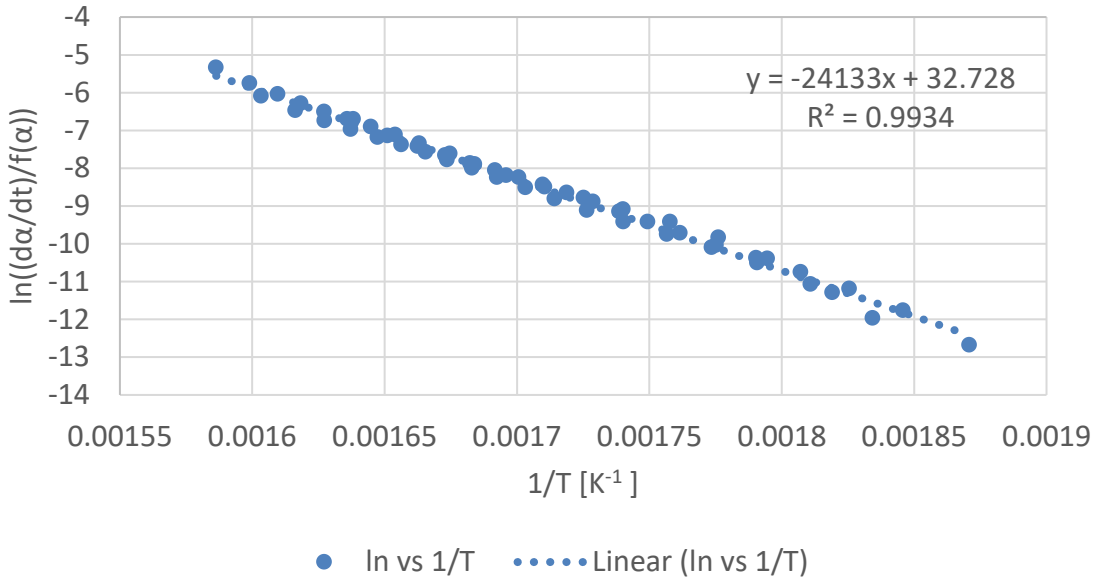


Finally, for the preexponential factor determination, results are plotted in Figure 13. Moreover, the equation obtained from the straight line found from this plot can be extracted, which is written down in expression (27) for the blend husk-straw sample as an example. From this expression, the activation energy is set again, for an accurate adjustment in the model validation, and final coefficients got through this method are displayed in Table 7.

$$ln\left(\frac{\frac{d\alpha}{dt}}{f(\alpha)}\right) = -24133 * \left(\frac{1}{T}\right) + 32.728 \quad (27)$$

Figure 13.

Results of the method for pre-exponential factor determination for blend husk-straw sample with the linear regression equation and the fitting coefficient (R^2).



As stated by Laougé and Merdun (Laougé and Merdun, 2020), this factor describe the reaction chemistry which is essential for the optimization in thermochemical conversion techniques performance using biomass. If the value of A remains high is an indicator of high molecular collision which requires an increase in the transferred heat, and thereby, an increase in E is necessary. In addition, it indicates the presence of loose junctional complex (Singh and Sawarkar, 2020); in Figure 19 and as exposed in section 4.5., a direct proportion relation between the pre-exponential factor and the activation energy is evidenced, including the data obtained in this isoconversional solution method for all samples. On the other hand, a low A value (regarding a limit below 10^9 s^{-1}) exposes that there is a restriction in the particle rotation of the activated complex contrasted with the initial reagent, meaning a large surface reaction (Laougé and Merdun, 2020); if this

reaction is not present under these conditions, it shows the tight junctional complex or closed complex (Singh and Sawarkar, 2020); furthermore, it also indicates the use of a porous material, which decompose with ease in an inert atmosphere (Santos et al., 2020).

Table 7.

Obtained data for parameters and deviation with experimental results in the isoconversional reaction scheme for rice husk (RH), rice straw (RS) and blend husk-straw (B H-S) samples.

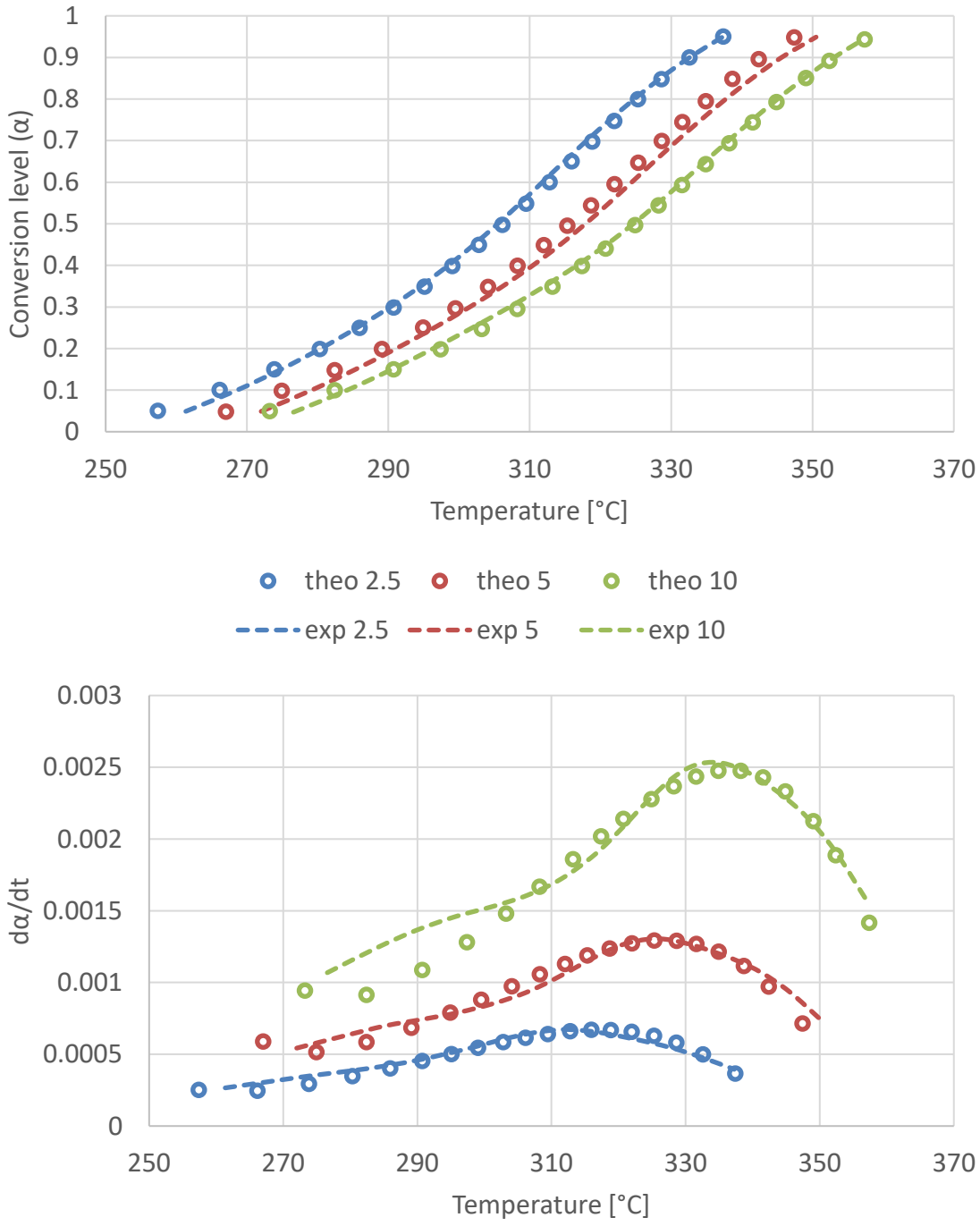
Biomass sample	Activation energy	Pre-exponential factor	Conversion function	Average Deviation
Symbol [units]	E [kJ/mol]	A	f(α)	AD [%]
RH	213.47	2.52×10^{15}	D3	7.00
B H-S	200.64	1.64×10^{14}	D3	4.70
RS	205.55	9.28×10^{14}	D3	6.61

As a comparison between the biomass samples in order to observe the effect of the addition of straw in the husk sample, it decreases the energy required for the material to degrade in an inert atmosphere and the collision between molecules in the material decrease, even though these values were slightly different among them. However, these values remains over the amounts found in the literature, as evidenced with the activation energy values below 160 kJ/mol (Lopes, F. et al., 2018; Laougé and Merdun, 2020; Mishra and Bhaskar, 2014; Singh and Sawarkar, 2020) and A magnitudes under 10^{10} s^{-1} (Saffe et al., 2019; Rueda-Ordóñez and Tannous, 2015). This demonstrated that in this temperature zone, a possible decomposition of cellulose is occurring, taking into account the values intervals stated for these coefficients and shown in Table 5 in section 4.2. related to the parallel reaction scheme discussion. Finally, analyzing the average deviation percentage for the biomass samples in this study, for the blend husk straw this value was found below 5%, which shows a proper fitting to the experimental values, despites the amount calculated

for the husk and straw samples reached a higher deviation. With a multiple reaction model performance such as parallel or consecutive reactions models in these biomasses a reduced deviation can be obtained, following the fact that multiple components are reacting at the same time, stated in previous biomass researches (Kumar et al., 2020; Grigiante et al., 2017). In addition, a higher deviation is found in this study for conversion values below 0.3, as seen in Figure 14.

Figure 14.

Comparison between experimental data and results from global reaction model performance for the blend husk-straw sample in terms of conversion level (upper plot) and its derivative as a function of time (downer plot).



3.4.2. Parallel reaction scheme – inert atmosphere.

In this scheme for a non-reactive environment, three reactions were selected as seen in Figure 15, which are considered for the three major structural components in biomass, which are hemicellulose, cellulose and lignin, taking into account the references found for similar studies for other biomass samples such as pine needle, bark and branch and shallow soil (Zhu and Liu, 2020), olive tree pruning and vine shoots (Sfakiotakis and Vamvuka, 2015), tobacco stem (Wang et al., 2019), empty fruit bunch and kernel shell (Rueda-Ordóñez et al., 2019) and beech and pine wood samples (Anca-Couce et al., 2014). This last work also contains a classification for the activation energy value according to each structural component regarding previous works, showing a probable range for hemicellulose among 75 and 220 KJ/mol, for cellulose between 180 and 250 KJ/mol and for lignin content from 20 to 200 KJ/mol. The model for each biomass sample in this study was compiled at certain ranges for all the parameters, shown in Table 5, for curves adjusting purposes from experimental data.

Results obtained in this reaction model are displayed in Table 8. A trend with a parabolic shape and positive direction is detailed for the third reaction from the rice straw content in the sample, whilst for the second reaction a direct influence is observed at high levels of the straw content in blend with an absence of any effect for low values of straw mass percentage; finally, values for this parameter in the third reactions shows an inverse effect from the straw content at low values of this factor, with a null influence for high

levels of this biomass content over the value of the discussed parameter. However, the difference between these values for all reactions is less than 5 kJ/mol, exposing a small magnitude in these effects. Comparing with the reference data, the highest values of activation energy were found for the second reaction and the lowest energies belonged to the third reaction of this model (Gyul'maliev et al., 2012; Santos et al., 2012; Sfakiotakis and Vamvuka, 2015), which agreed with the trend managed from the intervals defined for the iterative process, and found in the kinetic modeling performance in this study as well.

Table 8.

Obtained data from the iterations performed in independent parallel reaction scheme on inert atmosphere.

Biomass sample	Reaction Name	Reaction fraction	Activation energy	Pre-exponential factor	Average Deviation
Symbol [units]	Rn	Xn	E [kJ/mol]	lnA	AD [%]
RH	R1	0.29	101.02	$0.0886\beta+15.224$	2.75
	R2	0.35	180	$0.0029\beta^2-0.024\beta+30.346$	
	R3	0.35	66.69	$0.1486\beta+3.179$	
B H-S	R1	0.27	100	$0.0977\beta+14.96$	1.95
	R2	0.37	180.00	$0.0092\beta^2-0.097\beta+30.552$	
	R3	0.35	65.05	$0.1515\beta+5.0887$	
RS	R1	0.24	100	$0.1127\beta+15.656$	2.25
	R2	0.40	184.47	$0.0249\beta+31.985$	
	R3	0.35	69.44	$0.1634\beta+5.8636$	

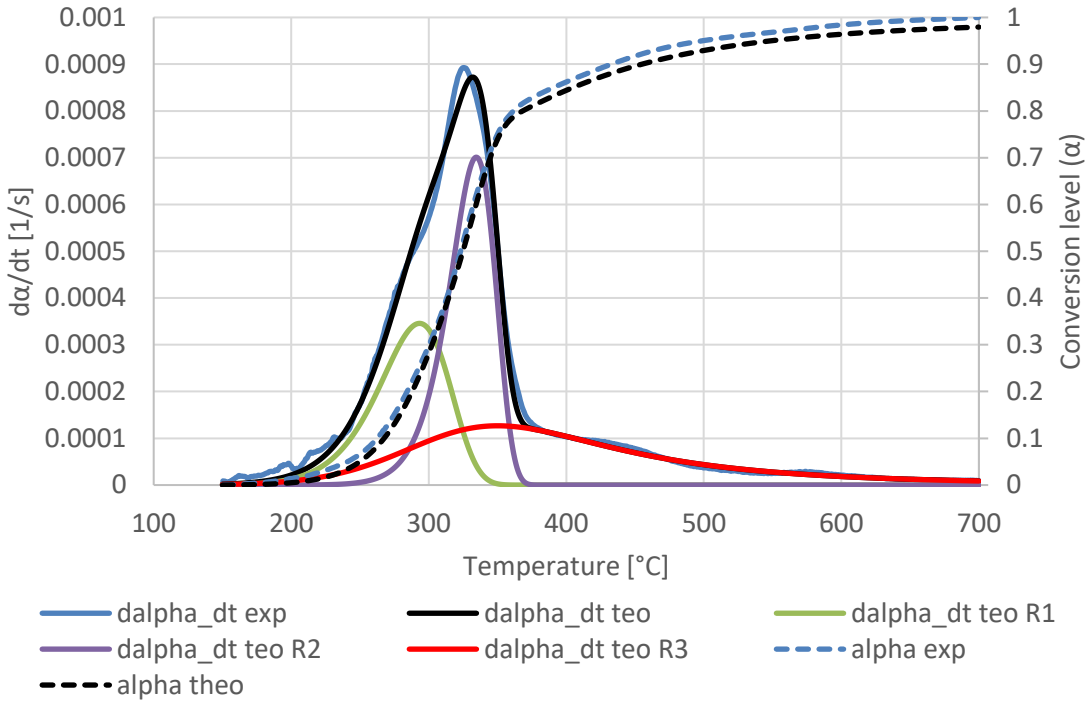
Now, for the pre-exponential factor determination in these schemes, regarding its magnitude as its natural logarithm (lnA) for a simpler appreciation, a negligible effect from the rice straw content in blend is detected for the hemicellulose content and for the cellulose reaction at low values of straw mass percentage. Furthermore, a direct influence from this factor is detected for the lignin content and for the cellulose reaction at high levels of rice straw content in the sample. Notice the use of the first-order reaction mechanism (F1-R1) as the conversion function in this scheme for the hemicellulose and cellulose contents and

the reaction mechanism with and n^{th} order (Fn) for the lignin content in the sample, remaining n=3 for all heating rates and biomass samples. This is consistent with previous works for various biomass samples (Sfakiotakis and Vamvuka, 2015; Santos et al., 2012) stating in this last research that the pyrolysis of lignin cannot be compiled with this scheme by first-order-kinetics, and showing that previous studies reported an improved description by the third-order reaction kinetics. The work performed by Anca-Counce et al. (Anca-Couce et al., 2014) managed the same reaction orders for hemicellulose and cellulose reactions, although for the lignin mechanisms this was set as first-order reactions. However, some other researchs set these reaction as free for iterative purposes (Wang et al., 2019; Zhu and Liu, 2020; Gyul'maliev et al., 2012).

The composition fractions obtained in this reaction model shows an influence of direct nature from the straw content in the sample for the cellulose content and an inverse effect over the reaction fraction regarded for the hemicellulose. Besides, an absence of change is exposed for the lignin content despites the variation of the straw percentage in blend. These fractions were close to those determined in previous studies of structural composition of rice husk and straw, which are shown in Table 4 and belongs to section 3.5.3. excluding the lignin content in both biomass materials which reached higher values than the references data and the hemicellulose content in the straw sample, with lower results than those observed in the literature.

Figure 15.

Parallel reaction scheme application to blend husk-straw mass conversion and its comparison with experimental results, β = 5 [°C/min], N_2 atmosphere, dα/dt variable is named as dalpha_dt.



At this point, average values of the mass fractions for each component, x_n, and their activation energies, E, were calculated. Then, the iterative process performed for the calculation of the Arrhenius parameters using the Solver add-in from the Microsoft® Excel® 16.0 software was carried out again, but setting the average values of E, and x_n, as fixed and the pre-exponential factor values as free for their further calculations, by the minimization of the average deviation, AD. Finally, a correlation for pre-exponential factor was stablished as a function of the heating rate in order to observe if there is a trend among these variables, as exposed in Table 8 as well and choosing a R^2 value above 0.95 as a criterion for a proper selection; this step is performed also in the parallel reaction model in oxidative atmosphere, and in the consecutive reaction models for both inert and oxidative

environments. For the hemicellulose an lignin components, these regressions presented a linear shape, whilst for the cellulose reaction mechanisms for rice husk and blend samples, it was necessary to apply a 2nd order polynomial regression in order to achieve the proposed fitting with experimental values. In previous works this step was carried out as well (Rueda-Ordóñez et al., 2019; Sfakiotakis and Vamvuka, 2015).

Finally, the average deviation percentage is calculated since the conversion derivative, ($d\alpha/dt$), with a value lower than 3 % for all samples, reaching the lowest value in the blend husk-straw sample. Notice that for the rice husk sample the highest average deviation percentage was obtained; this can be also observed in the plot contrasting this data with the experimental results for this biomass sample, where a wide difference at the beginning and at the end of the char formation zone is detected. In Figure 15 the curve for the theoretical value of α shows that at 700 °C it reaches a value below 1; thereby, the set of reactions finish at a higher temperature than that set in the upper limit of the kinetic model performance.

In this particular material, a component reacting above 370 °C can be added in order to improve the model fitting with the experimental values, which could have the same features as the lignin component or as a carbonaceous component (Zhu and Liu, 2020; Xu et al., 2019). From the previous studies mentioned before in this section, all of them reached an average deviation percentage lower than 5 %. As a contrast with the isoconversional reaction model, this fits better with experimental results due to the stablishment of multiple

components (Saffe et al., 2019) in the biomass materials reacting in any temperature zone without restriction.

3.4.3. Consecutive reaction scheme – inert atmosphere.

This model, different from the independent parallel reactions, considers each component as a product of the thermal decomposition of a previous compound in inert environment and so on, as shown in Figure 16. Studies performed for sugarcane straw (Rueda-Ordóñez and Tannous, 2018) and empty fruit bunch and kernel shell (Rueda-Ordóñez et al., 2019), used also three reaction mechanisms for modeling thermal decomposition in this environment.

Table 9.

Obtained data of coefficients from the iteration process and its deviation value in consecutive reaction scheme performance for all samples on inert atmosphere.

Biomass sample	Reaction Name	Reaction Start point	Activation energy	Pre-exponential factor	W Average Deviation	Average Deviation
Symbol [units]	Rn	Xn	E [kJ/mol]	lnA	W AD [%]	AD [%]
RH	[A]	1	103.10	0.0793β+15.795	1.19	1.97
	[B]	0.77	160	0.0225β+26.292		
	[C]	0.51	45.83	0.0659β-0.1971		
	[D]	0.17	-	-		
B H-S	[A]	1	100	0.0957β+15.292	0.39	1.61
	[B]	0.78	160	$0.0076\beta^2$-0.0621β+26.632		
	[C]	0.48	44.57	0.1333β+0.9274		
	[D]	0.28	-	-		
RS	[A]	1	100	0.0982β+15.967	0.92	1.93
	[B]	0.80	167.30	0.0333β+28.709		
	[C]	0.50	33.81	$0.0192\beta^2$-0.144β+0.2401		
	[D]	0.25	-	-		

Although four components are plotted in this model, this is based in three reaction mechanisms comprising the thermal decomposition stages of biomass samples, related to low-temperature volatile release, high-temperature volatile release and carbonization (Rueda-Ordóñez et al., 2019). Moreover, as evidenced in a previous research, the activation energies of the three reactions are similar in their values magnitude to those obtained for the structural components of the biomass (hemicellulose, cellulose and lignin) (Rueda-Ordóñez and Tannous, 2018). Values for all the coefficients of these mechanisms were displayed in Table 9. Considering now the effect produced by the content of rice straw in the blend over the activation energy for each component, a direct influence with a small magnitude is detected for the second reaction at high values of the straw content, attached to a null influence at low levels of this biomass sample. In the other hand, an inverse effect for the first and third reactions is exposed, including an absence of influence for this first reaction at high values of straw content in blend, with a larger magnitude for the third reaction rather than the first one. Some studies had been carried out using two reaction mechanisms for the kinetic modeling with this scheme, following the method stated by (Guo and Lua, 2001), which regards that all cellulosic components of this raw material decompose in two steps, degradating in the first one to intermediates material and after this to the final solid char and volatile matter (Weerachanchai et al., 2010) and after this work several studies were carried out, even though the isoconversional and independent parallel reactions have been developed more frequently. Despite this, analysis for biomass samples such as cassava pulp (Weerachanchai et al., 2010) and oil palm shell, fiber and kernel (Luangkiattikhun et al., 2007) were carried out using also two reaction mechanisms.

Furthermore, previous researches using three reaction mechanism have been performed for sugarcane bagasse and straw (Santos et al., 2012; Rueda-Ordóñez andTannous, 2018).

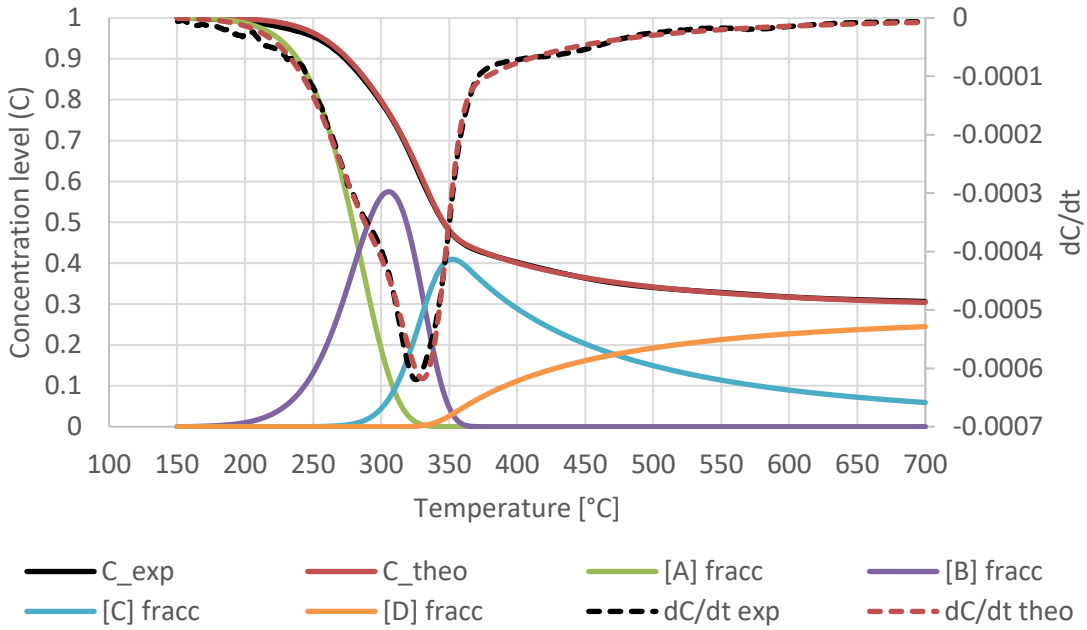
Now, the pre-exponential factor (in units of frequency: s^{-1}) shows a parabolic-shaped trend in a positive direction for the first reaction and in a negative direction for the third reaction; besides, in the second reaction a direct effect is observed, being this wider at high levels of rice straw content in blend. As seen in previous works for biomass samples using this model with two mechanisms (Weerachanchai et al., 2010; Luangkiattikhun et al., 2007), values from this parameter for the second reaction were registered as higher than those belonging to the first reaction. Moreover, studies that involve three reaction mechanisms (Santos et al., 2012; Rueda-Ordóñez and Tannous, 2018) registered the highest values in the second reaction and the lowest for the third mechanism, which is the same trend observed in the present research. A relation between values of activation energy and pre-exponential factor is detected and will be shown in Figure 20 and Figure 21 and discussed in section 4.5.

In all the biomass samples and in the two first mechanisms, the conversion function carried out was set as first-order (n=1), whilst for the third mechanism was set a conversion function of third order (n=3). This is consistent with the research developed by Santos et al. (Santos et al., 2012) and in the study performed by Rueda-Ordóñez and Tannous (Rueda-Ordóñez andTannous, 2018), where conversion functions used were of first-order nature for all the reaction mechanisms. For the two-step consecutive reactions models, this

parameter was set as free for an iteration performance (Luangkiattikhun et al., 2007; Weerachanchai et al., 2010). Further, discussing about the start point for each component reaction, excluding the first component which point was set as one in all biomass samples, a direct influence is revealed in the second component from the rice straw content in the sample; in addition, parabolic trends from the same factor are observed, with a positive direction for the third component and with a negative sense for the last one.

Figure 16.

Consecutive reactions scheme performance and a contrast with experimental values, to blend husk-straw sample, β = 5 [°C/min], N_2 atmosphere.



Using the same step performed in the independent parallel reactions scheme, the value of the preexponential factor was defined as a function of the heating rate β, in order to observe a possible trend among them, setting the frequency factor to a natural logarithm

scale (lnA). Thus, all these coefficients had a linear trend with a positive slope, regarding the coefficient R^2 higher than 0.95 as a value for fitting checking for its acceptance, as shown in Table 9, excluding the second mechanism in the blend sample and the third reaction in the straw material. Therefore, a 2^{nd} order polynomial shape was used in order to predict these trends for the last mechanisms mentioned. According to Rueda-Ordóñez et al. (Rueda-Ordóñez et al., 2019), this assumption is based in several studies that reported this frequency factor as a fitting parameter in solid state kinetics, and it has a lack of valid physical meaning.

Finally, in order to assess the general fitting of the theoretical values obtained with the experimental results achieved in this study, the average deviation percentages, s (%), for the conversion derivative and the concentration value were calculated, finding deviations below 2 % for the first parameter and below 1.2 % for the second criteria. This shows that this scheme achieved a higher fitting than the isoconversional reaction and the independent parallel reaction models in terms of the conversion derivative deviation. From the studies with the two-step consecutive reactions models (Weerachanchai et al., 2010; Luangkiattikhun et al., 2007), deviations over 5% were registered. In the other hand, in the works with three reaction mechanisms, this percentage was determined below 3 % (Santos et al., 2012; Rueda-Ordóñez and Tannous, 2018). This demonstrates that the addition of the third mechanism improves the curve fitting with the experimental values.

3.4.4. Parallel reaction scheme – oxidative atmosphere

In an oxidative atmosphere both volatile matter and fixed carbon content react with the oxygen content in the air. Thus, six reactions were considered remaining three main structural components of biomass (hemicellulose, cellulose and lignin) but separating each one into the volatile matter and carbonaceous material fractions. Thereby, reaction R1 and R4 belong to volatile matter and carbonaceous material of hemicellulose, R2 and R5 for cellulose, and R3 and R6 for lignin, respectively. As seen in Figure 17 and according to Lopes, F. et al. (Lopes, F. et al., 2018) the decomposition of the lignin content does not stand out in a specific temperature range as the other components. This has a very complex chemical composition, and it is present in a wide temperature range (Valente et al., 2015). Besides, in the study performed by Ding et al. (Ding et al., 2019) the main structural components were separated according to its reactivity with inert and oxidative atmospheres. However, the shuffled complex evolution method was carried out.

It worth noticing that the iteration intervals for each variable were equal for both reactions of volatile matter and char in each structural component (see Table 5) and results obtained in the performance of this reaction model are shown for all biomass samples in Table 10. In the case of the activation energy, lower values for the solid char reactions were detected for the reactions of the first and fourth components (R1 and R4) and an inverse influence from the straw content in the blend is exposed. For reactions related to cellulose content decomposition (R2, R5), an absence of effect from the straw content is observed,

regardless of the volatile matter or solid char belonging as well. Finally, in the case of reactions involving lignin content thermal conversion (R3, R6) a direct effect is made by the straw content in the sample, and higher values were evidenced for the solid char reactions as well. In a previous study (Lopes, F. et al., 2018) six-component were regarded in the oxidative atmosphere as well; also, values of activation energy obtained for the volatile matter reactions were higher than those for the solid char. From an analysis for beech wood (Ding et al., 2019) the lignin fraction energy was higher than the obtained in the present model.

Table 10.

Obtained results for coefficients values and the deviation with experimental data from parallel reaction scheme for all samples in oxidative atmosphere.

Biomass sample	Reaction Name	Reaction fraction	Activation energy	Pre-exponential factor	Function order	Average Deviation
Symbol [units]	Rn	Xn	E [kJ/mol]	lnA	n	AD [%]
RH	R1	0.21	149.70	0.0341β+26.366	1	3.09
	R2	0.16	180.00	0.0357β+31.252	1	
	R3	0.14	72.71	0.0931β+7.7044	3	
	R4	0.09	149.77	$0.0084\beta^2$-0.0993β+27.85	1	
	R5	0.19	180.00	$0.0062\beta^2$-0.0867β+25.95	1	
	R6	0.21	75.55	0.0919β+8.2634	3	
B H-S	R1	0.27	139.36	0.0682β+24.507	1	3.33
	R2	0.20	180.00	0.0661β+31.437	1	
	R3	0.14	79.73	0.0881β+8.9806	3	
	R4	0.03	126.68	0.0918β+23.065	1	
	R5	0.15	180.00	$0.0156\beta^2$-0.1926β+26.24	1	
	R6	0.21	84.37	0.0862β+9.887	3	
RS	R1	0.27	136.59	0.0679β+24.258	1	3.48
	R2	0.22	180.00	0.047β+31.971	1	
	R3	0.14	85.56	0.0716β+10.328	3	
	R4	0.03	116.14	0.1092β+21.244	1	
	R5	0.13	180.00	-0.0925β+27.154	1	
	R6	0.21	88.50	0.0571β+10.958	3	

The values of the pre-exponential factor were handled in this study with their natural logarithm magnitudes for a proper scale appreciation. The effect from the straw

content over this parameter is direct for the lignin and cellulose reactions and inverse for the hemicellulose reactions. Moreover, values for reactions of volatile matter were higher than those comprising solid char fractions for the hemicellulose (excluding the rice husk model) and cellulose. This is the opposite for lignin reactions where the values for solid char reactions were higher. According to a previous kinetic model analysis (Lopes, F. et al., 2018), higher values of lnA for the devolatilization reactions in the structural components were found with a wide difference from the results in this study (near 50%). Moreover, in a study carried out for grape marc biomasses (Valente et al., 2015), values for the hemicellulose content were higher than the other two structural components. In addition, those amounts from the cellulose reactions were located inside the interval formed by the values of the lignin content reactions. Finally, the char reaction here established (combustion) reached values even higher than those for the hemicellulose and cellulose contents, similar to the situation found in the study for beech wood samples and performed by Ding et al. (Ding et al., 2019).

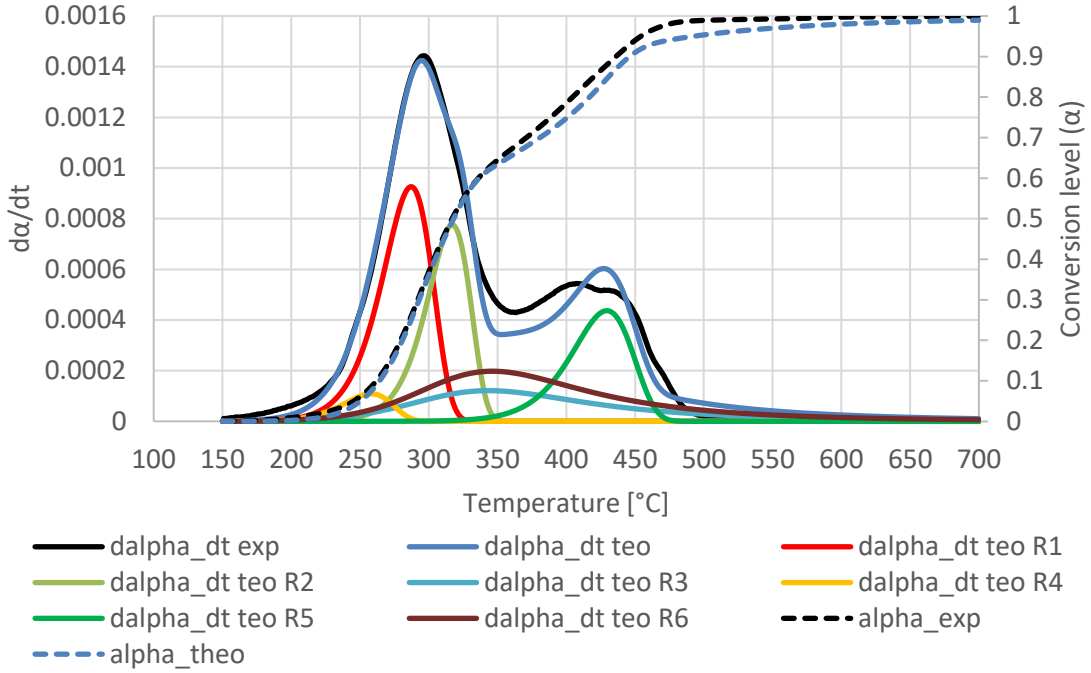
For this scheme performance, conversion functions of first order for hemicellulose and cellulose thermal degradation mechanisms were established for both solid char and volatile matter decomposition reactions. In contrast, third-order functions were applied for the decomposition mechanism of lignin for both volatile matter and solid char fractions. Regarding previous research with fourth components for pine waste samples (Zhu and Liu, 2020) in the reactions for the main structural components these orders were set as free, obtaining values between 1 and 3, adding that for the char reaction this order was near to

one. Moreover, in the study carried out by Lopes, F. et al. for guarana seed residue samples (Lopes, F. et al., 2018), all components regarded in the model had first-order reactions involved.

Then, for the fractions of these reactions obtained in this study for the consecutive reactions scheme, the rice straw content in blend applied a direct influence in R2 and R1 reactions, being this influence absent for this last reaction at high values of straw in the sample; for both lignin reactions a null effect from the rice straw mass percentage is detected, and finally, this influence is identified as the inverse for R4 and R5, with an absence of this trend in the straw for the hemicellulose reaction. Furthermore, fractions for volatile matter contents were higher than those from the solid char in the hemicellulose and cellulose reactions (excluding those from the last component in the rice husk sample) and were lower for the lignin content reactions. According to the study performed by Lopes, F. et al. (Lopes, F. et al., 2018) using the same amount of reactions from this study, the hemicellulose and lignin contents reactions show higher fractions in the devolatilization mechanisms rather than those for the solid char, being this trend opposite to the observed for the cellulose content reactions. Besides, in a research where four components were regarded (Zhu and Liu, 2020) higher fractions for hemicellulose and cellulose contents were determined, instead of the other two components.

Figure 17.

Curves of normalized mass and its derivative, from the performance of independent parallel reaction model for the blend husk-straw sample and a contrast with experimental data, β = 10 °C/min, synthetic air atmosphere.



Following the step performed in the schemes for the inert atmosphere, the preexponential factor in its natural logarithm magnitude was expressed also as a function of the heating rate to observe a possible trend, finding a linear behavior with a positive slope in almost all component reactions, excluding R4 and R5 for rice husk sample and R4 for the blend material due to the use of a 2nd order polynomial equation for the regression, and a linear trend with negative slope achieved in R5 for the straw sample. R^2 coefficient above 0.95 was stated to select a proper linear pattern for each component reaction. Finally, for the fitting assessment of this scheme with experimental results the average deviation percentage was used, obtaining average values between 3% and 3.5%, increasing this variable with the addition of straw in the blend. According to the curves detailed in Figure

17, the main deviation is evidenced in the char oxidation zone, obeying to the peak missing in this decomposition stage for the straw sample (see Figure 8). After consulting previous works, an average deviation percentage lower 3 % was achieved in them (Zhu and Liu, 2020; Lopes, F. et al., 2018) and another study achieved an R^2 value up to 0.94 (Ding et al., 2019).

3.4.5. Consecutive reaction scheme – oxidative atmosphere.

The same number of reactions used in the inert atmosphere were used for comparing its results with parallel reactions model in this medium, and with the consecutive reaction model in the oxidative atmosphere. The last component [D] is set as descriptive for the ash contents, due to its permanence as a straight line with the entire biomass content above 450 °C, as seen in Figure 18.

At the moment of the activation energy comparison among the biomass samples used in this study, whose values were displayed in Table 11, the rice straw content in a sample applied an inverse influence over the magnitude of the activation energy for the first mechanism. Besides, the second mechanism shows an even shorter influence from the same factor over the activation energy. Finally, the third reaction mechanism, which influences the third and fourth component showed a pronounced inverse effect from the straw content in the sample. Regarding now the reference data, in case of the two-step scheme performance to guarana seed residues (Lopes, F. et al., 2018) activation energies

were with a similar magnitude to those in the first and last mechanisms from this study. Moreover, as stated by Rueda-Ordóñez and Tannous (Rueda-Ordóñez and Tannous, 2018), the activation energies in synthetic air are expected to be higher than those from the inert atmosphere because of the presence of exothermic reactions in the oxidation of the volatile matter released, which produces an increase in the reaction rate and thereby, an increment in this energy.

Table 11.

Obtained results for consecutive reaction scheme performance and its deviation from the experimental data in oxidative atmosphere for all samples.

Biomass sample	Reaction Name	Reaction start point	Activation energy	Pre-exponential factor	W Average Deviation	Average Deviation
Symbol [units]	Rn	Xn	E [kJ/mol]	A	W-AD [%]	AD [%]
RH	[A]	1	107.90	$0.0696\beta+16.831$	0.32	2.22
	[B]	0.58	160.00	$0.0084\beta^2-0.0943\beta+26.425$		
	[C]	0.49	100.27	$0.0612\beta+11.157$		
	[D]	0.21	-	-		
B H-S	[A]	1	103.63	$0.0949\beta+16.011$	0.29	1.80
	[B]	0.55	160.00	$0.0115\beta^2-0.1024\beta+27.13$		
	[C]	0.45	73.33	$0.0956\beta+6.1863$		
	[D]	0.13	-	-		
RS	[A]	1	103.01	$0.0902\beta+16.205$	0.47	1.85
	[B]	0.55	161.21	$0.0373\beta+27.809$		
	[C]	0.44	50.52	$0.1023\beta+2.1073$		
	[D]	0.09	-	-		

Then, the preexponential factors obtained in this scheme were compared, using its natural logarithm magnitude as same as the previous schemes performed at this work; thus, in the first mechanism, the influence from the straw content fits with a positive parabolic shape. Further, in the second mechanism, a direct effect for this parameter with the rice straw content in the sample is detected. Finally, in the third mechanism, this proportion for this coefficient with the rice straw content in the blend is inverse. As seen in the next

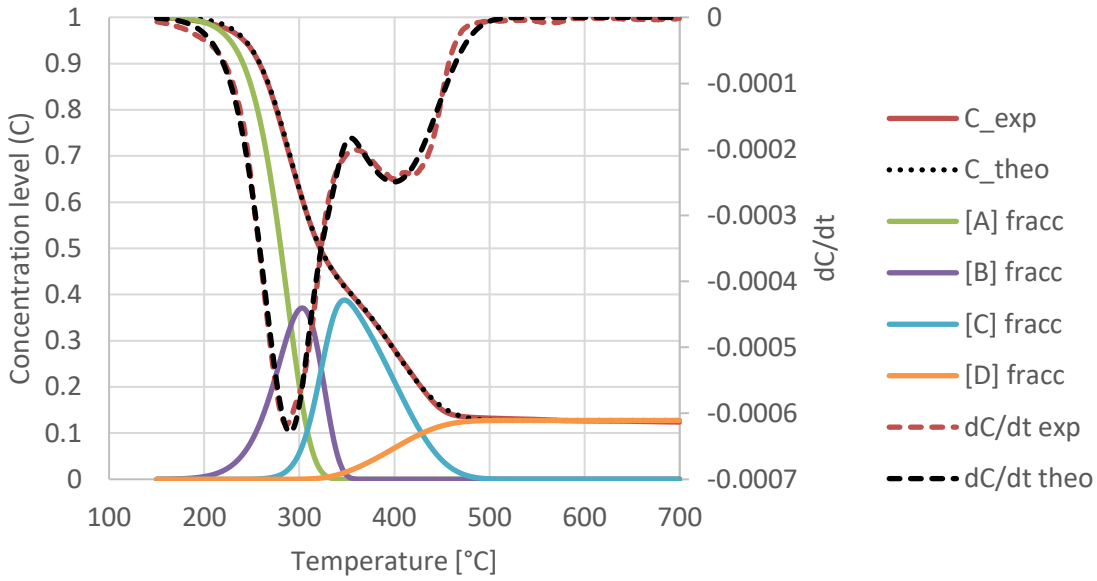
section, this frequency factor is expected to be directly proportional to the activation energy (see Figure 19).

Moreover, conversion functions used in this scheme were from first-order reactions for all the mechanisms, including those related to the components [C] and [D]. This is different in the model for the inert atmosphere where a third-order reaction is applied in the last mechanism, regarding that in the actual environment as a first step, and this third order was carried out for checking the model fitting with experimental values. Although this fitting percentage was higher than 5 %, thereby the reaction order was switched to one, improving the fitting with the experimental results. These reaction orders were used previously (Rueda-Ordóñez and Tannous, 2018), however, in the study performed by Lopes, F. et al. (Lopes, F. et al., 2018) with the two-step consecutive reactions, the first-order reaction is implemented in the first mechanism, and for the second one, a two-dimensional diffusion is applied, following a previous analysis performed with isoconversional reaction model.

Considering now the start points for each component of this scheme, stating previously that for the [A] component its value is one, in the second component [B] the straw content in blend produces an inverse effect in this parameter for low values, while for high content the influence is negligible; a similar effect was observed for [C] although this was present for all levels tested, as same for the fourth component [D], where a more significant influence is detected.

Figure 18.

Consecutive reaction scheme development and its comparison with experimental results to blend husk-straw sample, β = 5 °C/min, synthetic air atmosphere.



A correlation between the frequency factor and the heating rate is carried out, as same as the previous schemes performed in an inert atmosphere and the parallel in the oxidative medium; in this step, as shown in Table 11, a linear trend was detected for the three mechanisms with a positive slope in the biomass samples here studied, except for the second mechanism in the blend and husk sample due to its lack of fitting with this shape; hence there was implemented a 2nd order polynomial shape for these particular cases to obtain an R^2 coefficient higher than 0.95 which was the criteria selection for this correlations.

Finally, the average deviation percentages for the normalized mass curves and the mass conversion derivative were calculated, obtaining the highest fitting in the blend

sample, shown in Table 11. Comparing with the fitting of the independent parallel reactions, the present model achieved higher accuracy in terms of the α data from the experimental results. In the research made by Rueda-Ordóñez and Tannous (Rueda-Ordóñez and Tannous, 2018), the average deviation percentage, AD (%), was lower than 3 %, while for the study made for guarana seed residues (Lopes, F. et al., 2018), was lower than 1.5 %, although they used of only two reactions in its scheme. This can be due to the previous determination of the reaction model through the global reaction scheme performance in a defined temperature zone.

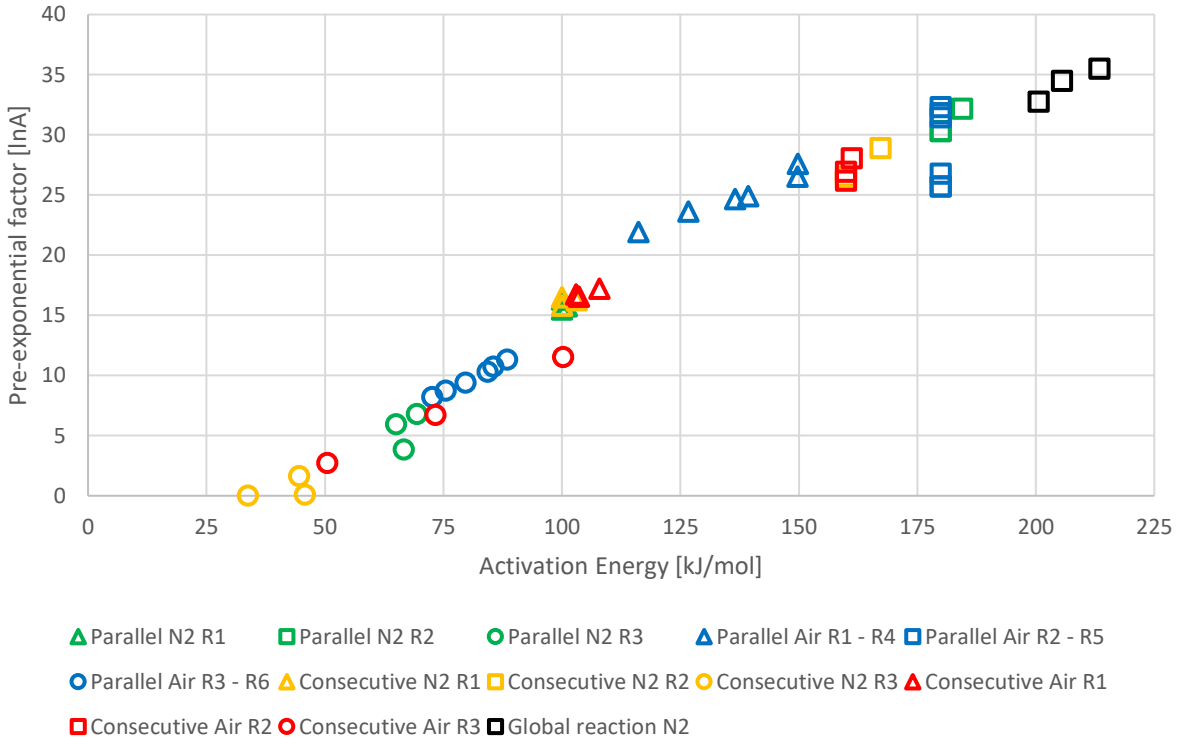
3.5.Comparison of the Arrhenius parameters.

This step is performed with the results from the kinetic modeling obtained in this study, to observe any possible trend and relation that could exist between these variables; a sorting and a comparison among the components handled in these schemes are developed as well. The points of intersection of data from the parallel reactions model are exposed as higher than those from the consecutive reactions model as seen in Figure 19, excluding the data obtained for the R3 reaction in the consecutive model in air atmosphere, which is distributed in the whole interval for lignin content, and the data from parallel and consecutive reactions models for the R1 reaction in an inert atmosphere which are located in the same point. Besides, determined data for the kinetic models in the oxidative atmosphere are found in higher values than the data from the inert atmosphere, confirming the fact stated by Rueda-Ordóñez and Tannous (Rueda-Ordóñez and Tannous, 2018) and

mentioned in the previous section. Notice that the results obtained in the global reaction scheme for inert atmosphere are located even higher than the last one for the cellulose reactions, showing that for this scheme, these reactions involved features related with this component in its temperature zone whose were performed.

Figure 19.

Sorting of pre-exponential factor values in natural logarithm magnitude vs activation energies in all the reactions for all the kinetic models in inert and oxidative atmospheres.

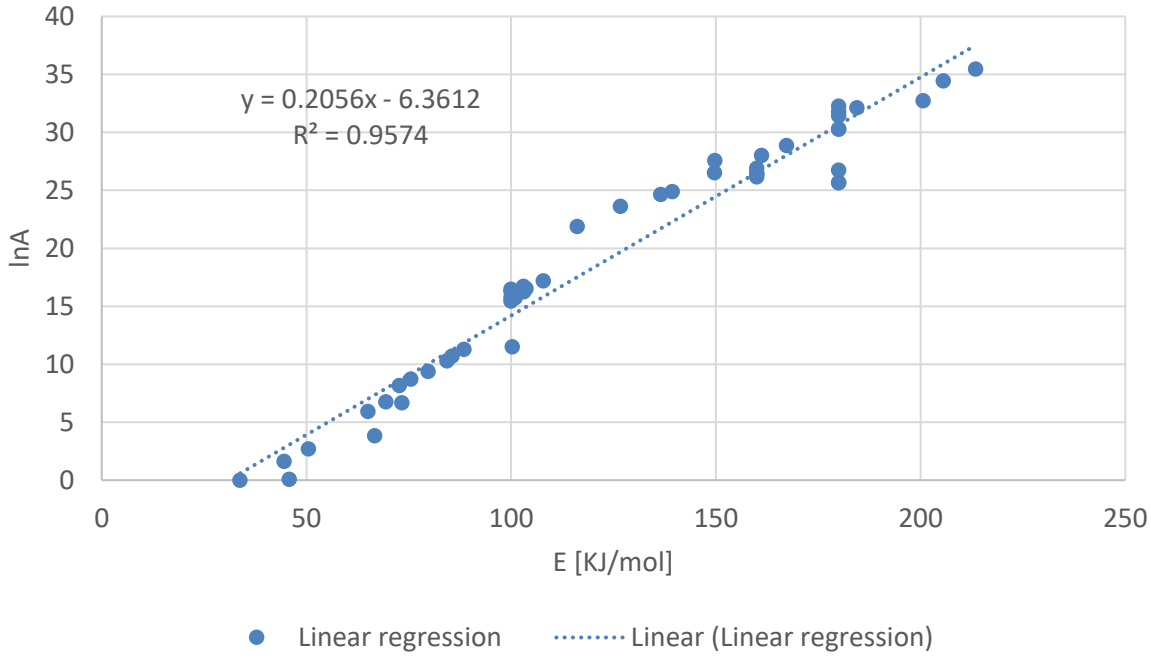


These points in the chart shaped a straight line with positive slope. Thus, in Figure 20 a trend line is plotted from the data obtained in the kinetic modeling performance using Microsoft® Excel® 16.0 software; the linear regression is included as an equation in the chart. This step is proposed as a possibility of use for future kinetic modeling studies with

the same biomass wastes, and as a method that can be replied for other biomass samples for a prediction of, E, and, lnA, in studies of the kinetics of thermal decomposition of these materials. Moreover, the R^2 coefficient calculated in this chart is above 0.95, which shows a proper fitting of the linear regression. A study carried out to black walnut samples (Xu et al., 2020) shows a similar analysis regarding the atmosphere analyzed and the temperature as well. This step follows the concept that a reaction model can be used to predict the trend of the solid pyrolysis accurately, if there is a linear correlation between these two parameters, called “compensation effects”.

Figure 20.

Linear regression and assessment with its fitting from the obtained data of pre-exponential factor values in natural logarithm magnitude vs activation energies, in all the reactions for all the kinetic models in nitrogen and synthetic air atmospheres.



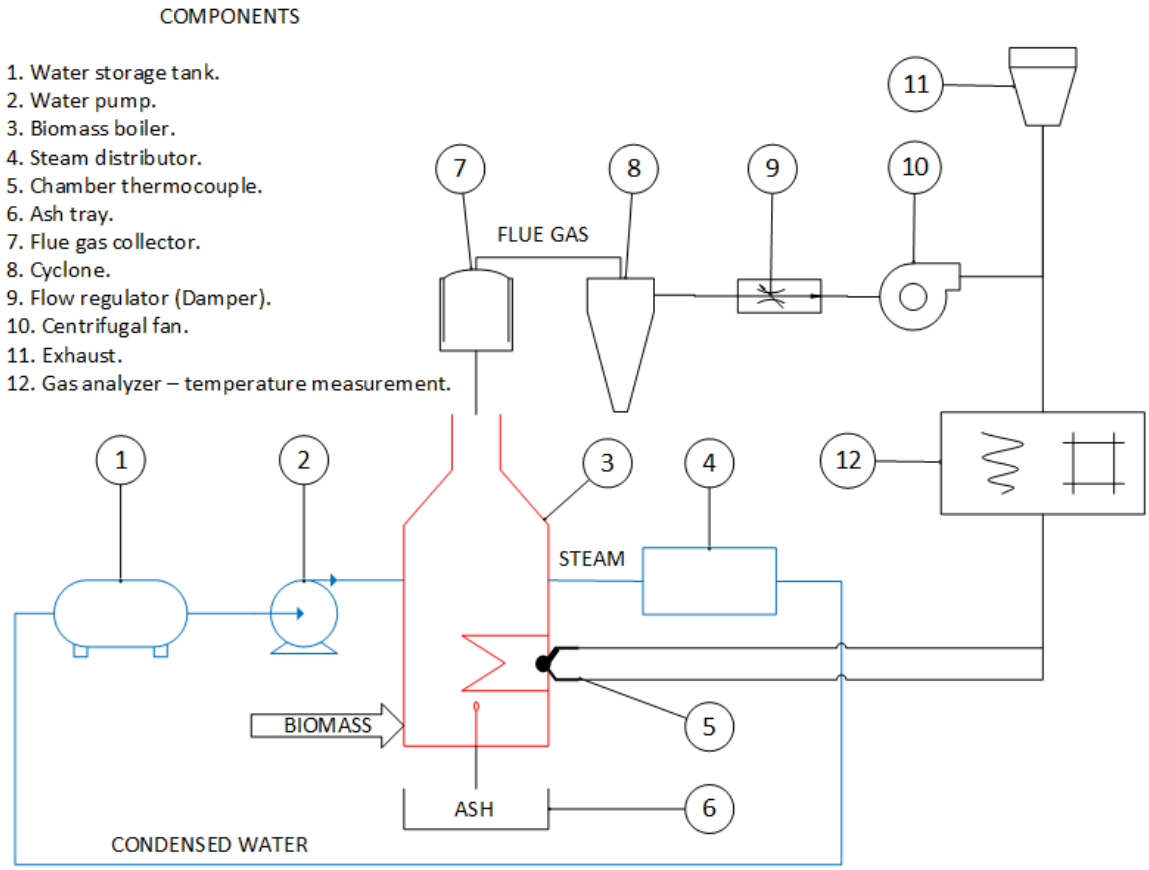
4. Enhancement technologies.

4.1. Combustion chamber

This appliance belongs to the Research Center for the sustainable development in the industry and energy (CIDES in Spanish) and is shown in Figure 21. Two process fluxes can be identified, these are the combustion gas flow line and the boiler water/steam flow line.

Figure 21.

Scheme of the combustion chamber and boiler for steam obtainment at a laboratory scale and used for this study.



In this study only the first process flux will be used, which is composed of a chamber, built with stainless steel and isolated in the inside with a ceramic coverage. This chamber has a thermocouple attached to the ceramic wall for the combustion gases measurement, and in the bottom, over the ash deposit, there is a burner which works with natural gas (methane) for the solid fuel ignition. Combustion gases are conducted through the tubes of the boiler, passing by a cyclone aimed for the particulate matter removal and then, these gases flow by a damper which controls the gases flux in order to set the air excess ratio in the combustion process, being this coupled to a centrifugal fan with a rotor diameter of 108 mm, assembled to an electric motor with a power of 1/7 HP and an angular speed of 3450 rpm being this gases finally taken away by an exhaust installed right after the centrifugal fan. From the rotor catalog, the performance curve is plotted for an axis speed of 1750 rpm, thus, enforcement of the affinity laws for fans was needed for the pressure and air flow determination with this new angular speed, as seen in equations (28) and (29) respectively (Salvador Escoda, 2019), where values with the subindex “O” represent the initial values for the calculation, setting the performance curve to the electric motor speed. Also, for the damper flux regulation, the flow air curve as a function of the percentage of opening is considered, using a condition of loose sealed damper, following the study performed by Millers and Pelite (Millers and Pelite, 2016). The performance curve from the rotor catalog, the flow air curve for the damper flux regulation and these last group of equations, which will be used also for the determination of the angle position of the damper for fixing of the real amount of air in combustion tests will be displayed in Appendix B.

$$q_v = q_{vo} * \frac{n_{rpm}}{n_{rpm_o}} \quad (28)$$

$$P_F = P_{FO} * \left(\frac{n_{rpm}}{n_{rpm_o}}\right)^2 \quad (29)$$

This chamber is coupled in the upper side with a lab-scaled pyrotubular boiler, connected to a pressure switch, which works in a range of 15 to 25 psi and controls the centrifugal fan directly (this is, if the maximum pressure is reached, the pressure switch turns off the centrifugal fan), and a thermocouple in order to measure the temperature of the water in the boiler. For the flue gas measurement, a Testo® 350 gas analyzes was used, which allows to obtain the amounts of CO, NO/NO_X, SO_2 and CxHy in ppm, which was coupled to the exhaust of the combustion chamber for this purpose.

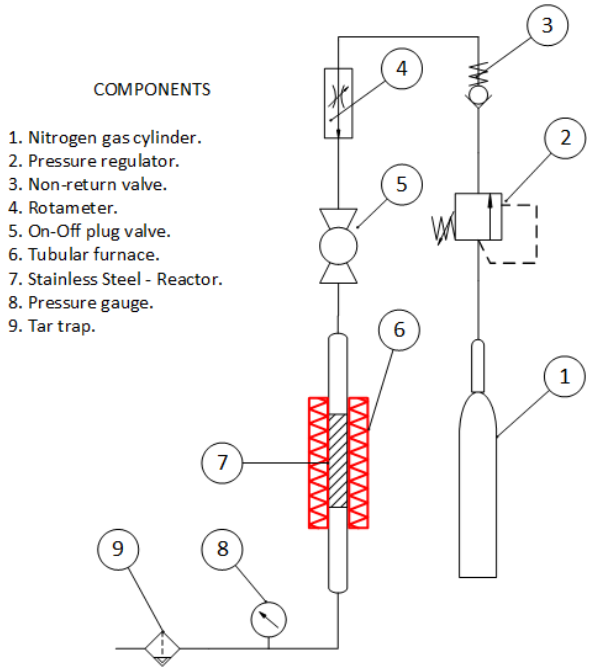
4.2. Pyrolysis reactor

For the development of the tests regarding this process, a laboratory pilot unit is used, drawn in Figure 22, which was assembled based on the project developed by Ferreira-Beltrán and Palencia-Blanco (Ferreira-Beltrán and Palencia-Blanco, 2015). This is composed of a vertical tubular reactor, made in stainless steel 304 as schedule 5S with a nominal diameter of 1 inch, with a length of 40 cm and external and internal diameters of 3.34 and 3.01 cm, respectively; in the internal section of the tubular reactor, a layette with mesh N° 40 and an internal diameter of 1.6 cm is built in the same material and attached to the upper cover of the external tube as a container for the biomass sample. Reactor heating is carried out through a Thermolyne® Sybron F21100 tube furnace which develops a power

of 1350 W working at 110 V, and it works with a heating rate of 15 °C/min. Further, a Cole-Parmer® cross-section area rotameter with a length of 150 mm for nitrogen fluxes among 0 – 50 ml/min is used for monitoring at the input, and a manometer of 60 (psi) is installed at the output of the reactor in order to seek for any obstruction in the system flux; one thermocouple is attached to the tubular furnace, which is standardized with the main temperature measured in the tubular reactor. The temperature calibration for the furnace thermocouple, the profile obtained alongside the reactor, which was used for the layette design and the calibration of the rotameter is added in the Appendix C.

Inert gas (N_2) is fed at the top of the reactor at a pressure of 15 psi, with a standard flux between [20 – 30] Nml/min (volume flow in ml/min at temperature and relative pressure conditions of 298 K and 1 atm respectively); previously, biomass sample is loaded in the layette, keeping a limit of 7.5 cm of height in order to avoid tar obstructions in the tubing installed after the reactor, this was observed in preliminary tests performed previously in the laboratory set-up. All these components were connected through stainless steel tubing 316/316L without welding with diameter ¼ in. (Swagelok®).

Figure 22.
Reactor set-up used for the pyrolysis analysis of biomasses in this study.



The product gases from the reaction are entrained by the inert gas to the released volatile matter (oil) condensation zone. Condensation section has just one trap, made of stainless steel, airtight sealed, which allow to the fluid to cool down to low temperatures using dry ice as cooling agent; in this zone, pyrolysis bio-oil is obtained. Non-condensable gases are taken out to the atmosphere.

4.3. Gasification reactor

Following the project developed by Paez-Duque and Suárez-Acelas (Paez-Duque and Suárez-Acelas, 2016), three fundamental zones are identified: pressure and flow

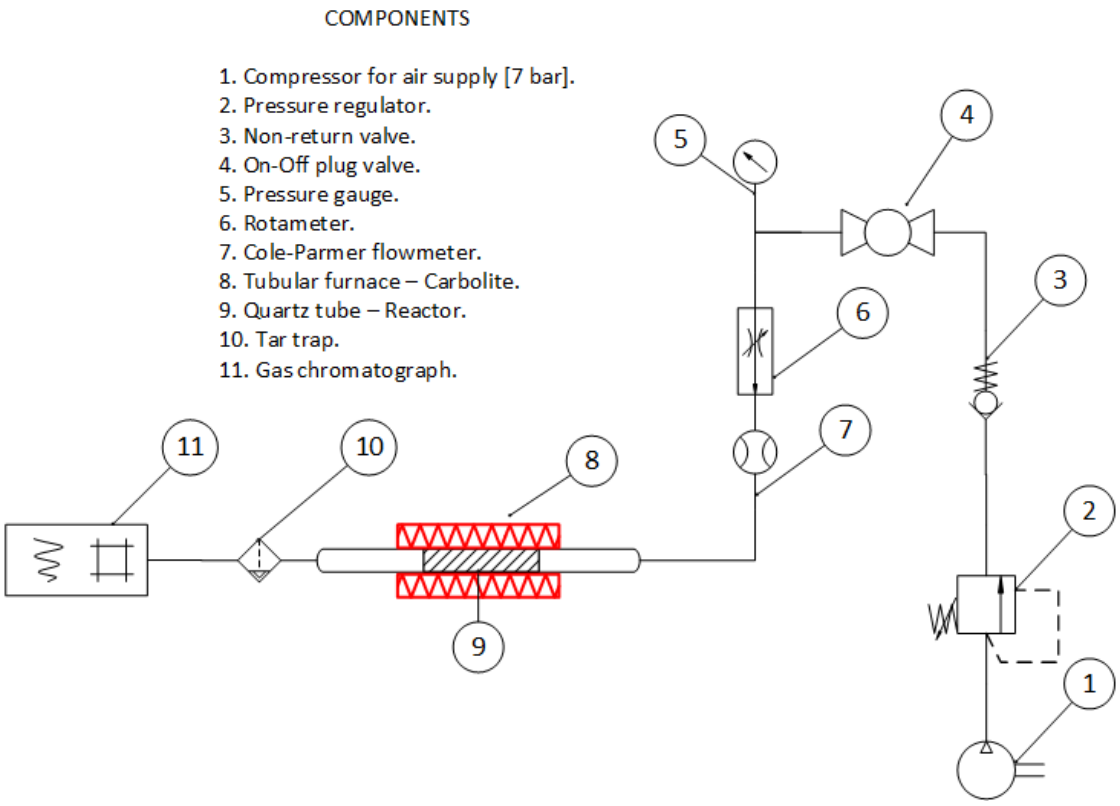
measurement stage, reaction stage and analysis stage. The proposed scheme is shown in Figure 23. The three zones named before are connected by stainless steel tubing 316/316L without welding with diameter ¼ in. (Swagelok®).

The compressed gas line comes from a general air compressor, for the entire laboratory building supply, which works at a pressure of 7 bar and contains a moisture filter in order to provide dry air. Measurement zone contains a Cole – Parmer® section-area-rotameter of 150 mm for compressed air line. This has a manometer which warrants the pressure measurement in the system.

Reaction zone is composed of a tubular reactor, made of quartz and set in a horizontal position with a length of 30 cm and external and internal diameter of 12 and 9.5 mm, respectively, which is heated through a small tubular furnace (Carbolite® MTF 10/15/130), set with a heating rate of 13 °C/min. Sample raw material is loaded as a fixed bed and held with quartz wool, based on Paez-Duque and Suárez-Acelas (Paez-Duque and Suárez-Acelas, 2016), using alumina layers up to its extreme points in order to subtract as much tar content as possible, produced in the devolatilization stage, to avoid damages in the gas chromatograph; besides, the addition of a tar trap cooled by dry ice was necessary in order to give a second stage of this substraction, especially for the volatile components with low condensation point.

Figure 23.

Laboratory-scale reactor set-up used for the gasification analysis of biomass samples.



Finally, the analysis zone has a gas chromatograph SRI8610C coupled to the reactor exit for the in-line detection performance of reaction products. This device uses He as carrier gas and is equipped with two packed columns for separation, one of them is the molecular sieve MS-13x and the other one is a Hayesep – D, both of them with a length of 6 in. Additionally, it has a HID detector (Helium Ionization Detector) and a TCD (Thermal Conductivity Detector) which are controlled using software PeakSimple 4.44 where the components are identified as peaks in a chart with a defined height (y-axis) and area, and located in their respective position in the horizontal axis (time of measurement).

The syngas compounds quantification was performed through previous measurements of gas blends contained in cylinders with specific compositions of 1 m^3 provided and certified by laboratory supplies facilities (CRYOGAS®, Linde - ©Messer Colombia). Regarding a minimum of three points of calibration for each component, these are plotted in a chart defined for values of volume percentage, vol%, as a function of the peak area, used for the determination of a trend line commonly shaped as a straight line using the software Microsoft® Excel® 16.0. Furthermore, the equation which features this trend line is obtained through the same software by a linear regression included in the graph. The calibration curves for each component analyzed in this study are exposed in Appendix D.

4.4. Stoichiometric analysis and reactor bed design for the thermochemical processes

4.4.1. Pyrolysis.

The carrier gas flux is determined using equation (30), stated by Vecino-Mantilla (Vecino-Mantilla, 2014), regarding a defined residence time, the porosity and the bed volume used for the biomass:

$$t = \left(\frac{A_T * h}{Q_{N_2}}\right) * \left(1 - \frac{\rho_{appar}}{\rho_{real}}\right) \quad (30)$$

Where *t* is the residence time of the gases, Q_{N_2} is the flow rate of N_2 at the operating conditions of the reactor (T, P), A_T is the cross-sectional area of the reactor in cm^2, h is the

bed height in cm, ρ_{appar} and ρ_{real} are the apparent and the real density of the biomass particles expressed in kg/m^3, according to Vecino-Mantilla (Vecino-Mantilla, 2014). In this assessment, the residence time selected was 30 seconds, in order to ensure the complete degradation of biomass samples regarding the condition of intermediate pyrolysis, as stablished by Tahir et al. (Tahir et al., 2019); the real density is taken from a previous study performed by the *Universitat Politècnica de València* (UPV, 2019) and the apparent one was measured using a 10-ml test tube, with the biomass sample previously prepared with the particle size selected for this thermochemical process; moreover, a linear regresssion for this last variable as a function of the rice straw content in the biomass sample was carried out, and is shown in the Appendix E.

4.4.2. Combustion.

A mass load in the combustion chamber was selected as 150 g, considering the lowest value of apparent density, being in this case for the straw sample, and determined through experimental loads previous to the main tests in the chamber, in order to check the maximum load possible in the laboratory set-up; for this thermochemical process, a complete and ideal combustion stoichiometry is regarded, as seen in equation (31). In this case, the chemical composition of the biomass is included considering the ultimate analysis performed in this study, and following the experimental results obtained and shown in Table 4, linear regressions for the mass content of each component measured in this analysis as a function of rice straw content in the sample were performed and included in

Appendix E, and the air is assumed as dry, due to the outcome of the lack of instruments for relative humidity measurement in real time at the moment of the combustion tests performance. Finally, as there is any content of sulfur in the biomass composition, the products generated in this reaction are carbon dioxide (CO_2), water (H_2O) and Nitrogen (N_2).

$$C_aH_bO_cN_d + (O_2 + 3.76N_2)_e \rightarrow n_1CO_2 + n_2H_2O + n_3N_2 \quad (31)$$

From this equation, the stoichiometric equilibrium is defined by the expressions (32) to (36), considering one mol of biomass and m_{sample} as the mass of the biomass sample measured in the combustion chamber; finally, x_i is the percentage taken from the ultimate analysis in mass basis, which is determined in section 3.5.2., divided by 100 % in order to handle a mass fraction value and M_i is the molar mass of each compound for the biomass sample.

$$z_i = \frac{(m_{sample} * x_i)}{M_i};\ z_i = [a, b, c, d];\ i = [C, H, O, N] \quad (32)$$

$$a = n_1 \quad (33)$$

$$b = 2 * n_2 \quad (34)$$

$$c + (2 * e) = (2 * n_1) + n_2 \quad (35)$$

$$d + (2 * 3.76 * e) = (2 * n_3) \quad (36)$$

Now, the theoretical mass of air is calculated using equation (37), regarding e value found in previous equation (36) and using the molar mass of the compounds of air. After this equation is stablished, the next defined variable is the air excess ratio (λ), as stated in

equation (38), which is the value between the real amount of air used in the process, over the theoretical amount of air defined in the previous stoichiometric relation.

$$m_{air_{theo}} = e * [(M_N * 2 * 3.76) + (2 * M_O)] \quad (37)$$

$$\lambda = \frac{m_{air_{real}}}{m_{air_{theo}}} \quad (38)$$

For the performance of each combustion tests in order to make the proper adjustment in the damper for the tests development, a time of 30 seconds since the biomass is ignited with assisted fire until the gas analyzer is started with its measurement routine of 5 minutes.

4.4.3. Gasification.

The sample mass was the reactor bed was calculated, regarding the bed volume to be used, stated in equation (39), where D_{int} is the internal diameter of the quartz tube used in the reactor and h is the bed length.

$$Vol_{bed} = \frac{pi * D_{int}^2}{4} * h \quad (39)$$

The length necessary to reach the desired temperature in the tubular furnace is determined by using a thermocouple inside the quartz tube, when the furnace is at the maximum or the desired temperature, and the thermocouple is located at the beginning in one extremity and then is placed 1 cm forward to the other side of the tube, in order to

generate a temperature profile from the measurements, which is shown in Appendix F; in this way, the length selected for the reactor volume calculation is of 3 cm, and the mass required for the fulfillment of this bed volume was determined through equation (40), where the apparent density is chosen through the correlation displayed in Appendix E.

$$m_{bed} = rho_{bed} * Vol_{bed} \quad (40)$$

In this process, as same as combustion, the next step is to determine the amount of oxygen required for a condition of ideal complete combustion for each biomass sample analyzed. This information is used further for the calculation of the theoretical and real amount of air used in each test, this last distributed in the whole time interval of the analysis by the air flow regulation through the rotameter in the experimental set-up. The stoichiometric expression for the real phenomena in this thermochemical conversion is shown in equation (41), which is proposed in molar units and is used for the mass balance calculation.

$$C_aH_bO_cN_d + (O_2 + 3.76N_2)_e \rightarrow n_1CO_2 + n_2CO + n_3CH_4 + n_4H_2O + n_5H_2 + n_6N_2 + Tar + Char \quad (41)$$

In this last expression a, b, c and d values are taken from the ultimate analysis (as seen in Table 4). At this point, the stoichiometric equilibrium is defined by the expressions (32) to (36) as well, considering one mol of biomass and in this case m_{sample} as the mass of the sample measured in the gasification reactor.

The theoretical mass of air is also calculated using equation (37); however, the real amount of air is determined through the equivalence ratio ER, following expression (42). According to Prabir Basu (Basu, 2018), a lower value of ER (< 0.2) results in incomplete gasification, excessive char formation and a low heating value for the syngas. Also, a high value for ER (> 0.4) takes the reaction near to a complete combustion, producing compounds such as CO_2 and H_2O rather than the expected syngas compounds (CO, H_2, among others). Therefore, ER is modified between the range of [0.2 – 0.3].

$$ER = \frac{m_{air_{real}}}{m_{air_{theo}}} \quad (42)$$

4.5. Experimental design for products composition test

Referring to all thermochemical processes, composed-central designs were applied, which consists in a complete factorial design with central points or a fractioned factorial design with resolution V, including the addition of "star points", used for curve modeling regarding each factor (Statgraphics, 2006); for the experimental analysis performance, software Statgraphics® will be used. In Table 12 are stablished all the factors used for each thermochemical conversion where 2 were used for combustion and pyrolysis and 3 were applied to the gasification reactor, and their low and high levels. For the intermediate pyrolysis the residence time is not taken into account, due to the low influence of this factor in the production of bio-oil, according to Vecino Mantilla et al. (Vecino Mantilla et al., 2014). In the case of the star points for this experimental design, the effect of temperature

for thermochemical processes will be observed in ranges of [300 – 550] °C for pyrolysis and [700 – 900] °C for gasification, being this last process also assessed varying ER value between [0.2 – 0.3] following Prabir Basu (Basu, 2018) by changing the gas flow rate and biomass residence time (Vonk and Piriou, 2019); moreover, in combustion, an analog factor will be assessed regarding the real amount of air in the test, which is the air excess ratio λ changing this value among [1.0 – 1.5]. Finally, the effect of rice straw mass concentration (% PA) in rice husk balance between [0 – 100 %] in all three reactors will be sized up.

Table 12.

Factors and values of high and low levels stated from the central composed designs for each thermochemical process performed using the biomass samples.

Thermochemical process	Factor	Low level	High level
Combustion	A: RS Content (% wt.)	14.65	85.35
	B: Air excess ratio (λ)	1.07	1.43
Gasification	A: RS content (% wt.)	20.27	79.73
	B: Temperature (°C)	740.54	859.46
	C: Equivalence ratio (ER)	0.22	0.28
Pyrolysis	A: RS content (% wt.)	14.65	85.35
	B: Temperature (°C)	336.61	513.40

As a discussion from the stablished response variables, which are exposed in Table 13, for the combustion process the flue gas temperature was set as this type of variable and the SO_2 composition was not included due to register of zero ppm in all tests, giving this a fact that the biomass samples here used are absent of sulfur content, regarding that this content was not measured in the ultimate analysis, shown in section 3.5.2.. Further, in the gasification process the response variables for the higher heating value, HHV, and the

H_2/CO ratio are included, which are obtained from the volume composition of the syngas produced measured through gas chromatography method obtaining here the volume content of N_2, H_2, CH_4, CO and CO_2; the HHV is calculated using the standard ASTM D3588 – 98 and the H_2/CO ratio is used as a potential value in a further exploitation for fuel synthesis (Lopes, I. et al., 2019). Finally, for the pyrolysis tests the syngas content produced could not be measured due to the lack of instruments for this step.

Table 13.

Response variables stablished from the central composed designs for each thermochemical process assessment using the biomass samples.

Thermochemical process	**Response Variable**	**Units**
Combustion	CO Concentration.	ppm
	NO/NO_X Concentration.	ppm
	C_XH_Y Concentration.	ppm
	Maximum temperatura in chamber	°C
Gasification	CO Percentage.	[%] vol.
	H_2 Percentage.	[%] vol.
	CH_4 Percentage.	[%] vol.
	CO_2 Percentage.	[%] vol.
	Higher heating value excluding N_2 (HHV)	[MJ/Kg]
	H_2/CO ratio	[wt./wt.]
Pyrolysis	Bio-oil mass yield.	[%] wt.
	Bio-char mass yield.	[%] wt.

4.6. Results from the experimental designs performance

4.6.1. Pyrolysis.

Bio-oil mass yield.

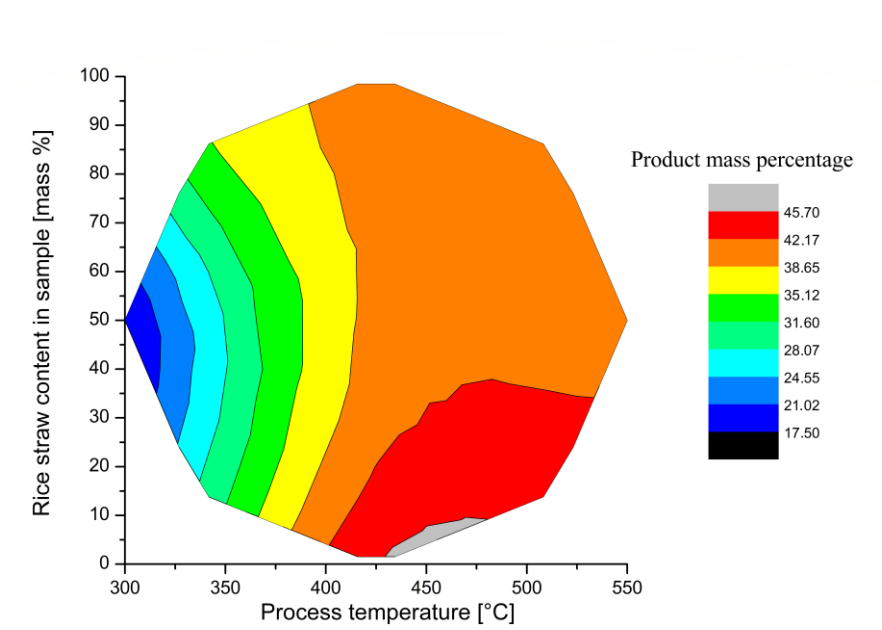
Results obtained from the tests carried out following the experimental analysis are shown in Appendix G. As seen in Figure 24, the process temperature applies a direct effect over the bio-oil obtainment; this effect is remarkable in the first half of the range of variation of the factor aforementioned where a null influence from the rice straw content is observed. This trend is consistent with results obtained in previous studies for rice husk samples (Natarajan and Ganapathy, 2009; Vieira et al., 2020), adding that for this last reference the influence was remarkable at the whole interval of temperature assessed, and for rice straw samples as well (Jin et al., 2019) where is observed a raise in the amount of pyrolysis gas produced due to the breaking of little chain fluid segments into non-condensable gases; another study for this last biomass in vacuum pyrolysis also detected this influence (Fukuda, 2015) where is stated that at high temperatures, the volatile matter yield increase, although the secondary cracking of the pyrolysis vapors into gas is favored, decreasing the oil yield.

In the other hand, at high values of temperature its effect becomes negligible and the straw mass percentage turns into predominant with an inverse influence in a short magnitude. Worth noticing that the bio-oil mass yield found for rice husk samples in the previous references mentioned were higher than the data obtained from the studies for rice

straw samples, excluding the vacuum pyrolysis results. A high composition of cellulose in a biomass material might lead to this trend, giving high liquid and gas yield through this process (Fukuda, 2015; Tai and Chen, 2016).

Figure 24.

Contour plots with the results obtained from the bio-oil mass yield following the experimental design carried out using rice waste biomasses.



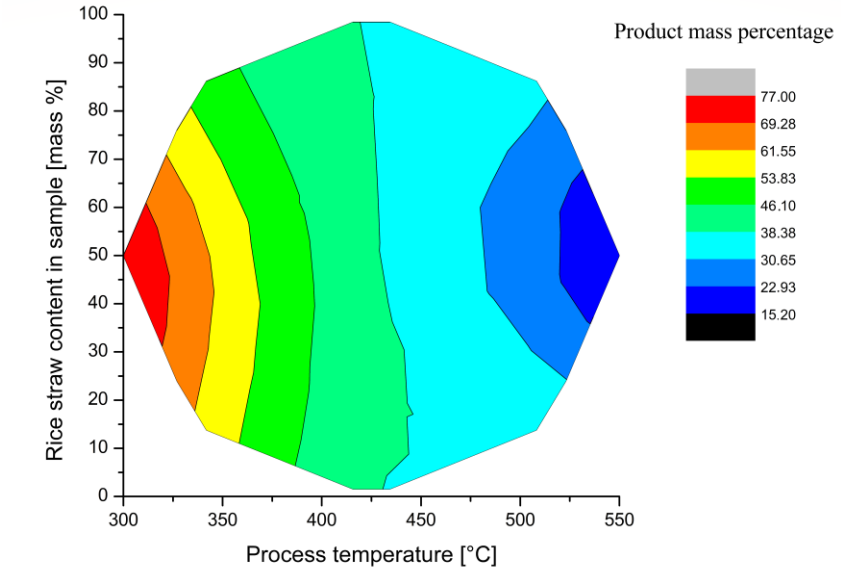
Bio-char mass yield.

Now, for the mass yield in this derivate from the pyrolysis process, a remarkable influence of inverse nature from the temperature can be observed, with a null effect from the rice straw content in the sample, as exposed in Figure 25. This same trend was found in previous studies for rice husk samples (Kumar-Gupta et al., 2016; Gautam and

Chaurasia, 2020); following the stated at the last work mentioned before, at low temperatures the pyrolysis process was partially complete, which resulted in high yields of char; furthermore, when the temperature increases, the cracking reaction of high-molecular-weight hydrocarbons intensifies, leading to a decrease in the production of this product. A similar influence is detected for rice straw analysis (Yakout et al., 2017) where is stablished that this effect could take place due to the raise of organic compound volatilization as temperature increases.

Figure 25.

Contour plots with the results obtained from the biochar mass yield measurement following the experimental design performed using rice waste biomasses.



The lignin content in biomass influence in a direct way the obtainment of the char yields in pyrolysis process (Tai and Chen, 2016; Fukuda, 2015), considering that lignin

content in rice husk is higher than the straw sample; however, according to this last author, even though high ash content tends to inhibit the production of bio-oil, components such as sodium and potassium possess a catalytic effect on the thermal degradation of biomass during pyrolysis and may lead to low degradation temperatures; thus, this may turn into a higher volatile release and higher gas production, which is in agreement with the higher amount of ash content in the rice husk rather than the rice straw samples.

4.6.2. Syngas composition (Gasification)

In Appendix G is included the table where are shown the results for the mass balance in all the experimental tests, in order to check the closure of this balance and to observe the amounts of solid char remaining in the reactor, the mass of the produced syngas and the condensed volatile matter in the tar trap and in the alumina layers as well. Moreover, in Appendix G as well, the results of the syngas composition measurement are displayed, and the high heating values for each experiment carried out are included.

In order to give a coherent discussion about the trends observed from the experimental results, the typical gasification reactions are considered, which represents the interactions taking place between the solid char remaining from the pyrolysis thermal stage and the gasyfing medium, which is in this case air taken from the local environment (see section 5.3.); these reactions are shown in Table 14 which were taken from Prabir Basu (Basu, 2018) and are divided in two stages: The first one is for the combustion step, which

releases energy from the exothermic reactions R5, R4 and R8 present here and generates H_2O and CO_2, and then the reduction step arises taking into account the interactions from reactions R1, R2, R3 and R9 with these new components, and obtaining finally methane. These last reactions were regarded in previous works for rice husk and sawdust analysis (Susastriawan et al., 2019) and for rice husk only in a downdraft gasifier (Ma et al., 2015) as well.

Table 14.

Typical gasification reactions used in previous studies concerning this thermochemical process using air in a fixed bed condition.

Code	Reaction	Reaction type
R5	$C + O_2 \rightarrow CO_2 - 394\ [kJ/mol]$	Oxidation reaction
R4	$C + 0{,}5O_2 \rightarrow CO - 111\ [kJ/mol]$	Carbon reaction
R8	$H_2 + 0{,}5O_2 \rightarrow H_2O - 242\ [kJ/mol]$	Oxidation reaction
R1	$C + CO_2 \leftrightarrow 2CO + 172\ [kJ/mol]$	Boudouard (Redox.)
R2	$C + H_2O \leftrightarrow CO + H_2 + 131\ [kJ/mol]$	Water-gas
R3	$C + 2H_2 \leftrightarrow CH_4 - 74.8\ [kJ/mol]$	Hydrogasification
R9	$CO + H_2O \leftrightarrow CO_2 + H_2 - 41.2\ [kJ/mol]$	Shift reaction

In previous studies related to simulation models for prediction of syngas composition, obtained from biomass gasification analysis in fixed bed, through the method of the minimization of Gibbs free energy (Damiani and Trucco, 2010; Sittisun et al., 2018; Khonde et al., 2019), the condition of the equilibrium of the reactions is stated, based on the assumption of a high residence time provided in the reactor, obtaining a reliable fitting with experimental data from biomass samples in the gas composition determination. In this sense, for the following discussion in the measurement of the syngas components, this fact is taken into account as well.

Le Châtelier-Braun principle states that for an endothermic reaction, an increase in temperature results in a shift of the equilibrium towards the products; in the other hand, at an exothermic reaction, this equilibrium shifts towards the reactants if the temperature increases (Keszei, 2012). Considering the set of reactions for reduction (R1, R2, R3 and R9) this principle explains properly the trends found for the synthesis of these components, being this principle also used for the discussion in a previous study about sugarcane bagasse gasification (Lopes, I. et al., 2019).

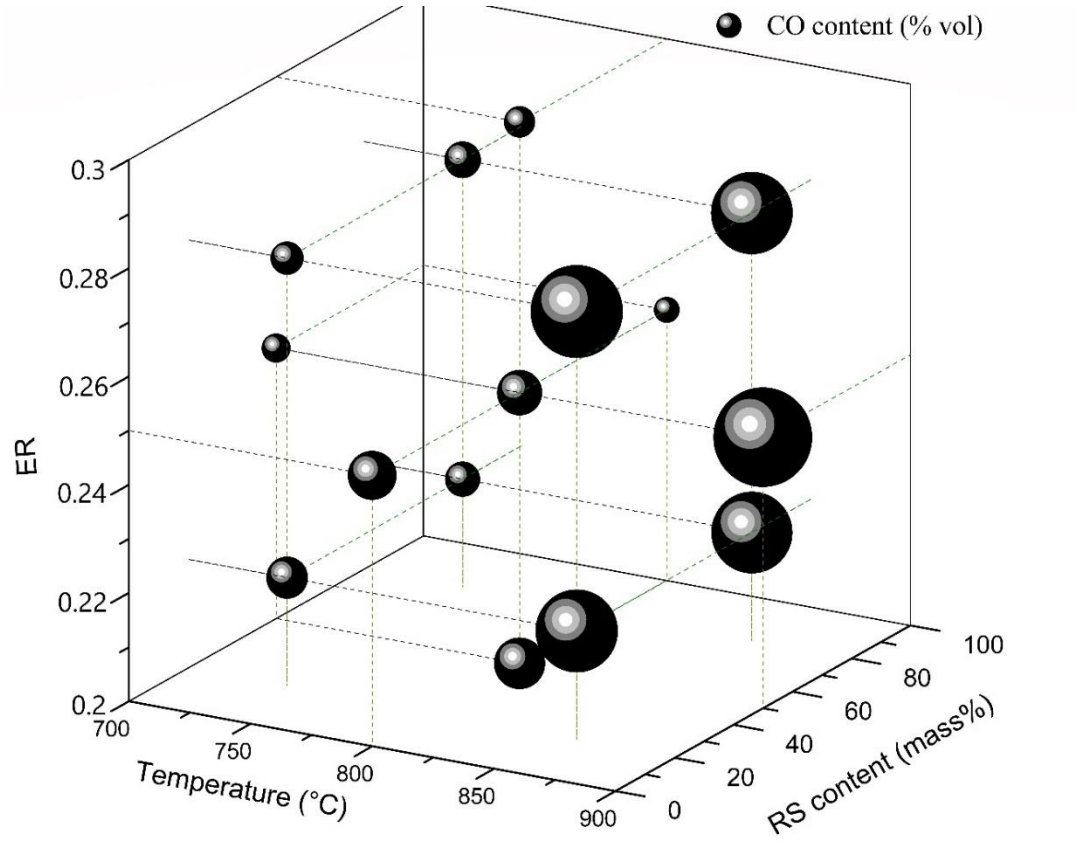
CO content.

In Figure 26 comparisons between the different levels of the factors and the star points from all tests considering the volume percentage of carbon monoxide are exposed; from this chart, it is clear the direct influence applied by the temperature over the production of this component, seen at all levels of rice straw content in the sample; This is consistent with a previous study performed for husk samples with a wide effect (Khonde and Chaurasia, 2016) even though above a certain temperature this production starts decreasing. This is different for the ER and the straw content in the biomass sample, which do not show a remarkable effect, observing similar magnitudes even for low and high levels of the straw mass percentage and at the moment of varying the equivalence ratio as well. Taking into account previous studies assessing the effect of the ER, for husk samples this factor applies an inverse effect (Ma et al., 2015); and for rice straw analysis this influence

is from a direct nature (Ngamchompoo, 2018), observing that these effects were of a short magnitude as well. Regarding Le Châtelier principle (Keszei, 2012) for this component, which is described by endothermic reactions R1 and R2 and by exothermic reaction R9 as seen in Table 14, if a raise in the temperature is carried out, this conducts to an increment in this constituent at R1 and R2 as a product and at R9 as a reactant.

Figure 26.

Comparison of measurements of CO content from the tests performed following the central composed design applied to this thermal decomposition process.



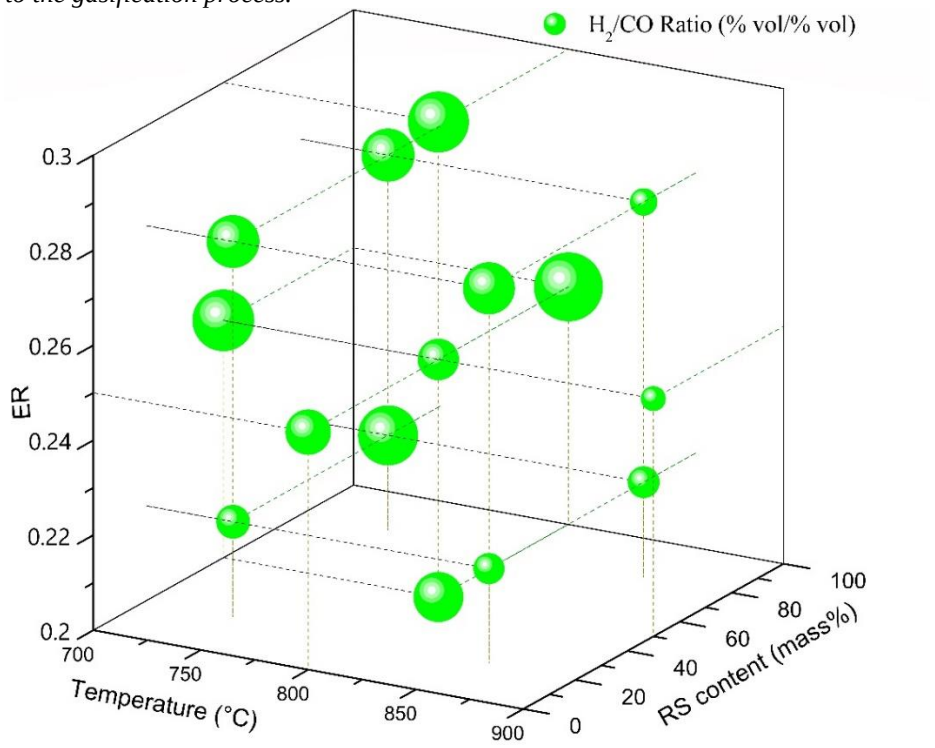
H_2/CO ratio.

An outcome took place in the hydrogen composition measurement from the produced syngas, due to the use of helium as carrier gas which presents a similar thermal conductivity with the hydrogen, producing an overlap in the curve of the last component mentioned before, following the gas chromatography method using a thermal conductivity detector (TCD) which is evidenced in previous works as well (Toonen and Van Loon, 2013; Snavely and Subramaniam, 1998). Therefore, the quantification of this gas is performed by difference, regarding that its value added with those from the other components considered at this study comprises the 95 vol% of the whole syngas produced, whilst the other 5 vol% is constitued by hydrocarbon compounds with more carbon atoms in their molecules. A deeper discussion about this component is added in Appendix H.

Thereby, the H_2/CO ratio is considered and discussed, which is an indicator for potential of this fuel as its use for biofuels synthesys through other processes (Lopes, I. et al., 2019; Dhanavath et al., 2018), as seen in Figure 27 at low values of rice straw content in biomass blend, the ER influence is predominant and with a positive trend excluding the other factors whose influence is not observed, whilst for high values of straw mass percentage, the temperature takes place as the predominant influence although with an inverse nature, being this opposite to the other factors which influence is absent. At central levels of straw content, both ER and temperature share the influence with similar magnitude, despites the first one is direct and the last one is of an inverse nature; finally, at

central levels of temperature and ER, the rice straw content shows a positive influence over the calculation of this ratio. Regarding the temperature effect, this trend has been detected in a previous work (Lopes, I. et al., 2019). Finally, according to Le Châtelier principle (Keszei, 2012), an explanation to the inverse effect from the temperature to the H_2/CO ratio can be made through reaction R9 which is exposed in Table 14, due to the switch of the equilibrium towards the reactants obeying a temperature raise, being the hydrogen and carbon monoxide stated in this reaction as product and reactant, respectively.

Figure 27.
Comparison among calculations of H_2/CO ratio from the tests performed following the experimental design stablished to the gasification process.



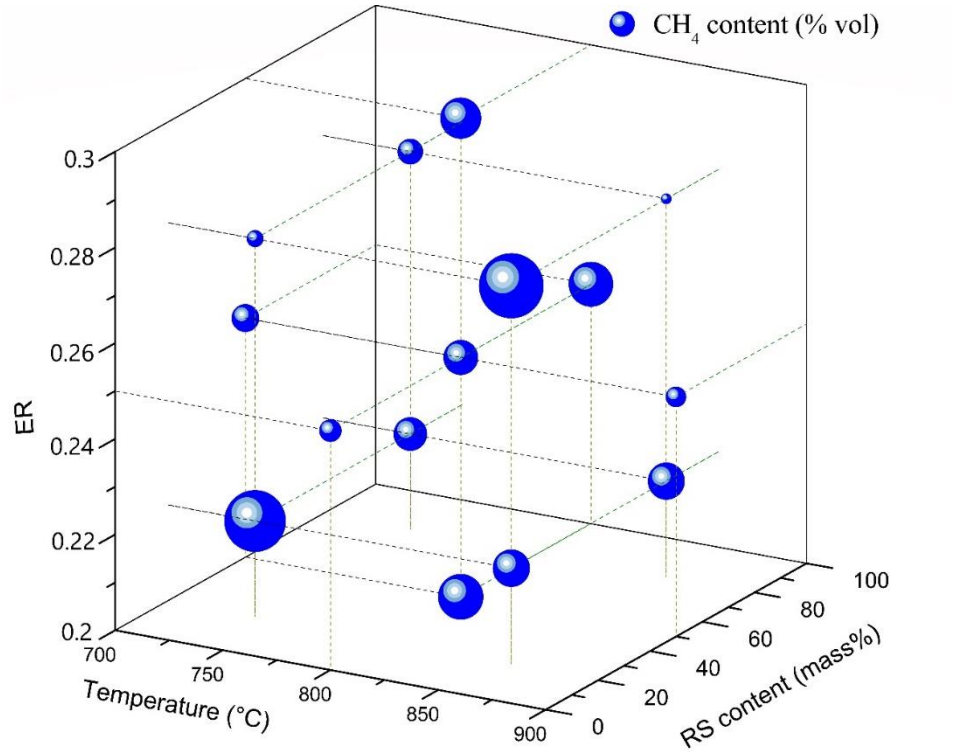
CH_4 content.

A contrast between the measurements carried out for this component and the variations of the factors is plotted in Figure 28; notice that in this component, the maximum value registered does not exceed the 5% over the total volume in the syngas produced in these tests. This is consistent with results found in previous works (Ma et al., 2015; Susastriawan et al., 2019; Ngamchompoo, 2018). There is not a significative trend found from any factor in the production of this compound in the syngas, this is, the equivalence ratio applies a direct influence at high temperatures for low levels of rice straw in sample, however, at low temperatures this effect is of an inverse nature; for high content of straw in the sample both inverse influences from the ER were observed, although this was more pronounced for high temperatures rather than a lower level of this last factor.

As detailed in previous analysis in rice husk samples, the maximum amount measured of this component has been found at low levels of ER and temperature (Ma et al., 2015) and at a half level of ER keeping the temperature in the same level (Susastriawan et al., 2019); for rice straw samples this composition kept as a constant at all levels of ER and measurement of temperatures (Ngamchompoo, 2018), finding a direct effect from the temperature as well (Khonde and Chaurasia, 2016).

Figure 28.

Comparison of measurements of CH_4 content from the tests carried out following the experimental design applied to the gasification process.



CO_2 content.

Opposite from the influence observed for the carbon monoxide production, the temperature applies an inverse effect over this composition in the syngas for all levels of rice straw mass percentage and equivalence ratio, although it was in a shorter magnitude. moreover, the effects from these two last factors are neligible, being this fact similar to the previous component discussed. A recent study for rice straw shows an effect of direct nature from the equivalence ratio (Ngamchompoo, 2018); in the case of rice husk samples, this effect has been found as inverse (Ma et al., 2015), and regarding the temperature influence, this has been found as inverse as well, similar to the trends observed at this work

(Khonde and Chaurasia, 2016). As stated in Le Châtelier principle (Keszei, 2012), in the carbon dioxide this inverse influence can be explained following reactions R1 and R9 shown in Table 14 which are of nature endothermic and exothermic, respectively. Thereby, when the temperature increase takes place, this component leads to a reduction on its composition at R1 as reactant and at R9 as product.

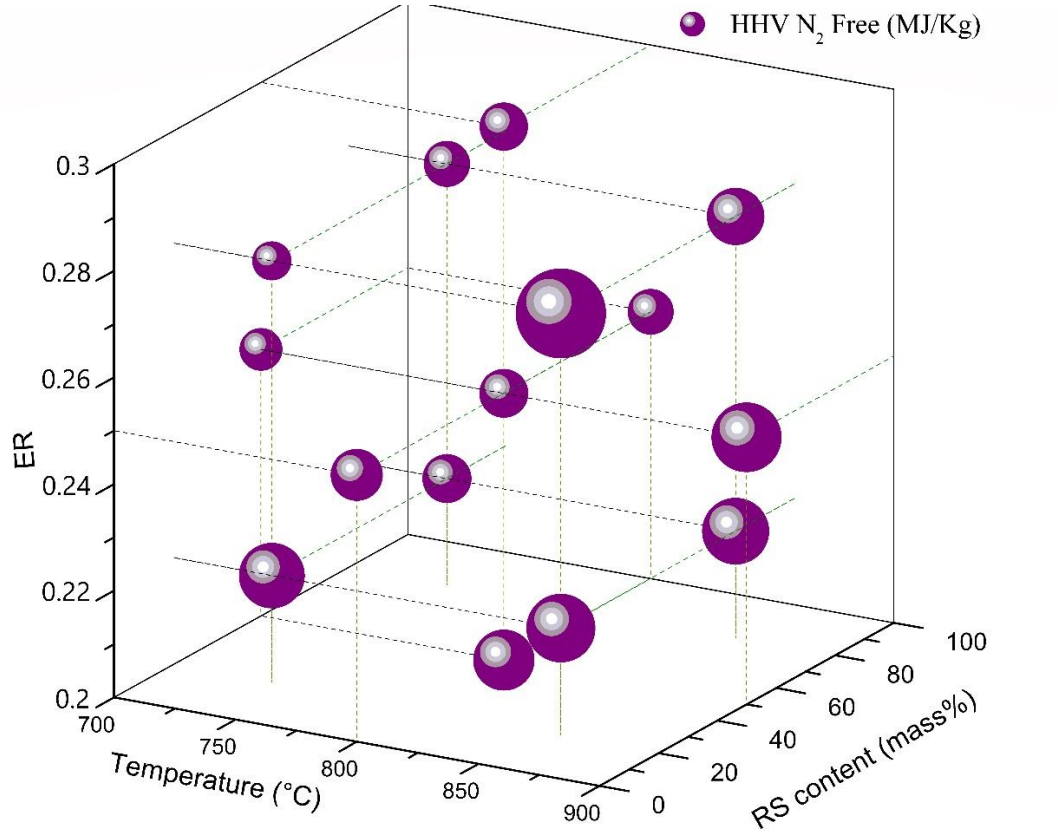
Higher heating value of syngas

The temperature shows a positive trend over this response variable, as seen for high and central values of rice straw contents despites of the variation of the equivalence ratio (see Figure 29); at low values of rice straw mass percentage, this factor keeps with the same effect for high levels of ER, although if this last factor is switched to its low value the temperature influence dissapears. Now considering the influence from the equivalence ratio, at low levels of straw content the effect for this response variable is direct from the factor in discussion if the process temperature is low; however, if the temperature increases, this trend switch to an inverse nature. Despite from this fact, in the other levels of straw content, the equivalence ratio does not show a significative influence over the heating value of the syngas, even though for central levels of rice straw content in blend the ER showed an inverse parabolic trend with short magnitude in the half level of temperature. A previous study shows an inverse influence made by the equivalence ratio for rice husk samples (Ma et al., 2015) in this amount and for the temperature as well, which in this work was set as a response variable; however, another study revealed that an absence of influence from the

ER is present from the downer limit stablished in this study, although it influences directly for lower values of this ratio (Susastriawan et al., 2019); finally, for rice straw samples, the effect over the heating value is from a direct nature (Ngamchompoo et al., 2018) similar to the influence over the process temperature, which is set as a response variable as well.

Figure 29.

Comparison among calculations of high heating value (HHV) from the tests performed following the central composed design applied to this thermochemical process.



Flue gas mass composition (Combustion).

In Appendix G results from measurements performed in these tests are shown. Considering a previous research (Sullivan and Ball, 2012), combustion process for lignocellulosic materials takes place through three unique stages: pre-ignition is the first one, where solid fuels are heated releasing its moisture content and occurring the whole decomposition of hemicellulose before the volatilization starts, including the partial volatilization of cellulose and lignin.

Further, the other two stages take place simultaneously, which are the flaming combustion of the volatile matter and carbon monoxide released, and glowing combustion of the solid char. Previous to these combustion steps, two competing reactions may be part for the cellulose content, which comprises in one part the formation of levoglucosan molecules which are the precursor to a large number of subsequent volatile decomposition species that oxidize in flaming combustion. If low thermal energy is surrounding the sample, this may block the formation of components with volatile features, resulting in solid primary char production, which can react by high exothermic reactions taking place helped by the presence of alkali metal cations. Those ones are common in the ash contents of biomass samples. On the other hand, the lignin presents high resistance to chemical and enzymatic decomposition and its degradation can be slow in a wide temperature interval (Sullivan and Ball, 2012).

Now, regarding the combustion steps performing at the same time, reactions occurring in these stages are exothermic. For the flaming combustion, subsequent intermediate species derived from the levoglucosan decomposition are present and, thereby, allow to increase of hydrocarbon and fuel components emissions due to the partial oxidation of them. On the other hand, the separation of these volatiles from the reaction zone following the nature of turbulent diffusion flames results in further quenching of these components through loss of heat or reactants (Sullivan and Ball, 2012).

In the case of the glowing combustion, high efficiency features, little smoke production and trends of fully oxidized products belong to this type of oxidation. That type of combustion occurs at higher surrounding of oxygen content near to the char material, which has a porous surface and higher carbon constituents, and leading to production of carbon dioxide and carbon monoxide as well (Sullivan and Ball, 2012).

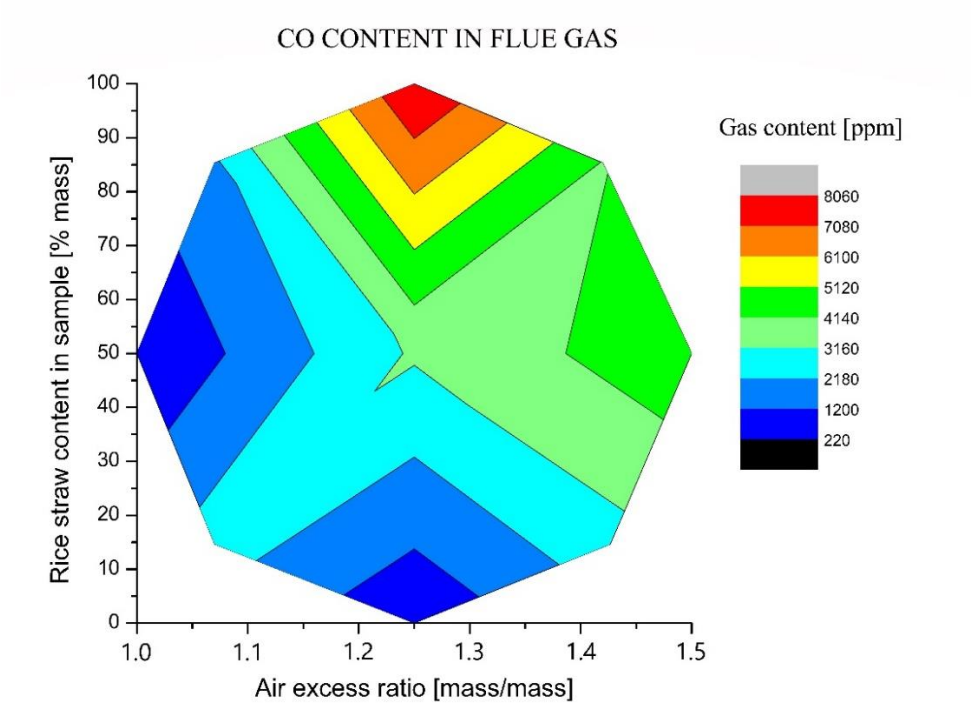
CO Emissions.

Now, as seen in Figure 30, a strong direct influence from the rice straw content is exposed considering the star points data, as well as the effect observed from the air excess ratio, even though this was weaker than that from the first factor mentioned. In addition, this raise trend is detailed regarding both factors in their high and low levels, increasing this content at the moment of switching them to their high values. Thus, the addition of rice straw to the rice husk for its use as solid fuel in combustion process increase CO emissions.

On the other hand, the increase in the air excess ratio may lead also to a raise in this component in a shorter extent. Considering its lower levels of cellulose, lignin and ash content, this leads to the presence of the flaming combustion of the released volatile matter from levoglucosan decomposition in a major proportion with release of partial oxidized components in the flue gas (Sullivan and Ball, 2012).

Figure 30.

Contour plot with data obtained from the CO emissions measurement in the combustion tests performance following the central composed design for rice waste biomasses.



Previous studies of pollutant emissions for rice husk samples showed a decrease in these concentrations as the excess air percentage increases (Janvijitsakul and Kuprianov, 2008); this trend is appreciated as well in the measurement performed by Duan et al. (Duan

et al., 2018) with the increment of the secondary air flow rate. However, an analysis of cofiring of coal and rice straw pellets (Unchaisri and Fukuda, 2017) shows that the addition of the biomass sample increased widely the CO emissions in a direct way. A similar effect is also observed with the raise of the air excess ratio in a shorter effect.

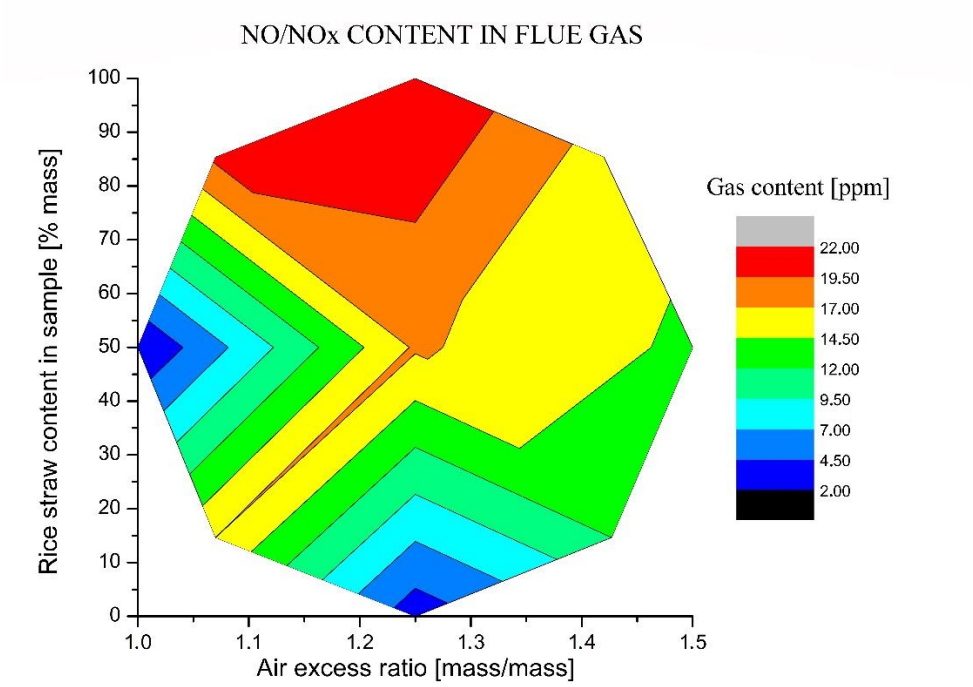
NO/NOx Composition.

For the comparison of these emissions, results were plotted in Figure 31. Specifically, worth noticing previously that the highest emission registered was less than 25 ppm. This plot allows to note the direct influence of the increase in the rice straw in these emissions through the data obtained in the star points. In this case, the higher nitrogen content in this biomass as measured in the ultimate analysis is regarded, although these compositions are below 2 mass%.

From the variation of the air excess ratio, however, considering the measurement performed at high and low levels of both factors, a short inverse influence is detected from λ at both levels of rice straw content in the sample. Thereby, this factor did not apply a remarkable effect over the emission of these gases. An increase of these concentration has been found product of the increment of the excess air percentage for rice husk samples (Janvijitsakul and Kuprianov, 2008; Duan et al., 2018). On the other hand, for rice straw analysis, these concentrations got reduced when the primary or secondary air ratio increased (Okasha, 2007; Migo-Sumagang et al., 2020).

Figure 31.

Contour plot with data obtained from the NO/NO_X content measurement in the combustion tests performance following the central composed design for rice waste biomasses.



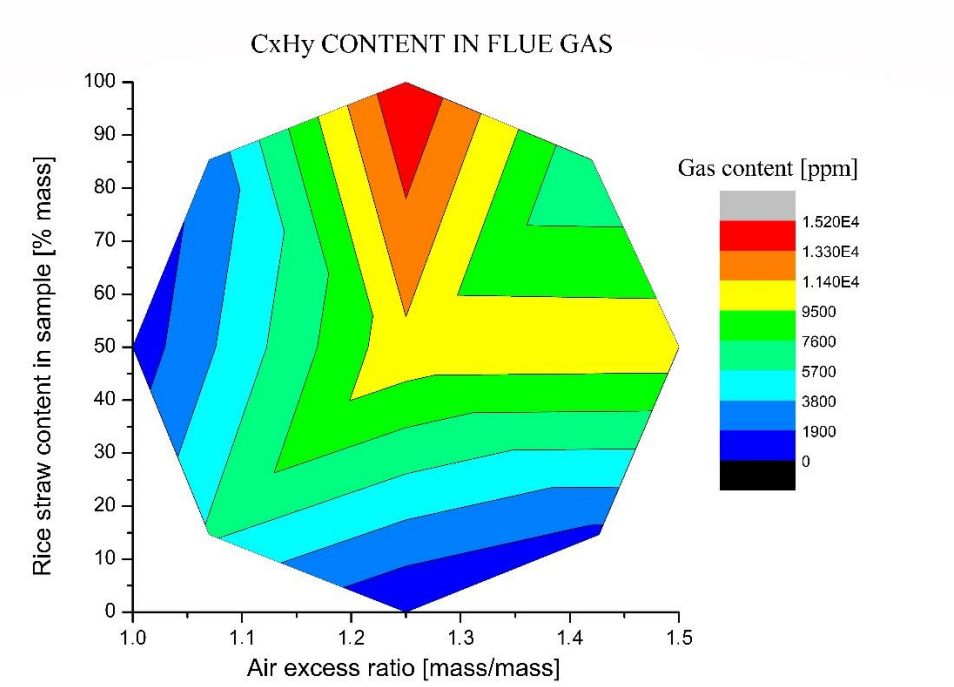
CxHy concentration.

Following Figure 32, notice the direct influence made by the variation of rice straw content in the solid fuel over the emissions produced for these gases at high values of λ, being this effect inverse at low level of this last factor. From the star points values, the rice straw content shows a remarkable influence of direct proportion over the production of these hydrocarbon compounds, similar to the applied from the air excess ratio, although this last effect was in a lower magnitude, affecting only from the lowest star point to the central level test carried out.

In rice husk samples, the amounts of ash are higher than the measured in the straw material; therefore, as described before, the addition of straw content in the sample leads to the presence of a higher release of levoglucosan and its further decomposition, turning into a higher performance of flaming combustion (Sullivan and Ball, 2012). Applying a direct influence over the release of hydrocarbon components from the combustion process, the lower emissions of hydrocarbons in the tests where the husk is predominant is due to its higher trend towards the solid char glowing combustion, considering the more extended reaction of lignin as well.

Figure 32.

Contour plot with data obtained from the C_XH_Y concentration measurement in the combustion tests performance following the central composed design for rice waste biomasses.

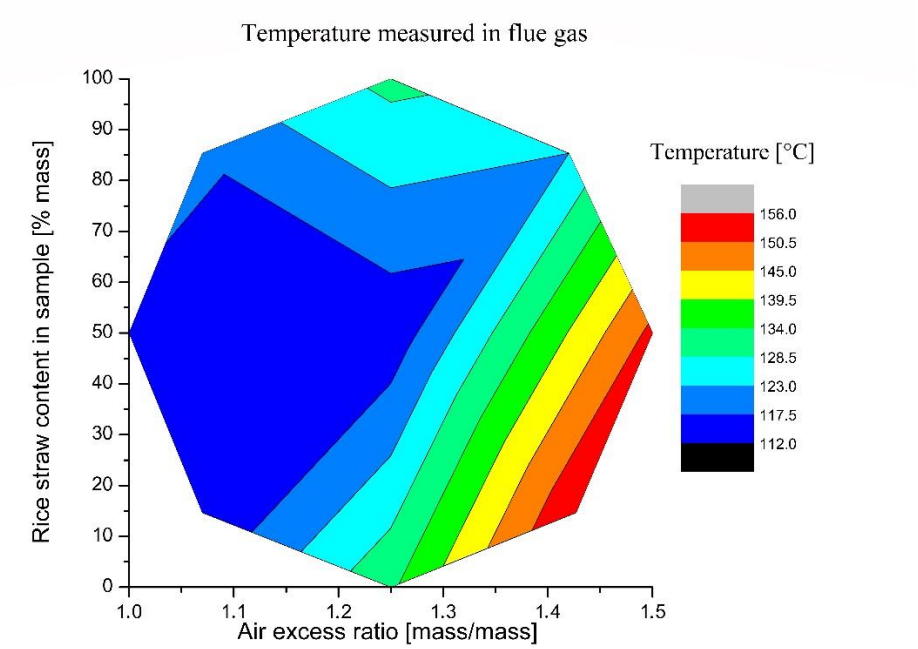


Wall temperature – Combustion chamber.

The direct influence of the air excess ratio in this variable is prominent, regarding the star points in the central level of rice straw content and at a low level of rice straw content in sample, as seen in Figure 33. This trend can be evidenced as well for rice straw samples (Migo-Sumagang et al., 2020) and for rice husk samples (Duan et al., 2018; Okasha, 2007). A shorter and inverse effect from the rice straw content in the sample is detected over the magnitude of this property, only at high levels of air excess ratio.

Figure 33.

Contour plot with data obtained from the chamber temperature measurement in the combustion tests performance following the central composed design for rice waste biomasses.



These trends are consequence of the higher proportion of the solid char glowing combustion, which possess highly exothermic features and occur by the larger content of ash in the husk samples, including its higher content of lignin, which applies a slower decomposition and a resistance over the chemical degradation. Moreover, the air excess ratio promotes a higher oxidation in the fuel reactants, releasing thermal energy to the system. In the other hand, for the formation of levoglucosan molecules which are the precursors of flaming combustion, are required high amounts of energy due to the endothermic nature of this process (Sullivan and Ball, 2012); this stage takes place by the lower presence of ash in the straw samples.

5. Conclusions

From the physico-chemical characterization, higher amounts of volatile matter and fixed carbon content was evidenced for the rice straw samples; this is consistent with the carbon and hydrogen contents and its heating value. On the other hand, higher amounts in the ash and oxygen content in the ultimate analysis were detected for the rice husk samples. However, these exposed trends do not guarantee an advantage for one biomass material over the other sample in a further exploitation in thermochemical conversions. Although the structural composition was performed, its results were not used due to several inconsistencies among them and the results found in the literature.

Considering the kinetic modeling performed to the thermogravimetry analysis carried out using the biomass samples, consecutive reactions model which is based on the mass concentration gave the lowest average deviation. Besides, this deviation is slightly higher in the independent parallel reaction model which is related with the mass conversion and its derivative. Despites the global reaction model showed the largest deviation from the three schemes applied in inert medium, this has been used widely as a preliminar step for the other models due to the determination of parameters for single components and definition of temperature zones for their thermal decomposition reactions. Further, the dependence of parallel and consecutive models in the structural composition of biomasses (HC, C, L) provides a high accuracy over the kinetic modeling of thermal degradation, compared in this study with data from previous researches.

Finally, from the mass yields of products and their compositions obtained at the thermochemical conversion processes, the temperature was the most influent over the hydrogen and carbon monoxide production syngas produced by gasification; this influence is present as direct over the production of bio-oil and as inverse over the biochar mass yield in pyrolysis tests. This property indicates the thermal energy present in the process, which is the key for decomposition reactions which are featured as endothermic. Moreover, the rice straw content in the biomass sample presents a remarkable influence of direct nature in combustion process, mostly over the production of hydrocarbons and carbon monoxide in the flue gas; this effect is related with the ash content in the biomass samples due to its role as catalyst for reactions of solid char formation in the previous stage of combustion.

The variation of air input set as a factor influences the combustion process as well, considering the oxygen supply as reactant for oxidation reactions; these are featured by their exothermicity which leads to an increase of the thermal energy in the surrounds.

Therefore, the addition of the rice straw to the rice husk samples improved the compositional features in the blend; however, this addition did not show any improvement over the thermal and energy features in the blend from its use for fuels or derivates production for industrial purposes, through the processes of combustion, gasification and pyrolysis.

References

Abu Bakar, M. & Titiloye, J. Catalytic pyrolysis of rice husk for bio-oil production. Journal of Analytical and Applied Pyrolysis, vol. 103, pag. 362 – 368 (2013). DOI: http://dx.doi.org/10.1016/j.jaap.2012.09.005Aguilar, J. Alternativas de aprovechamiento de la cascarilla de arroz en Colombia. Monografía. Sincelejo, Sucre, Colombia: Universidad de Sucre, 2009. URL: http://repositorio. unisucre.edu.co/bitstream/001/211/2/333.794S571.pdf.

Alves-Rocha, E. et al. Kinetics of pyrolysis of some biomasses widely available in Brazil. Journal of Thermal Analysis and Calorimetry, vol. 130, pag. 1445 – 1454 (2017). DOI: 10.1007/s10973-017-6138-2.

Anca-Couce, A. et al. How to determine consistent biomass pyrolysis kinetics in a parallel reaction scheme. Fuel, vol. 123, pag. 230 – 240 (2014).

Ashoor, S. & Sukumaran, R. Mild alkaline pretreatment can achieve high hydrolytic and fermentation efficiencies for rice straw conversion to bioethanol. Preparative Biochemistry & Biotechnology (2020) DOI: https://doi.org/10.1080/10826068.2020.1744007.

ASTM D1105 – 96 (Reapproved 2013). Standard Test Methods for Preparation of Extractive-Free Wood. ASTM International (Committee D07), West Conshohocken, PA, United States, (August 1st, 2013). DOI: 10.1520/D1105-96R13.

ASTM D1106 – 96 (Reapproved 2013). Standard Test Methods for Acid-Insoluble Lignin in Wood. ASTM International (Committee D07), West Conshohocken, PA, United States, (August 1st, 2013). DOI: 10.1520/D1105-96R13.

ASTM D1110 – 84 (Reapproved 2013). Standard Test Methods for Water Solubility of Wood. ASTM International (Committee D07), West Conshohocken, PA, United States, (August 1st, 2013). DOI: 10.1520/D1110-84R13.

ASTM D3588 – 98. Standard Practice for Calculating Heat Value, Compressibility Factor, and Relative Density of Gaseous Fuels. ASTM International (Committee D03), West Conshohocken, PA, United States, (April 1st, 2017). DOI: 10.1520/D3588-98R17E01.

ASTM D5373 - 16. Standard Test Methods for Determination of Carbon, Hydrogen and Nitrogen in analysis samples of Coal and Carbon in Analysis Samples of Coal and Coke. ASTM International (Committee D05), West Conshohocken, PA, United States, (September 1st, 2016). DOI: 10.1520/D5373-16.

ASTM D5865/D5865M - 19. Standard Test Methods for Gross Calorific Value of Coal and Coke. ASTM International (Committee D05), West Conshohocken, PA, United States, (June 1st, 2019). DOI: 10.1520/D5865_D5865M-19.

ASTM E11 – 20. Standard Specification for Woven Wire Test Sieve Cloth and Test Sieves. ASTM International (Committee E29), West Conshohocken, PA, United States, (April 1st, 2020)

ASTM E1755 – 01 (Reapproved 2015). Standard Test Method for Ash in Biomass. ASTM International (Committee E48), West Conshohocken, PA, United States, (June 1st, 2015). DOI: 10.1520/E1755-01R15.

ASTM E1756 – 08 (Reapproved 2015). Standard Test Method for Determination of Total Solids in Biomass. ASTM International (Committee E48), West Conshohocken, PA, United States, (June 1st, 2015). DOI: 10.1520/E175608R15.

ASTM E872 - 82 (Reapproved 2019). Standard Test Method for Volatile Matter in the Analysis of Particulate Wood Fuels. ASTM International (Committee E48), West Conshohocken, PA, United States, (June 1st, 2015). DOI: 10.1520/E0872-82R19.

Basu, Prabir. Biomass Gasification, Pyrolysis and Torrefaction: Practical design and Theory. Chapter 1 & 7. 3rd Edition. Academic Press, 2018. ISBN: 9780128130407.

Chang, K. et al. Enhanced Enzymatic Hydrolysis of Rice Straw Pretreated by Oxidants Assisted with Photocatalysis Technology. Materials, 11, 802 (2018). DOI: 10.3390/ma11050802

Chen, D. et al. Comparative study on the pyrolysis behaviors of rice straw under different washing pretreatments of water, acid solution, and aqueous phase bio-oil by using TG-FTIR and Py-GC/MS. Fuel, vol. 252, pag. 1 - 9 (2019). https://doi.org/10.1016/j.fuel.2019.04.086

CREG – Comisión de Regulación de Energía y Gas. Estadísticas de los Sectores Eléctrico, Gas Natural y GLP Colombiano: 2010 – 2018. Consumo Anual Total en el Departamento de Casanare. URL: https://www.creg.gov.co/sectores/energia-electrica.

Damiani, L. & Trucco, A. An Experimental Data Based Correction Method of Biomass Gasification Equilibrium Modeling. Journal of Solar Energy Engineering, Vol. 132:031011, pag. 1 – 11 (2010). DOI: https://bibliotecavirtual.uis.edu.co:2236/10.1115/1.4001463.

DANE. Boletín Técnico Encuesta Nacional de Arroz Mecanizado – ENAM-: II Semestre 2017. Edición en 2018. URL: https://www.dane.gov.co/files/investigaciones/boletines/arroz/bol_arroz_IIsem17.pdf.

Dhanavath, K. et al. Oxygen-steam gasification of karanja press seed cake: Fixed bed experiments, ASPEN Plus process model development and benchmarking with sawdust, rice husk and sunflower husk. Journal of Environmental Chemical Engineering, vol. 6, pag. 3061 – 3069 (2018).

Ding, Y. et al. Kinetic model and parameters study of lignocellulosic biomass oxidative pyrolysis. Energy, vol. 181, pag. 11 – 17 (2019).

Dong, Q. et al. Pyrolysis behavior of raw/torrefied rice straw after different demineralization processes. Biomass and Bioenergy, vol. 119, pag. 229 - 236 (2018). https://doi.org/10.1016/j.biombioe.2018.09.032.

Duan, F. et al. Pollutant emission characteristics of rice husk combustion in a vortexing fluidized bed incinerator. Journal of Environmental Sciences (2013), vol 25, pp. 335 – 339.

EPA - United States Environmental Protection Agency. Global Greenhouse Gas Emissions Data (Based on data from IPCC 2014). [Online: 17/05/2019] – Available at: https://www.epa.gov/ghgemissions/global-greenhouse-gas-emissions-data.

Evtuguin, D. et al. Characterization of an acetylated heteroxylan from Eucalyptus globulus Labill. Carbohydrate Research, Vol. 338, Pag. 597 – 604 (2003). DOI: https://doi.org/10.1016/S0008-6215(02)00529-3

Fang, M. et al. Experimental study on rice husk combustion in a circulating fluidized bed. Fuel Processing Technology, Vol. 85, Pag. 1273 – 1282 (2004).

Ferreira-Beltrán, D. Palencia-Blanco, C. Utilización de catalizadores heteropoliácidos para el mejoramiento de la producción de aromáticos a partir de pirólisis de llanta usada. Thesis to request to title of Chemical Engineer. Universidad Industrial de Santander, Bucaramanga, 2015.

Friedman, H. Kinetics of thermal degradation of char-forming plastics from thermogravimetry. Application to a phenolic plastic. Journal of Polymer Science Part C: Polymer Symposia, vol. 6:1, pag. 183 – 195 (1964). DOI: https://doi.org/10.1002/polc.5070060121.

Fukuda, Suneerat. Pyrolysis Investigation For Bio-Oil Production From Various Biomass Feedstocks in Thailand. International Journal of Green Energy (2015), Vol. 12, Pag. 215 – 224 (2015).

Gautam, N. & Chaurasia, A. Study on kinetics and bio-oil production from rice husk, rice straw, bamboo, sugarcane bagasse and neem bark in a fixed-bed pyrolysis process. Energy, vol. 190 – 116434, pag. 1 – 13 (2020). DOI: https://doi.org/10.1016/j.energy.2019.116434.

Ghaly, A. & Mansaray, K. Comparative Study on the thermal degradation of rice husks in various atmospheres. Energy Sources, vol. 21:10, pag. 867-881 (1999). DOI: 10.1080/00908319950014254.

Goenka, R. et al. Kinetic Analysis of Biomass and Comparison of its Chemical Compositions by Thermogravimetry, Wet and Experimental Furnace Methods. Waste Biomass Valor, Vol. 6, pag. 989 – 1002 (2015). DOI: 10.1007/s12649-015-9402-3

Grigiante, M. et al. Analysis of the impact of TG data sets on activation energy (Ea). Journal of Thermal Analysis and Calorimetry, vol. 129, pag. 553 – 565 (2017). DOI: 10.1007/s10973-017-6122-x.

Guo, J. & Lua, A. Kinetic study on pyrolytic process of oil-palm solid waste using two-step consecutive reaction model. Biomass and Bioenergy, vol. 20:3, pag. 223 – 233 (2001). DOI: https://doi.org/10.1016/S0961-9534(00)00080-5.

Gyul'maliev, A. et al. Mathematical Simulation of the Pyrolysis of Biomass for the Manufacture of Synthesis Gas and Coke. Solid fuel chemistry, vol. 46, pag. 164 – 167 (2012). DOI: 10.3103/S0361521912030056.

Han, J. et al. Development of the Process Model and Optimal Drying Conditions of Biomass Power Plants. ACS Omega, vol. 5, pag. 2811 – 2818 (2020). DOI: https://dx.doi.org/10.1021/acsomega.9b03557.

Havilah, P. et al. Combustion characteristics and kinetic parameter estimation of *Lantana camara* by thermogravimetric analysis. Biofuels, vol. 10:3, pag. 365 – 372 (2019). DOI: 10.1080/17597269.2016.1259521.

Hrbek, J., & Vreugdenhil, B. (2020, January 30). The past, present and future for biomass gasification [Webinar]. In IEA Bioenergy Webinars. Retrieved from https://www.ieabioenergy.com/publications/iea-bioenergy-webinar-the-past-present-and-future-for-biomass-gasification/

Hu, Y., et al. Investigation on the co-pyrolysis mechanism of seaweed and rice husk with multi – method comprehensive study. Renewable Energy, Vol. 132, Pag. 266 – 277 (2019).

Janković, B. Kinetic analysis of the nonisothermal decomposition of potassium metabisulfite using the model-fitting and isoconversional (model-free) methods. Chemical Engineering Journal, vol. 139, issue 1, pag. 128 – 135 (2008). https://doi.org/10.1016/j.cej.2007.07.085

Janvijitsakul, K. & Kuprianov, V. Major gaseous and PAH emissions from a fluidized-bed combustor firing rice husk with high combustion efficiency. Fuel Processing Technology, Vol. 89, Pag. 777 – 782 (2008).

Jin, X. et al. Co.pyrolysis of rice straw and water hyacinth: Characterization of products, yields and biomass interaction effect. Biomass and Bioenergy, vol. 127 – 105281, pag. 1 – 7 (2019). DOI: https://doi.org/10.1016/j.biombioe.2019.105281.

Keszei, E. Chemical Thermodynamics, An Introduction. © Springer-Verlag Berlin Heidelberg (2012). DOI: 10.1007/978-3-642-19864-9.

Khonde, Ruta; Chaurasia, Ashish. Rice husk gasification in a two-stage fixed bed gasifier: Production of hydrogen rich syngas and kinetics. International Journal of Hydrogen

Energy, Vol. 41, Pag. 8793 – 8802 (2016). DOI: http://dx.doi.org/10.1016/j.ijhydene.2016.03.138.

Khonde, R. et al. Prediction of product gas composition from biomass gasification by the method of Gibbs free energy minimization. Energy Sources, Part A: Recovery, Utilization, and Environmental Effects (2019), DOI: 10.1080/15567036.2019.1624890.

Kumar Gupta, N. et al. The effect of temperature and hemicellulose-lignin, cellulose-lignin and cellulose-hemicellulose of char yield from the slow pyrolysis of rice husk. Energy Sources, Part A: Recovery, utilization, and environmental effects, Vol. 38, Pag. 1428 – 1434 (2016). DOI: 10.1080/15567036.2014.941518.

Kumar, M. et al. Thermal degradation of rice husk: Effect of pre-treatment on kinetic and thermodynamic parameters. Fuel, vol. 268 - 117164, pag. 1 – 15 (2020). https://doi.org/10.1016/j.fuel.2020.117164

Laougé, Z. & Merdun, H. Pyrolysis and combustion kinetics of Sida cordifolia L. using thermogravimetric analysis. Bioresource Technology, vol. 299 – 122602, ´pag 1-7 (2020). https://doi.org/10.1016/j.biortech.2019.122602

Logan, S. The Origin and Status of the Arrhenius Equation. Journal of Chemical Education, Vol. 59, Number 4, (1982).

Lopes, F. et al. Combustion reaction kinetics of guarana seed residue applying isoconversional methods and consecutive reaction scheme. Bioresource Technology, vol. 219, Pag. 392 – 402 (2016). DOI: http://dx.doi.org/10.1016/j.biortech.2016.07.099.

Lopes, F. et al. Thermal decomposition kinetics of guarana seed residue through thermogravimetric analysis under inert and oxidizing atmospheres. Bioresource Technology, vol. 270, pag. 294 – 302 (2018). DOI: https://doi.org/10.1016/j.biortech.2018.09.021

Lopes, I. et al. Biomass gasification in fluidized beds: A review of biomass moisture content and operating pressure effects. Renewable and Sustainable Energy Reviews, vol. 94, pag. 998 – 1023 (2018). DOI: https://doi.org/10.1016/j.rser.2018.06.042.

Lopes, I. et al. Sugarcane bagasse gasification: Simulation and analysis of different operating parameters, fluidizing media, and gasifier types. Biomass and Bioenergy, vol. 122, pag. 433 – 445 (2019). DOI: https://doi.org/10.1016/j.biombioe.2019.01.051.

Luangkiattikhum, P. et al. Non-isothermal thermogravimetric analysis of oil-palm solid wastes. Bioresource technology, vol. 99, pag. 986 – 997 (2008). DOI: 10.1016/j.biortech.2007.03.001

Luo, Q. et al. The hydriding kinetics of Mg-Ni based hydrogen storage alloys: A comparative study on Chou model and Jander model. International Journal of Hydrogen Energy, vol. 35, pag. 7842 – 7849 (2010). DOI: 10.1016/j.ijhydene.2010.05.073.

Ma, Z. et al. Gasification of rice husk in a downdraft gasifier: The effect of equivalence ratio on the gasification performance, properties, and utilization analysis of byproducts of char and tar. BioResources, vol. 10(2), pag. 2888 – 2902 (2015).

Mantananont, N. & Patumsawad, S. The effect of the combustion of rice husk with thai lignite in a fixed bed reactor on combustion characteristics and pollutant emissions. Energy Sources, Part A: Recovery, Utilization, and Environmental Effects, vol. 36:5, pag. 471 – 478 (2014). DOI: 10.1080/15567036.2011.638971.

Marques, G. Valorización de diferentes cultivos lignocelulósicos para la fabricación de pasta de papel: Caracterización química, modificación estructural de sus constituyentes orgánicos durante los procesos de cocción y blanqueo y aplicaciones

biotecnológicas. Project for application to PhD. degree in Chemical Sciences. Universidad de Sevilla, Sevilla, España (2010).

Marrugo, G. et al. Characterization of Colombian Agroindustrial Biomass Residues as Energy Resources. Energy & Fuels, Vol. 30, Pag. 8386 – 8398 (2016). DOI: 10.1021/acs.energyfuels.6b01596

Migo-Sumagang, M. et al. Optimization of a downdraft furnace for rice straw based heat generation. Renewable Energy, Vol. 148, Pag. 953 – 963 (2020). DOI: https://doi.org/10.1016/j.renene.2019.11.001

Millers, R. & Pelite, U. Survey of Control Characteristics of Circular Air Dampers in Variable Air Volume Ventilation Systems. Energy Procedia, vol. 96, pag. 294 – 300 (2016). DOI: 10.1016/j.egypro.2016.09.152

Mishra, G. & Bhaskar, T. Non isothermal model free kinetics for pyrolysis of rice straw. Bioresource Technology, vol. 169, pag. 614 – 621 (2014) http://dx.doi.org/10.1016/j.biortech.2014.07.045

Moore, W. & Johnson, D. Procedures for the chemical analysis of wood and wood products. Forest Products Laboratory Forest Service. U.S. Department of Agriculture (1967).

Natarajan, E. & Ganapathy, E. Pyrolysis of rice husk in a fixed bed reactor. World Academy of Science, Engineering and Technology, vol. 56, pag 504 - 508 (2009).

Ngamchompoo, W. et al. Experimental investigation on rice straw gasification in a cyclone gasifier. BioResources, vol. 13(4), pag. 7654 – 7670 (2018).

OECD – Organisation for Economic Co-operation and Development. Emission of air pollutants (Air emissions by source). [Online: 17/05/2019] – Available at: https://stats.oecd.org/Index.aspx?DataSetCode=AIR_EMISSIONS#.

Okasha, F. Staged combustion of rice straw in a fluidized bed. Experimental Thermal and Fluid Science, Vol. 32, pag. 52 – 59 (2007). DOI: 10.1016/j.expthermflusci.2007.01.006.

Páez-Duque, S. Suárez-Acelas, I. Evaluación de una unidad piloto a escala laboratorio de vaporreformado usando bajas concentraciones de agua. Thesis to request to title of Chemical Engineer. Universidad Industrial de Santander, Bucaramanga, 2016.

Paniagua, S. et al. Simultaneous thermogravimetric and mass spectrometric monitoring of the pyrolysis, gasification and combustion of rice straw. Journal of Thermal

Analysis and Calorimetry, vol. 121, pag. 603 – 611 (2015) DOI: 10.1007/s10973-015-4632-y.

Parés-Casanova, Pere M. & Kucherova, Irina. Nota técnica: Alternativas de gestión de la paja de arroz en la albufera de Valencia. 2017. DOI: 10.12706/itea.2017.015. URL: http://www.ivia.gva.es/documents/161862582/162455759/Nota+t%C3%A9cnica_Alternativas+de+gesti%C3%B3n+de+la+paja+de+arroz+en+la+Albufera+de+Valencia.pdf/cc127504-cf3c-4142-9345d33e5c56c649.

Pérez-Maqueda, L. & Criado, J. The accuracy of senum and yang's approximations to the Arrhenius integral. Journal of Thermal Analysis and Calorimetry. Vol 60, 909 – 915 (2000).

Press, W. et al. Numerical Recipes: The Art of Scientific Computing (Third Edition), Section 17.1 Runge-Kutta Method, Cambridge University Press (2007).

Qi, Boyang et al. Study of chemical looping co-gasification (CLCG) of coal and rice husk with an iron-based oxygen carrier via solid – solid reactions. Journal of the Energy Institute. (2017). https://doi.org/10.1016/j.joei.2017.12.006.

Reshad, A. et al. Thermal decomposition and kinetics of residual rubber seed cake and shell. Journal of Thermal Analysis and Calorimetry, vol. 129, pag. 577 – 592 (2017). DOI: 10.1007/s10973-017-6136-4.

Rueda-Ordóñez, Y. et al. An empirical model to obtain the kinetic parameter of lignocellulosic biomass pyrolysis in an independent parallel reactions scheme. Fuel Processing Technology, vol. 140, pag. 222 – 230 (2015). DOI: http://dx.doi.org/10.1016/j.fuproc.2015.09.001.

Rueda-Ordóñez, Y. et al. Assessment of the thermal decomposition kinetics of empty fruit bunch, kernel shell and their blend. Bioresource Technology, vol. 292 - 121923, pag. 1 – 11 (2019). DOI: https://doi.org/10.1016/j.biortech.2019.121923.

Rueda-Ordóñez, Y. & Tannous, K. Isoconversional kinetic study of the thermal decomposition of sugarcane straw for thermal conversion processes. Bioresource Technology, vol. 196, pag. 136 – 144 (2015). DOI: http://dx.doi.org/10.1016/j.biortech.2015.07.062.

Rueda-Ordóñez, Y. & Tannous, K. Drying and thermal decomposition kinetics of sugarcane straw by nonisothermal thermogravimetric analysis. Bioresource Technology, vol. 264, pag. 131 – 139 (2018). DOI: https://doi.org/10.1016/j.biortech.2018.04.064.

Saffe, A. et al. Pyrolysis kinetics of regional agro-industrial wastes using isoconversional methods. Biofuels, vol. 10:2, pag. 245 – 257 (2019). DOI: 10.1080/17597269.2017.1316144

Salvador Escoda S.A. Manual práctico de ventilación – catálogo técnico (con la colaboración de Soler & Palau), 2nd edition. Last review: (05/22/2020) [Online] Available at: https://www.salvadorescoda.com/tecnico/VE/Manual-Ventilacion.pdf.

Santos, C. et al. Thermal conversion of defective coffee beans for energy purposes: Characterization and kinetic modeling. Renewable Energy, vol. 147, pag. 1275 – 1291 (2020). https://doi.org/10.1016/j.renene.2019.09.052.

Santos, F. et al. Productive potential and quality of rice husk and straw for biorefineries. Biomass Conversion and Biorefinery, vol. 7, pag. 117 – 126 (2017). DOI: 10.1007/s13399-016-0214-x.

Santos, K. et al. Bagasse pyrolysis: A comparative study of kinetic models. Chemical engineering communications, vol. 199:1, pag. 109 – 121 (2012). DOI: 10.1080/00986445.2011.575906.

Sasauchi, K. (2019, May 27). Present situation and problems of small biomass gasification plants in Japan [Seminar session]. In EUBCE 2019 contents. Retrieved from https: https://www.eubce.com/wp-content/uploads/2019/02/3-present-situation-and-problems-of-small-scale-gasification-plants-in-Japan_K_Sasauchi.pdf.

Sattar, H. et al. Thermal and kinetic study of rice husk, corn cobs, peanut crust and khushab coal under inert (N_2) and oxidative (dry air) atmospheres. Renewable Energy, Vol. 149, Pag. 794 – 805 (2020) https://doi.org/10.1016/j.renene.2019.12.020.

Scopus® – Registered trademark of Elsevier B.V. Analyze search results. [Online 18/05/2020]. Available at: https://bibliotecavirtual.uis.edu.co:2150/search/form.uri?display=basic

Sfakiotakis, S. & Vamvuka, D. Development of a modified independent parallel reactions kinetic model and comparison with the distributed activation energy model for the pyrolysis of a wide variety of biomass fuels. Bioresource Technology, vol. 197, pag. 434 – 442 (2015). DOI: http://dx.doi.org/10.1016/j.biortech.2015.08.130.

Singh, S. & Sawarkar, A. Thermal decomposition aspects and kinetics of pyrolysis of garlic stalk. Energy Sources, Part A: Recovery, Utilization, and Environmental Effects, pag. 1 – 12 (2020). DOI: 10.1080/15567036.2020.1716891.

Sittisun, P. et al. Biomass gasification in a fixed bed downdraft reactor with oxygen enriched air: a modified equilibrium modeling study. Energy Procedia, vol. 160, pag. 317 – 323 (2019). DOI: 10.1016/j.egypro.2019.02.163.

Snavely, K. and Subramaniam, B. Thermal Conductivity Detector Analysis of Hydrogen Using Helium Carrier Gas and HayeSep® D Columns. Journal of Chromatographic Science, Vol. 36, pag. 191 - 196, 1998. DOI: https://doi.org/10.1093/chromsci/36.4.191

Statgraphics®. Diseño de experimentos – Diseño de superficie de respuesta. Statpoint, Inc. – Rev. 09/14/2006 (Online) last review: 05/22/2020. Available at: https://www.statgraphics.net/wp-content/uploads/2011/12/tutoriales/DDE%20-%20Diseno%20de%20Superficies%20de%20Respuesta.pdf.

Sullivan, A. & Ball, R. Thermal decomposition and combustion chemistry of cellulosic biomass. Atmospheric Environment, vol. 47, pag. 133 – 141 (2012). DOI: https://doi.org/10.1016/j.atmosenv.2011.11.022.

Susastriawan, A. et al. Comparison of the gasification performance in the downdraft fixed-bed gasifier fed by different feedstocks: Rice husk, sawdust, and their mixture. Sustainable Energy Technologies and Assessments, vol. 34, pag. 27 – 34 (2019). DOI: https://doi.org/10.1016/j.seta.2019.04.008.

Tai, H. & Chen, C. Analyzing the pyrolysis kinetics of rice straw, bagasse, and mixtures thereof and product energy yield. Journal of the Chinese Institute of Engineers, vol. 39:3, pag. 381 – 389 (2016). DOI: https://doi.org/10.1080/02533839.2015.1112249.

TAPPI T 203 cm 99. Alpha-, beta- and gamma-cellulose in pulp. TAPPI© (Chemical Properties Committee of the Process and Product Quality Division), Peachtree Corners, GA, United States (1999).

Toonen, A. & Van Loon, R. Hydrogen Detection with a TCD using Mixed Carrier Gas on the Agilent Micro GC. Application Note. © Agilent Technologies, Inc. 2013. [Online] Available at: https://www.srainstruments.fr/wp-content/uploads/2018/08/5991-3199EN_Hydrogen-detection-with-a-TCD-using-mixed-carrier-gas.pdf. Last review: 07/29/2020.

Tsai, T., Chang, Y. Fast pyrolysis of rice husk: Products yields and compositions. Bioresource Technology (2007), vol 98, pp. 22 – 28.

Unchaisri, T. & Fukuda, S. Co-firing of coal and rice straw pellet in a circulating fluidized-bed reactor. Energy Procedia, vol. 138, pag. 766 – 771 (2017). DOI: 10.1016/j.egypro.2017.10.051.

UPV – Universitat Politècnica de València. Resultados y discusión: Cascarilla de arroz de Arrocerías Herba, S.A. y Paja de arroz de Catarroja (Valencia). [Online] Last review (22/05/2019). Available at: http://www.upv.es/resiagri/ficheros/i0106.pdf; http://www.upv.es/resiagri/ficheros/i0003.pdf.

Valente, M. et al. Investigation of grape marc combustion using thermogravimetric analysis. Kinetic modeling using an extended independent parallel reaction (EIPR). Fuel processing technology, vol. 131, pag. 297 – 303 (2015).

Vecino-Mantilla, S. Desarrollo de un método extractivo de la fracción fenólica presente en el bio-oil producido por pirólisis intermedia. Project presented as request for application to Master's Degree in Chemical Engineering. Universidad Industrial de Santander, Bucaramanga, 2014.

Vecino Mantilla, S. et al. Comparative study of bio-oil production from sugarcane bagasse and palm empty fruit bunch: Yield optimization and bio-oil characterization. Journal of Analytical and Applied Pyrolysis, vol. 108, pag. 284 – 294 (2014). DOI: http://dx.doi.org/10.1016/j.jaap.2014.04.003.

Vieira, F. et al. Optimization of slow pyrolysis process parameters using a fixed bed reactor for biochar yield from rice husk. Biomass and Bioenergy, vol. 132 – 105412, pag. 1 – 11 (2020). DOI: https://doi.org/10.1016/j.biombioe.2019.105412.

Vonk, G. & Piriou, B. Comparative analysis of wood and solid recovered fuels gasification in a downdraft fixed bed reactor. France, Waste Management, vol. 85, pp. 106 - 120 (2019).

Vyazovkin, S.; Wight, C. Model-free and model-fitting approaches to kinetic analysis of isothermal and nonisothermal data. Thermochimica Acta, 340 – 341, Pag. 53 – 68 (1999).

Vyazovkin, S. et al. ICTAC Kinetics Committee recommendations for performing kinetic computations on thermal analysis data. Thermochimica Acta, vol. 520, pag. 1 – 19 (2011). DOI: 10.1016/j.tca.2011.03.034.

Wang, C. et al. Catalytic performance of potassium in lignocellulosic biomass pyrolysis based on an optimized three-parallel distributed activation energy model. Bioresource Technology, vol. 281, pag. 412 – 420 (2019). https://doi.org/10.1016/j.biortech.2019.02.118.

Wang, T. et al. Combustion behavior of refuse-derived fuel production from sewage sludge and rice husk/wood sawdust using thermogravimetric and mass spectrometric analyses. Journal of Cleaner Production, Vol. 222, Pag. 1 – 11 (2019) https://doi.org/10.1016/j.jclepro.2019.03.016.

Weerachanchai, P. et al. Comparison of pyrolysis kinetic models for thermogravimetric analysis of biomass. Suranaree Journal of Science and Technology, vol. 17 (4), pag. 1 – 14 (2010).

Weldekidan, H. et al. Energy Conversion Efficiency of Pyrolysis of Chicken Litter and Rice Husk Biomass. Energy & Fuels, Vol. 33, Pag. 6509 – 6514 (2019) DOI: 10.1021/acs.energyfuels.9b01264

Xu, X. et al. Comparative Pyrolysis Characteristics and Kinetics of Typical Hardwood in Inert and Oxygenous Atmosphere. Applied Biochemistry and Biotechnology (2020), vol. 190, pag. 90 – 112 (2020). DOI: https://doi.org/10.1007/s12010-019-03089-9.

Yakout, S. Physicochemical characteristics of biochar produced from rice straw at different pyrolysis temperature for soil amendment and removal of organics. Proceedings of the National Academy of Sciences, India Section A: Physical Sciences, vol. 87, pag. 207 – 214 (2017). DOI: 10.1007/s40010-017-0343-z.

Yin, Y. et al. Kinetic Analysis of Co-Firing of Corn Stalk and Paper Sludge Using Model-Fitting and Model-Free Methods. Journal of Energy Resources Technology, vol. 142/042301, pag. 1 – 8 (2020).

Zhao, S. et al. Experimental Investigation of Rice Straw and Model Compound Oxidative Pyrolysis by in Situ Diffuse Reflectance Infrared Fourier Transform and Coupled Thermogravimetry−Differential Scanning Calorimetry/Mass Spectrometry Method. Energy & Fuels, vol. 29, pag. 4361 – 4372 (2015). DOI: 10.1021/acs.energyfuels.5b00583

Zhu, H. & Liu, N. Thermal decomposition of biomass and shallow soil mixtures. Fire safety journal (2020), DOI: https://doi.org/10.1016/j.firesaf.2020.102990

Appendixes

Appendix A

Table 15.

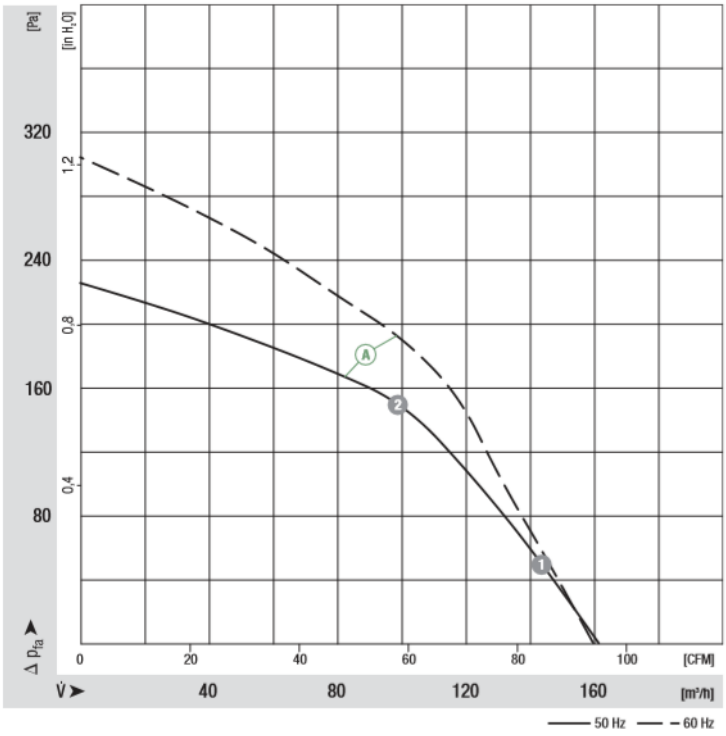
List of reaction models used for the reaction kinetics description used by Jankovic (Jankovic, 2008).

No.	Symbol	Reaction model	f(α)	g(α)
1	P1	Power law	$4 \propto^{3/4}$	$\propto^{1/4}$
2	P2	Power law	$3 \propto^{2/3}$	$\propto^{1/3}$
3	P3	Power law	$2 \propto^{1/2}$	$\propto^{1/2}$
4	P4	Power law	$(2/3) \propto^{-1/2}$	$\propto^{3/2}$
5	R2	Phase-boundary controlled reaction (Contracting area, i.e., bidimensional shape)	$2(1-\propto)^{1/2}$	$[1-(1-\propto)^{1/2}]$
6	R3	Phase-boundary controlled reaction (Contracting volume, i.e., tridimensional shape)	$3(1-\propto)^{2/3}$	$[1-(1-\propto)^{1/3}]$
7	F1	First-order (Mampel)	$(1-\propto)$	$-ln(1-\propto)$
8	A2	Avrami-Erofe'ev (m=2)	$2(1-\propto)[-ln(1-\propto)]^{1/2}$	$[-ln(1-\propto)]^{1/2}$
9	A3	Avrami-Erofe'ev (m=3)	$3(1-\propto)[-ln(1-\propto)]^{2/3}$	$[-ln(1-\propto)]^{1/3}$
10	A4	Avrami-Erofe'ev (m=4)	$4(1-\propto)[-ln(1-\propto)]^{3/4}$	$[-ln(1-\propto)]^{1/4}$
11	D1	One-dimensional diffusion	$1/(2 \propto)$	$\propto^2$
12	D2	Two-dimensional diffusion (bidimensional particle shape) Valensi equation	$[-ln(1-\propto)]^{-1}$	$(1-\propto)\ln(1-\propto)+\propto$
13	D3	Three-dimensional diffusion (tridimensional particle shape) Jander equation	$(3/2)(1-\propto)^{2/3}[1-(1-\propto)^{1/3}]^{-1}$	$[1-(1-\propto)^{1/3}]^2$
14	D4	Three-dimensional diffusion (tridimensional particle shape) Ginstling-Brounshtein	$(3/2)[(1-\propto)^{-1/3}-1]^{-1}$	$(1-(2 \propto)/3)-(1-\propto)^{2/3}$

Appendix B

Figure 34.

Parametric curve of operation of centrifugal fan with a rotor diameter of 108 mm, working at 1800 rpm.*



**Source: centrifugal fans and blowers (version 07). Ebm papst, Germany (2007). [Online] Available at: https://www.ebmpapst.com/media/content/info-center/downloads_10/catalogs/centrifugal_fans_1/Centrifugal_fans_2007_EN.pdf last review: [07/01/2020]*

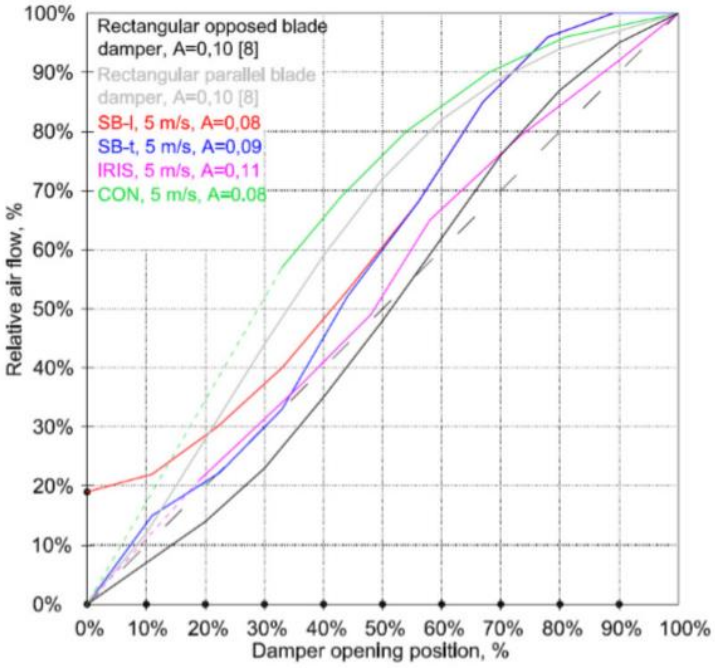
Table 16.

Equations applied for the real air flow determination and the opening angle calculation in the damper.

Description	*Equation*
Obtained parametric equation at the electric motor speed (3450 rpm) based in the catalog data.	$\Delta P_{pump} = -0.011 * Q_{fan}^2 - 0.1039 * Q_{fan} + 1086.8$
Equation of the curve regression performed from the experimental data of the single blade damper without sealing (Millers & Pelite, 2016)	$\%Qfan = 1x10^{-9} * \%_{opening}^6 - 4x10^{-7} * \%_{opening}^5 + 1x10^{-5} * \%_{opening}^4 + 0.0017 * \%_{opening}^3 + 0.0496 * \%_{opening}^2 + 0.0848 * \%_{opening} + 19.043$

Figure 35.

Control features of various tested dampers (Millers & Pelite, 2016) at similar air flow velocities, approaching in the single blade damper without a sealing (SB-l) in the present study.



Appendix C

Figure 36.

Calibration curve and equation for the temperature measured by the furnace and the measured through an additional thermocouple connected to a multimeter.

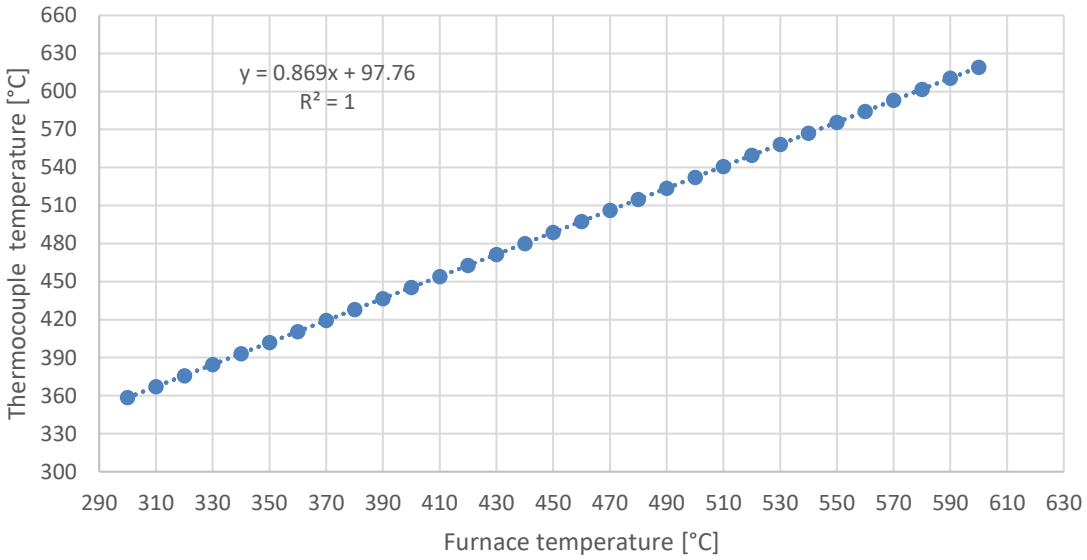


Figure 37.

Temperature profiles measured all along the pyrolysis reactor, at the center of its cross-sectional area, at various constant temperatures [°C] set in the furnace.

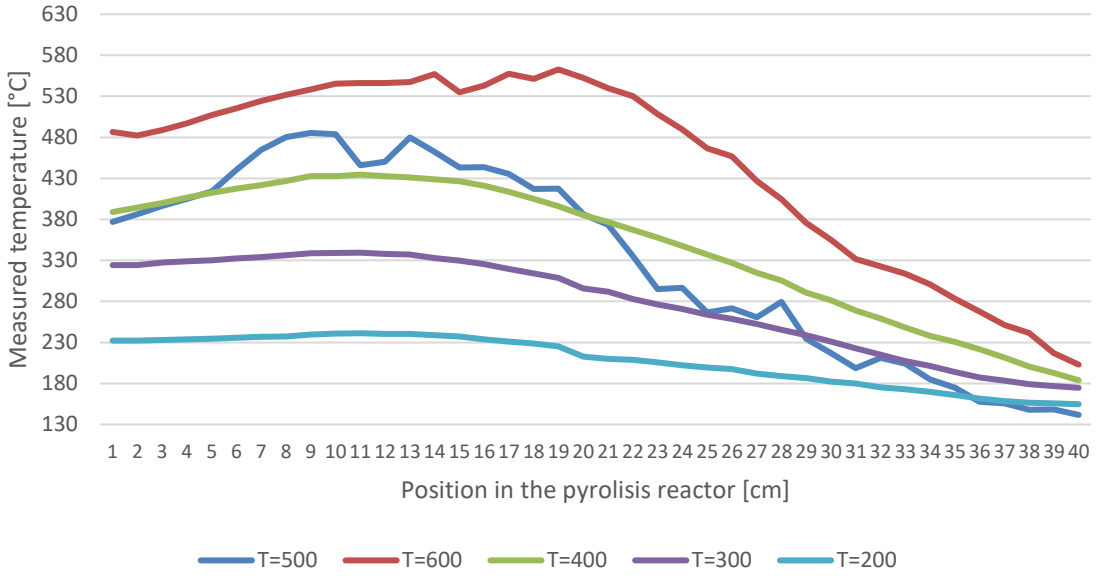
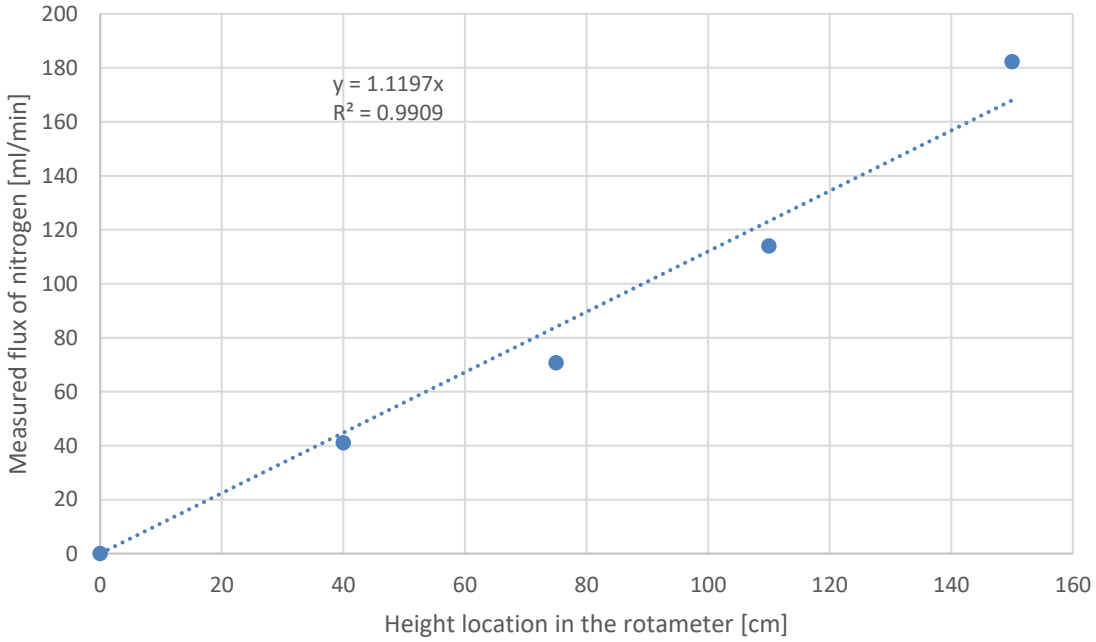


Figure 38.

Calibration curve for the flux regulation of nitrogen in the rotameter.



Appendix D

Figure 39.

Linear regression performance over the nitrogen content measurement in the gas chromatograph in terms of its peak area, as a function of the volume percentage of this component in the gas sample.

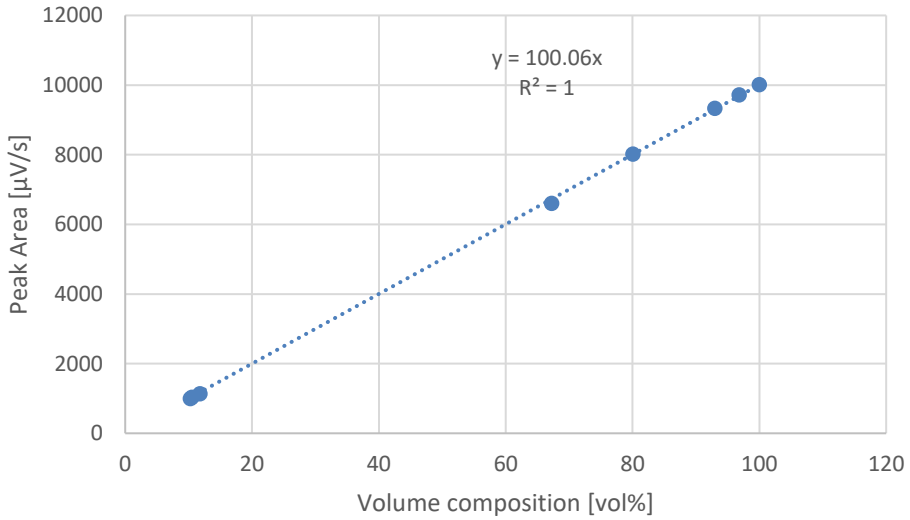


Figure 40.

Linear regression performance over the hydrogen content measurement in the gas chromatograph in terms of its peak area, as a function of the volume percentage of this component in the gas sample.

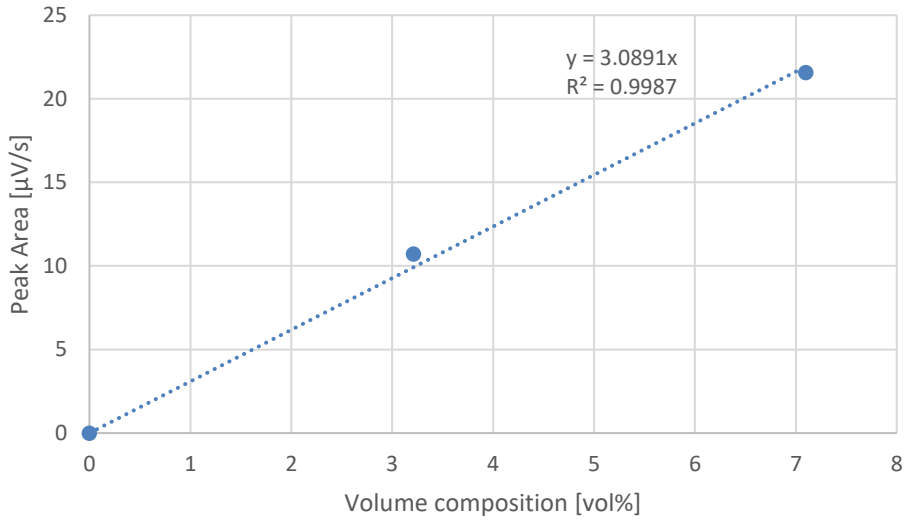


Figure 41.

Linear regression performance over the methane content measurement in the gas chromatograph in terms of its peak area, as a function of the volume percentage of this component in the gas sample.

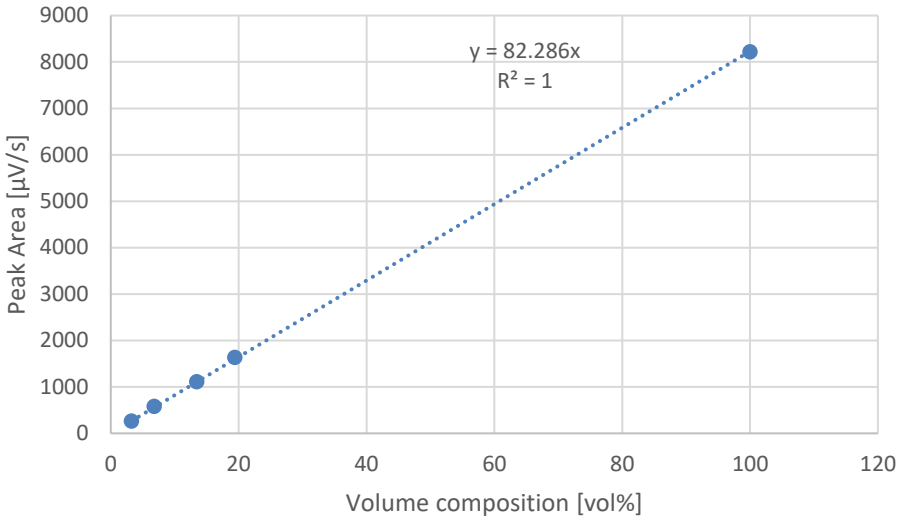


Figure 42.

Linear regression performance over the carbon monoxide content measurement in the gas chromatograph in terms of its peak area, as a function of the volume percentage of this component in the gas sample.

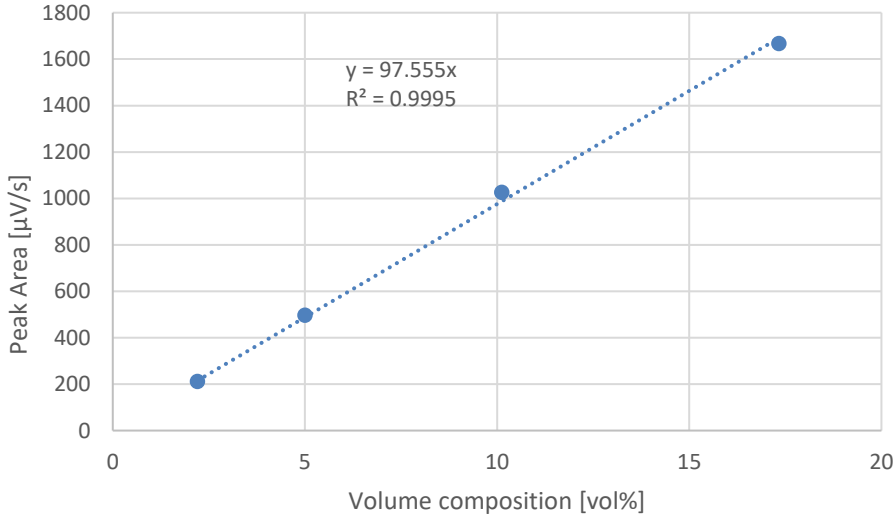
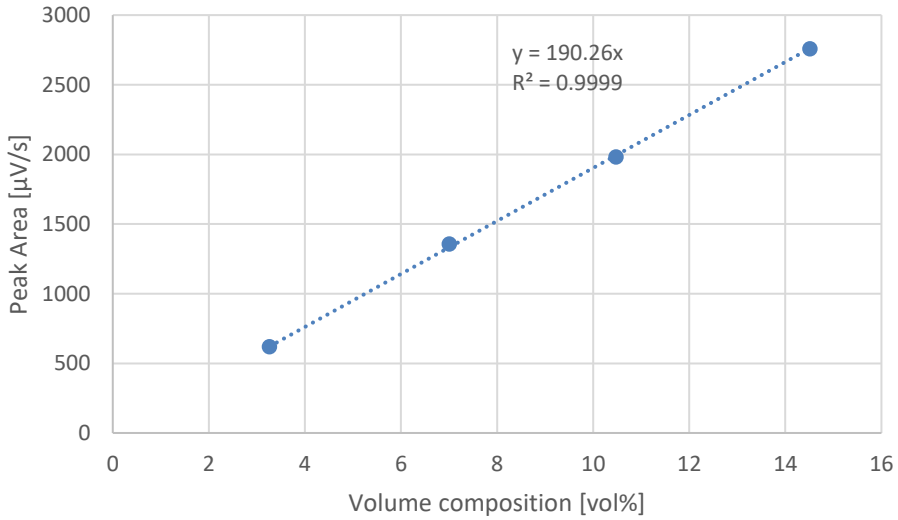


Figure 43.
Linear regression performance over the carbon dioxide content measurement in the gas chromatograph in terms of its peak area, as a function of the volume percentage of this component in the gas sample.



Appendix E

Figure 44.

Correlation for the linear regression performed to the experimental data obtained from the loose bulk density measurement as a function of the rice straw mass percentage in the sample.

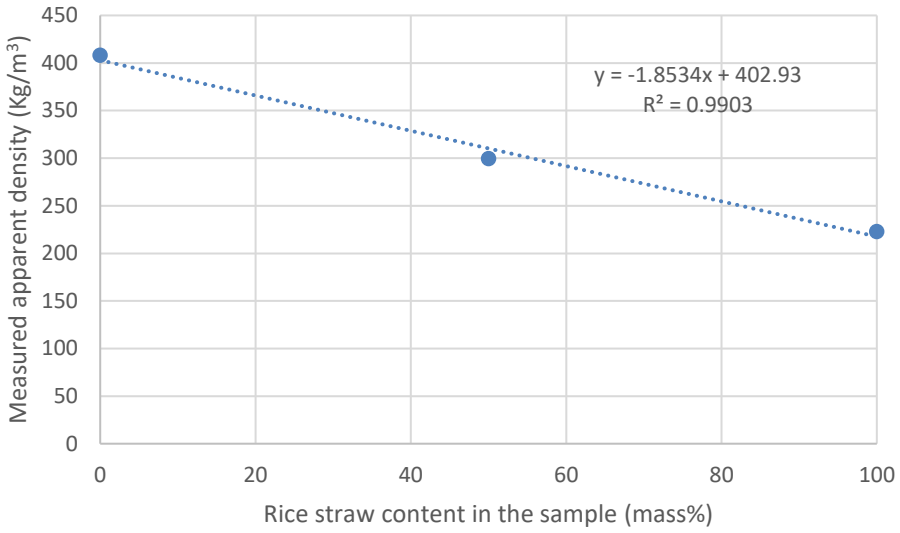


Figure 45.

Correlation from the linear regression applied in the experimental results of the ash content measurement as a function of the rice straw content in the biomass blend.

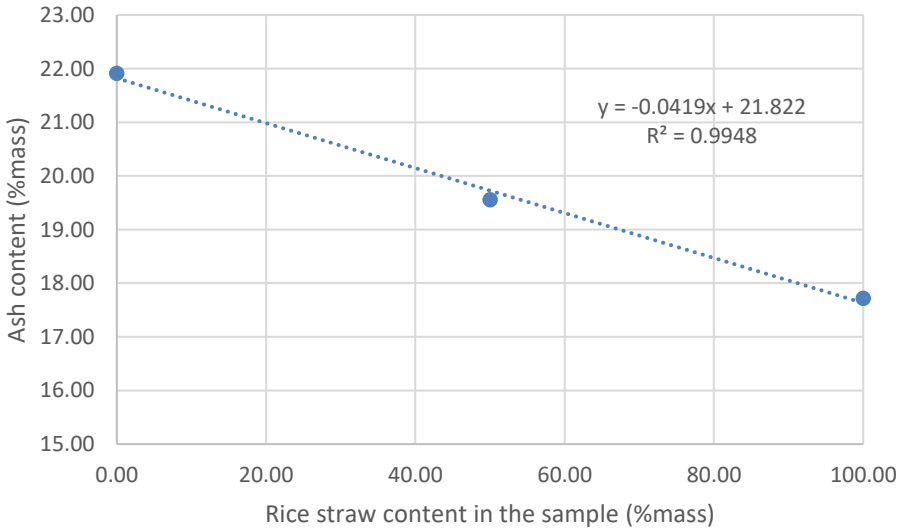


Figure 46.

Linear regression performance over the tests data obtained for the carbon content measurement, as a function of the rice straw mass percentage in the sample.

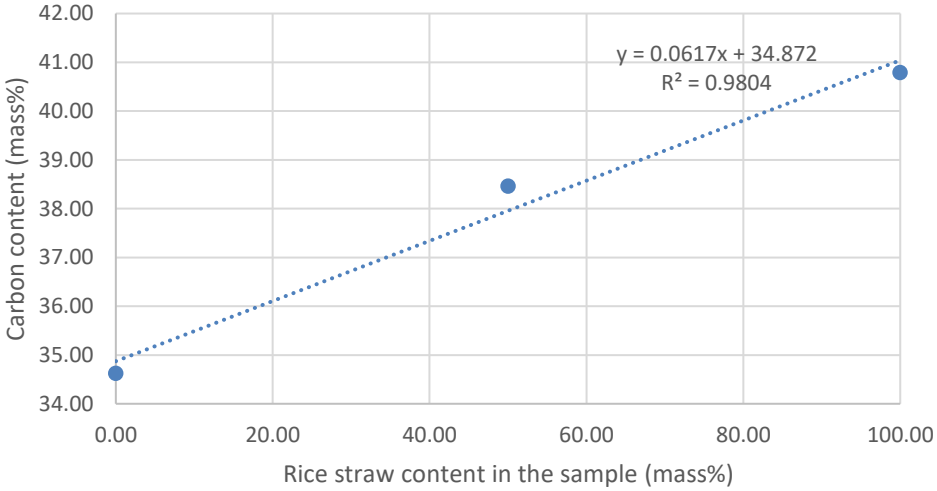


Figure 47.

Correlation obtained since the linear regression application over the experimental results of the hydrogen content determination, as a function of the rice straw content in the biomass blend.

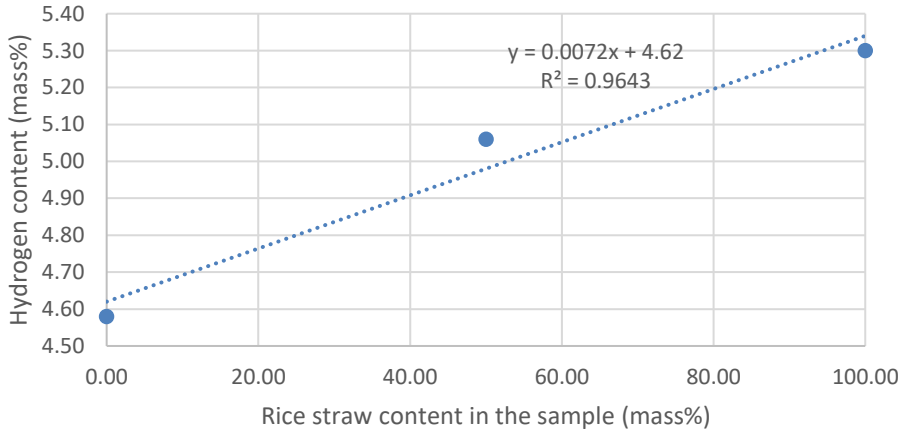


Figure 48.

Linear regression application in the experimental results obtained from the nitrogen content measurement in the biomass sample, as a function of its rice straw content.

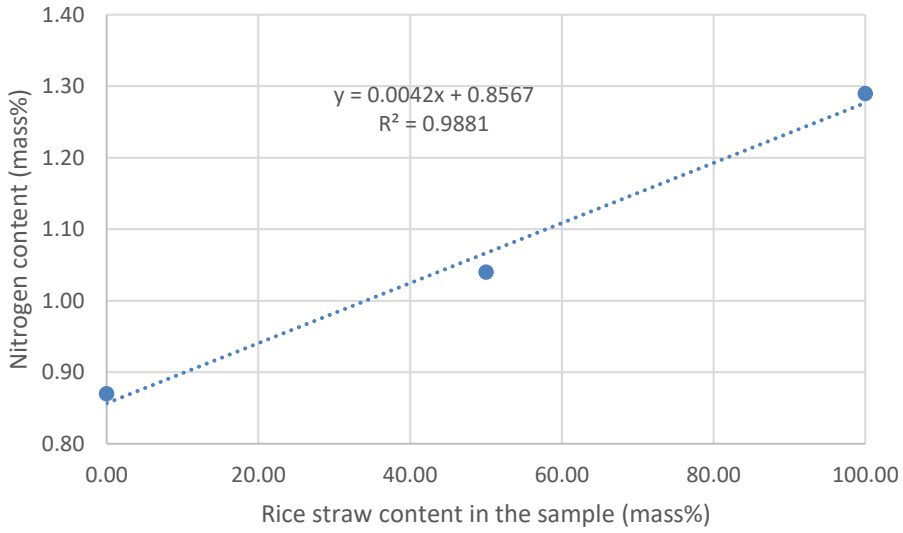
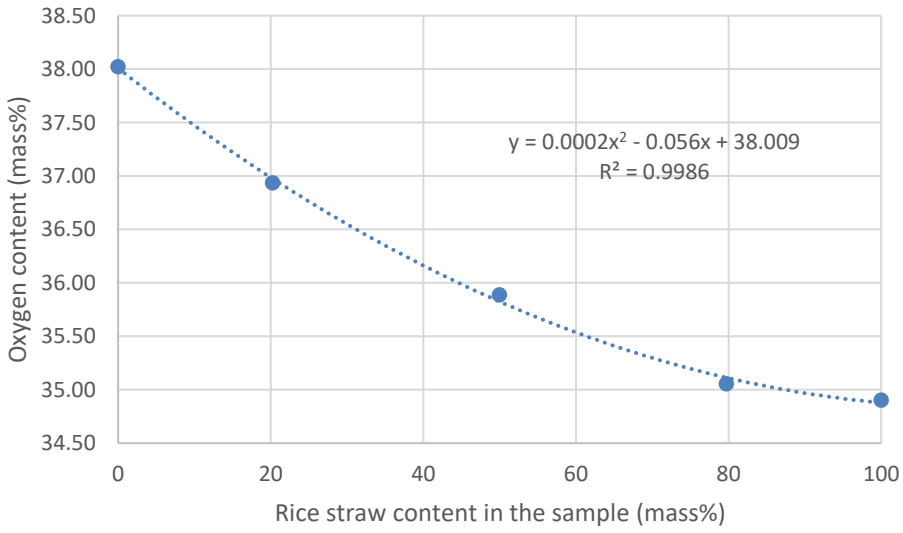


Figure 49.

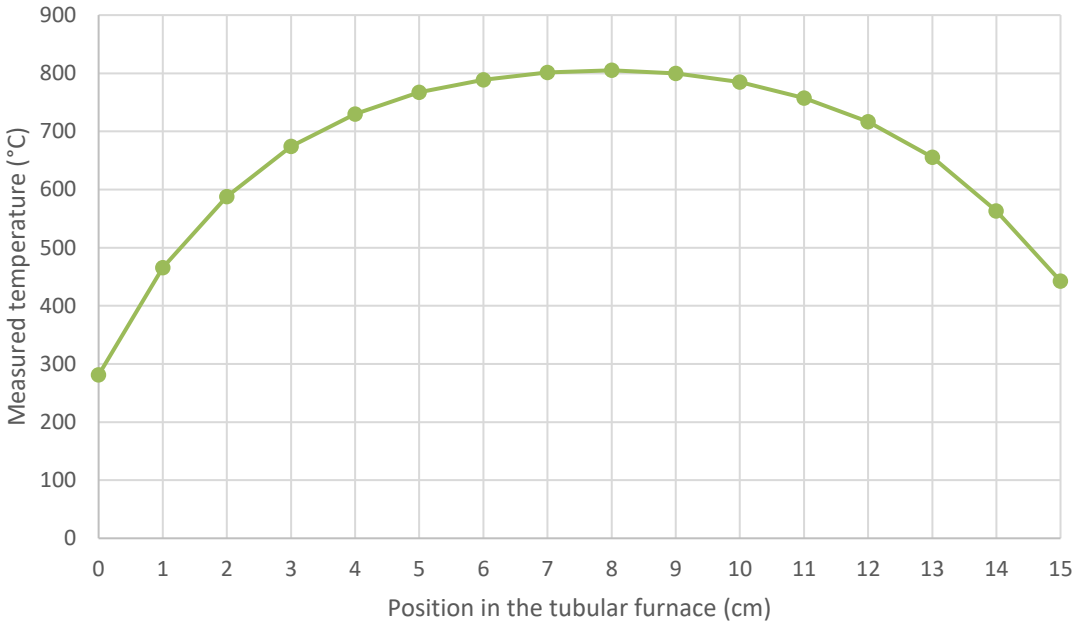
Linear regression performance in the tests data obtained for the oxygen content determination, as a function of the rice straw content in the biomass sample.



Appendix F

Figure 50.

Temperature profile measured in the quartz reactor using the tubular furnace at 805 °C in the experimental set-up for the fixed bed gasification analysis.



Appendix G

Table 17.

Results of bio-oil and solid char mass yields obtained from the tests performed in the pyrolysis reactor.

Temperature [°C]	Rice Straw content [mass%]	Bio oil percentage [mass%]	Bio char percentage [mass%]
425	50	37.20	38.83
336.6	14.64	28.38	60.71
425	100	39.54	37.90
425	50	40.28	39.08
513.4	14.64	44.44	35.82
336.6	85.35	34.21	51.16
425	50	41.28	39.37
425	0	45.69	38.66
513.4	85.35	41.29	31.85
550	50	41.05	15.27
300	50	17.54	76.92

Table 18.

Mass balance calculation from the products mass yields obtained in the gasification tests performance.

N° Test	Temp [°C]	% RS	ER	Tar yield (mass%)	Char yield (mass%)	Syngas yield (mass%)	Total (mass%)
15	740.54	20.27	0.220	27.42	14.65	56.49	98.56
11	740.54	20.27	0.279	27.18	9.97	56.98	94.13
5	740.54	79.73	0.220	26.45	9.37	57.52	93.34
2	740.54	79.73	0.279	29.47	7.95	62.58	100
4	859.46	20.27	0.220	27.40	12.37	60.23	100
6	859.46	20.27	0.279	19.09	12.34	68.57	100
3	859.46	79.73	0.220	29.10	8.79	62.11	100
10	859.46	79.73	0.279	19.65	4.96	66.16	90.77
1	900	50	0.25	27.24	8.55	64.21	100
8	700	50	0.25	24.44	10.29	57.12	91.85
19	800	100	0.25	23.59	8.12	62.07	93.78
13	800	0	0.25	34.21	12.18	53.61	100
16	800	50	0.3	22.42	8.75	64.29	95.46
7	800	50	0.2	26.23	12.90	58.20	97.33
9	800	50	0.25	26.47	9.47	61.06	97.00
12	800	50	0.25	20.32	8.14	58.59	87.05
14	800	50	0.25	18.19	7.44	58.14	83.77
17	800	50	0.25	22.96	13.58	63.46	100
18	800	50	0.25	21.88	11.48	60.43	93.79

Table 19.

Results of syngas composition measurement through the gas chromatograph and its calculated heating value following the experimental design carried out for gasification process tests for rice waste biomass samples.

Temp. [°C]	% RS	ER	HHV [MJ/kg] (N_2 free basis)	HHV [MJ/kg] (N_2 Included)	Volume composition percentage (%) H_2	CH_4	CO	CO_2
740.54	20.27	0.220	7.34	3.02	6.05	4.40	8.78	18.55
740.54	20.27	0.279	5.00	1.72	5.57	1.22	6.94	16.69
740.54	79.73	0.220	7.12	2.73	9.87	2.39	7.41	17.19
740.54	79.73	0.279	6.44	2.35	8.11	1.84	7.72	16.42
859.46	20.27	0.220	10.96	5.04	16.02	2.66	17.32	12.65
859.46	20.27	0.279	14.28	8.69	28.25	4.63	19.45	13.75
859.46	79.73	0.220	10.95	5.20	17.25	2.65	17.07	13.37
859.46	79.73	0.279	7.79	3.10	8.36	0.77	17.23	12.32
900	50	0.25	10.03	4.27	11.29	1.46	20.87	10.08
700	50	0.25	5.73	2.03	6.66	1.99	6.14	17.23
800	100	0.25	6.73	2.61	8.65	3.19	5.46	18.91
800	0	0.25	7.12	2.66	8.75	1.61	10.33	15.04
800	50	0.3	6.53	2.45	7.06	2.93	6.61	17.75
800	50	0.2	9.51	4.14	14.45	3.25	10.81	16.18
800*	50*	0.25*	6.86	2.76	7.84	2.49	9.59	16.89

*Average value.

Table 20.

Results obtained from flue gas composition and its temperature measurements performed from the combustion experimental tests.

% RS	λ	CO Production**	NOx Production**	NO Production**	CxHy Production**	T max chamber [°C]
1	1	4098	16	16	5820	123
1	-1	2042	20	20	2480	118
-1	-1	2648	17	17	5975	112
-1	1	1285	8	8	1425	156
0	α	4898	14	14	10785	152
α	0	8048	22	22	15170	130
0	-α	222	2	2	695	117
-α	0	407	3	3	0	133
0*	0*	3286	17	17	10912	114

*Averaged values;
**Units in parts per million [ppm].

Appendix H

In Figure 51, a comparison between the results obtained from the factors variations is shown; a direct effect from the temperature variation can be observed, which is more remarkable at low levels of straw content in the sample; further, the equivalence ratio applies a similar influence, although in a shorter extent. If the straw content rise, the temperature influence decreases widely keeping the same trend and the ER switchs to an inverse effect over the production of this component in a small magnitude as well; the influence from the temperature and the ER remains at central levels of straw mass percentage. The straw content in sample does not apply a significant effect, even though its decrease allows a higher production of hydrogen at high temperatures.

The influence from the temperature is consistent with previous studies for rice husk gasification in fixed bed using air as gasifying medium (Khonde & Chaurasia, 2016) and for rice straw analysis (Ngamchompoo, W., 2018), where the ER performed a direct effect over the production of this component; however, for rice husk samples, this last factor applied an inverse trend (Ma, Z. et al., 2015) thereby, the effect of the rice straw content and the equivalence ratio in sample is not remarkable over the hydrogen production. Following Le Châtelier principle (Keszei, E., 2012), the hydrogen content is managed by R2 which is endothermic and R3 that is of an exothermic nature as detailed in Table 14; if a temperature increment takes place in the gasification process, this leads to an increase in the contents of this component at R2 as a product and at R3 as a reactant.

Figure 51.

Comparison of measurements of H_2 content from the tests performed following the central composed design applied to the gasification process analysis.

